MEMS Design: The Geometry of Silicon Micromachining

Thesis by
Ted J. Hubbard

In Partial Fulfillment of the Requirements
for the Degree of
Doctor of Philosophy

California Institute of Technology
Pasadena, California

1994

(Defended April 1, 1994)

© 1994
Ted J. Hubbard
All rights Reserved

Acknowledgments

To my advisor Erik for all his advice, counsel, and for helping me see the orchard for the trees.

To everyone in Dr. Tai's lab and at JPL for helping with the fabrication.

To the Thomas lunch gang for making three years seem too short.
A special thanks to my fellow Canadians, Andrew and Jim.

To Grandpère.

MEMS Design:
The Geometry of Silicon Micromachining

by

Ted J. Hubbard

In Partial Fulfillment of the
Requirements for the Degree of
Doctor of Philosophy

Abstract

The design of MEMS (Micro Electro Mechanical Systems) on the millimeter to micron length scales will be examined in this thesis.

A very broad base of knowledge has been developed concerning the etching processes commonly used in MEMS fabrication. The fundamental problem we have sent out to study is how to model the shape transformations that occur in MEMS fabrication. The ultimate goal is to determine the required input mask geometry for a desired output etched shape.

The body of work begins with the crystal structure of silicon and ends with etched shapes. The underlying crystal structure causes different rates for different directions; this behavior has been modeled to obtain rate models. The information in these rate models has then been used in a number of shape modelers. High level models like the Eshape model provide not only simulation but a framework for true design. Other models such as the Cellular Automata model take a different approach and provide flexible and robust simulators. The tools were used to develop real world MEMS applications such as compensation structures.

As important as the individual models, is the ability to integrate them together into a coherent design tool and allow information to flow between different parts. This synthesis allows a fuller understanding of the etching process from start to finish.

It is important to note that while this thesis deals with etching, the methods developed are very general and are applicable to many shape transformation processes.

Contents

1 Introduction **1**

1.1 Design . . . 1

1.2 Historical Perspective . . . 3

1.3 VLSI vs. MEMS . . . 6

1.4 MEMS CAD . . . 6

1.5 Thesis Overview . . . 7

1.5.1 Contributions . . . 8

1.5.2 Limitations . . . 9

1.5.3 MEMS design . . . 10

2 MEMS Background **12**

2.1 MEMS Fabrication Techniques . . . 12

2.1.1 Bulk wet micro machining process steps . . . 12

Disadvantages . . . 14

2.1.2 Other etching methods . . . 14

Bulk dry etching . . . 14

Surface micro machining . . . 17

Laser micro machining . . . 17

LIGA . . . 17

2.2 Crystals and Shapes . . . 18

2.2.1 Why use silicon? . . . 18

2.2.2 Crystal planes . . . 19

2.2.3 Corner and shape classifications . . . 20

2.2.4 Spoke patterns 23

2.3 Shape Transformations 26

2.3.1 Examples of shape transformations 26

2.3.2 Minkowski transforms 30

2.3.3 MEMS shape modelers 32

Wulff-Jaccodine 32

Slowness 33

Discussion 35

3 Rate Modeling **37**

3.1 Introduction 37

3.2 Two Dimensions 38

3.2.1 Two Parameters 38

Three Parameters 41

3.2.2 Three Dimensions 44

Three Parameters 44

Four Parameters 46

3.3 3D $\Rightarrow$ 2D (100) Projections 51

3.3.1 General Projections 51

3.4 Generality 53

3.5 Summary 58

4 Shape Modeling **59**

4.1 Introduction 59

4.2 Wafer Cuts 60

4.3 Limit Shapes 60

4.3.1 Linear shapes 66

4.3.2 Why are limit and linear shapes important? 67

4.4 Shape Library 67

4.5 Uncertainty 69

4.5.1 Noise 69

4.5.2 Misalignment 69
4.6 Peg Limit Shape 74
4.7 Summary 74

5 Eshapes **75**
5.1 Introduction 75
5.1.1 Prior work 75
5.2 Mathematical Derivation 77
5.2.1 Shapes 77
5.2.2 Envelopes 79
5.2.3 Eshapes 81
5.2.4 Corners 82
5.2.5 Time Evolution 86
5.3 Limit Shape 86
5.4 Time Scaling 87
5.5 Design Inversion 89
5.6 Comparison with Experiment 90
5.6.1 Test patterns 90
5.6.2 Spoke patterns 91
5.7 Extension to Three Dimensions 94
5.7.1 Exact solution 94
5.7.2 Approximate three dimensional solution 96
5.8 Summary 97

6 Cellular Automata **99**
6.1 Introduction 99
6.2 Modeling Methods 100
6.2.1 Scaling 101
6.2.2 Empirical vs. theoretical 101
6.3 Two Dimensional Algorithm 102
6.4 Three Dimensional Extension 105

6.5 Full Three Dimensional Algorithm 105

6.5.1 Two dimensions vs. Three dimensions 109

6.6 Computational Cost 109

6.6.1 Area vs. volume calculations 110

6.7 Cellular Automata Advantages 110

6.8 Implementation 111

7 Synthesis **112**

7.1 Design Paths 112

7.1.1 Linear zones 113

7.2 Time Plots 113

7.2.1 Design inversion 114

7.3 Path Plots 116

7.4 Negative Time 119

7.5 Possible and Impossible Shapes 120

7.6 Model Comparisons 127

7.6.1 How do the models differ? 128

7.6.2 Itemized comparisions 128

7.6.3 Disadvantages 130

7.6.4 Advantages 133

7.7 Design Approaches 133

8 Applications **135**

8.1 Compensation Simulation and Optimization 135

8.1.1 Introduction 135

8.1.2 Experiments 136

8.1.3 Optimization and Design Guidelines 137

8.1.4 Quality versus quantity compensation 137

8.1.5 Observations 138

8.1.6 Hole Compensation 140

8.1.7 Folded Compensation 142

Area versus linear constraints 144

8.1.8 Limitations 145

8.1.9 Three Dimensions 146

8.1.10 Summary 146

8.2 Compensation Fuses 148

8.2.1 Introduction 148

8.2.2 Previous Compensation Techniques 148

8.2.3 Compensation Tuning 150

8.2.4 Fuses 151

8.2.5 Masking 151

8.2.6 Summary 151

8.3 Application Examples 153

8.3.1 Introduction 153

8.3.2 Spiral Springs 154

8.3.3 Slotted Fan 154

8.3.4 Valves 158

8.3.5 Circular Structures 161

9 Conclusion **167**

9.1 Summary 167

9.2 Future Work 168

9.2.1 Information Standards 168

9.2.2 Robust/tolerant shapes 168

9.2.3 Etch rate data (Standard test patterns) 168

9.2.4 Improved models 169

9.3 Wish List 171

A **173**

A.1 Implementation 173

A.2 Link between Eshape and Minkowski operations 175

A.3 Trapezoidal correction for beams 177

A.4 Comparison of EDP, KOH, and TMAH etches 177

A.5 Table of abbreviations 178

List of Figures

1-1 Manufacturing, Analysis, and Design. 2

2-1 Oxide masking layer. 13
2-2 Patterning oxide masking layer. 15
2-3 Wafer etching. 16
2-4 Silicon basis cell. 19
2-5 Silicon plane densities and symmetries. 21
2-6 Qualitative (100) wafer etch rate diagram. The x axis is parallel to the wafer flat. 22
2-7 Definition of pegs and holes. 22
2-8 Definition of convex and concave corners. The unetched mask is dark, the etched bottom is light, and the beveled walls are grey. 23
2-9 Spoke pattern geometry. 24
2-10 Spoke tip geometry. 25
2-11 Experimental spoke patterns for (100) wafer in EDP. 27
2-12 Shape transformation examples: (A) painting, (B) profilers, (C) cams. . . . 29
2-13 Example of Minkowski Addition (convex/convex). The slope diagrams are shown below. 31
2-14 Example of Minkowski Addition (convex/nonconvex). + signs mean that the vector is used, - signs mean that the negative of the vector is used. The slope diagrams are shown at the bottom of the figure. 31
2-15 Wulff-Jaccodine method. 32
2-16 Corner evolution. 34
2-17 Slowness method geometry. 35

3-1 Two dimensional basis representations. 39
3-2 2D, two parameter results. 41
3-3 2D, three parameter results. 43
3-4 3D, three parameter model regions. 45
3-5 3D, three parameter model results. 47
3-6 3D, four parameter model regions. 48
3-7 3D, four parameter model results. 50
3-8 Minimum projection. 52
3-9 Projections onto cones. 53
3-10 Modeled (100) projection. 54
3-11 Experimental (100) projection. 55
3-12 Modeled (110) projection. 56
3-13 Experimental (110) projection from the literature [65]. 57

4-1 Different etchants for (100) wafer. Outer contours show etch rate at surface, inner contours show etch rate at greater depths. 61
4-2 EDP/KOH-like etchant from (100) wafer to (110) wafer. Outer contours show etch rate at surface, inner contours show etch rate at greater depths. . 62
4-3 Limit shape (inner shape) for hypothetical elliptical etch rate diagram (outer shape). 63
4-4 Sampling of a shape. 64
4-5 Limit shapes for Figure 4-2. Outer contours show limit shape at surface, inner contours show limit shape at greater depths. 65
4-6 Limit and linear shapes. 66
4-7 Shape Library. 68
4-8 Rates with noise level of 50 percent of (111) rate. Outer contours show etch rate at surface, inner contours show etch rates at greater depths. 70
4-9 Limit shapes for Figure 4-8. Outer contours show limit shape at surface, inner contours show limit shape at greater depths. 71
4-10 Rates with five degree misalignment. Outer contours show etch rate at surface, inner contours show etch rate at greater depths. 72

4-11 Limit shapes for Figure 4-10. Outer contours show limit shape at surface, inner contours show limit shape at greater depths. 73

5-1 A qualitative example of an etch rate diagram. The formula for this rate in terms of angle θ is given above the figure. Etchants such as KOH and EDP have (100) etch rate diagrams which are very similar to the above figure. . . 76

5-2 Evolution of corners. 78

5-3 (A) Corner evolving to envelope of tangents. (B) Intersection of two adjacent tangents near a corner. 80

5-4 Hypothetical two dimensional etch rate diagram (top), corresponding Eshapes (center), and Etched shape (bottom). Note that the two etchants are not real etchants. The initial mask shape was the cross shaped hole shown at the bottom of the Figure. 83

5-5 Definition of convex and concave corners.The unetched mask is dark, the etched bottom is light, and the beveled walls are grey. 84

5-6 Summary of Eshape analysis: The etch rate is first transformed into an Eshape diagram. Then each corner is tangent-matched to the Eshape, and the appropriate Esection is extracted. The initial mask (shaded region) evolves to the surrounding curve. Concave corners use interior Esections, while convex corners use exterior Esections. The three corners shown are, starting at the top in counterclockwise order, concave, convex, and convex. 85

5-7 Time evolution of a shape in a single etch. The initial mask on left is repeated at different scales. The output shapes are on the right. The effective etch time is inversely proportional to scale. 88

5-8 EDP or KOH etching: (A) diamond mask evolves to octagon. (B) modified diamond evolves to approximate diamond. (C) Eshape for (A). (D) Eshape for (B). 89

5-9 Etch rate diagram for (100) silicon in KOH and associated Eshape. 91

5-10 (A) Initial mask shapes; the squares are 0.8 mm across. (B) Predicted shapes derived from Figure 5-9. Compare with Figure 5-11. In both A and B, The top row of figures represents "pegs" while the bottom row represents "holes". 92

5-11 (A) (100) silicon etched with KOH at 60°C for two hours. The largest square is 0.8 mm across. (B) (100) silicon etched with KOH at 60°C for one hour. Compare any shape in this figure with the corresponding shape in Figure 5-11 A. In both A and B, The top row of figures represents "pegs" while the bottom row represents "holes". 93

5-12 (A) Initial spoke pattern. (B) Simulated etch using Eshape method with KOH etchant. Compare with Figure 5-1. (C) Spoke pattern etched in KOH. (D) Spoke pattern etched in EDP. Both patterns are approximately 1.5 centimeters across and both were etched for several hours. Note that the end regions on the simulations agree with the observed experiments. 95

5-13 Cross and diamond shaped holes. (A: top) KOH etch simulation extension to three dimensions (B: bottom) View from an oblique angle. Compare with Figure 5-11. 98

6-1 Silicon basis cell. 102

6-2 Silicon basis cell viewed from above, size indicates depth. 103

6-3 Classification of planes based on neighbors. 104

6-4 Sample of Cellular Automata algorithm output. 106

6-5 Cellular automata algorithm output for initially cross shaped pegs. 107

6-6 Experimental output shapes for initially cross shaped pegs. 108

7-1 EDP etchant: (A) limit shape, (B) linear shape, general shapes (C) and (D). 113

7-2 Sampling of a shape. 114

7-3 Radius versus time plots. 115

7-4 Extrapolation and interpolation of linear shapes. 115

7-5 (A) and (B) distance parameters versus time; (C) distance parameter versus distance parameter. 117

7-6 Two dimensional paths from zero time. Some paths are linear, some are not. 118

7-7 Paths forward and backward in time. 119

7-8 Running etch simulators backwards in time will not recreate the initial shape if lines disappear. 121

7-9 Design paths. 122

7-10 (A) possible hole shape; impossible hole shapes (B), (C), and (D). 123

7-11 Holes, pegs and self intersecting shapes. 124

7-12 Contradictory three dimensional parts of self intersecting shape. 125

7-13 Isotropic etching of a rectangular peg and removal of cusps. 126

7-14 Backward simulations which yield impossible input shapes: (A) rectangular hole in isotropic etchant; (B) diamond hole in EDP-like etchant. 127

7-15 Graphical comparison of different methods. 131

7-16 Comparison of different methods. 132

8-1 Successive degradation of initially square peg. 136

8-2 Initial mask of array of compensation structures including uncompensated rectangles (lower left and upper right). 137

8-3 Evolved shapes at different times. (A) uncompensated rectangle; (B) fin compensation; (C) bar compensation; (D) rectangular compensation. . . . 138

8-4 Output shapes: (A) 4 1/2 hours (B) 6 hours; the array is about 1 cm by 1 cm. 139

8-5 (A) diamond mask evolves to octagon. (B) modified diamond evolves to approximate diamond. (C) compensation for isosceles triangle. 140

8-6 Experimental output shape for diamond hole compensation. 141

8-7 Initial mask for snake-like compensation. 142

8-8 Two samples of snake-like compensation after etching $\sim$ 7 hrs (left) and $\sim$ 14 hrs (right) in EDP. 143

8-9 Progressive etching of a a folded compensation structure. Time increases from A to D. 144

8-10 Compressed version of folded compensation. Note staggered holes. 145

8-11 Extension of simulation to third dimension. Simulation proceeds from top left to bottom right. 147

8-12 Schematic representation of compensation techniques. (A) uncompensated; (B) square compensation; (C) bar compensation. 149

8-13 Web compensation.(A) webs are permanent (B) (111) planes slowly etch through webs. 150

8-14 Compensation tuning. An anisotropic etch is followed by an ~ isotropic etch and a second anisotropic etch. 152

8-15 Compensation fuses (A) Stable fuse with some variable parameters. (B) Unstable fuse exposes convex corners. 153

8-16 Uncompensated spiral spring mask/design (A), and expected output (B). Compensated spiral spring mask/design (C) and simulated output (D). . . 155

8-17 Compensated spiral spring (A) and uncompensated spiral spring (B) two dimensional simulations. Contours represent two dimensional shape at different times. 156

8-18 Etched spiral spring. 156

8-19 Overhead view of slotted fan design. 157

8-20 Cross-sectional view of slotted fan design. 158

8-21 Two dimensional simulation of slotted fan design (one quarter circle). Original mask and two dimensional output contours are shown. 159

8-22 Three dimensional simulation of etched slotted fan (one quarter circle, one sided etch only). 160

8-23 Preliminary valve design mask, actuation perpendicular to flow. Interlocking raised pegs control flow. 161

8-24 Preliminary valve design mask, actuation along flow, pegs within holes control flow. 162

8-25 Simulated three dimensional output shapes for part a of first valve. 163

8-26 Simulated three dimensional output shapes for part b of first valve. 164

8-27 Two dimensional simulations for annular mask. 165

8-28 Three dimensional simulations for annular mask. In this oblique view, the mask is etched for longer times and increasing depths in the following order: west, north, south, and east. 166

A-1 Links between different design tools. 174

A-2 Main menu screen. 175

A-3 Eshape submenu screen. 176

A-4 Trapezoidal I/A as a fraction of square I/A versus normalized width. Top curve is θ =35.3 degrees, bottom curve is θ =45 degrees. 178

A-5 Comparison of EDP, KOH, and TMAH etches. 179

List of Tables

2.1 Typical values for mechanical properties. 19

3.1 2D, two parameter model matrices and equations. 40

3.2 2D, three parameter model matrices and equations. 42

3.3 3D, three parameter model matrices and equations. 46

3.4 3D, four parameter model matrices and equations. 49

6.1 Number of neighbors for etching planes. 104

A.1 Common abbreviations. 180

Chapter 1

Introduction

1.1 Design

The design of MEMS (Micro Electro Mechanical Systems) on the millimeter to micron length scales will be examined in this thesis.

While MEMS structures have been fabricated for many years, their design has been almost entirely informal trial and error. A more formal MEMS design approach is presented below, which substantially reduces the number of experimental prototypes required to fabricate a MEMS structure, and provides considerable insight into effective MEMS design.

In a generalized manufacturing process (see Figure 1-1), an initial plan or mask is made. Next the fabrication process (using that plan or mask) produces an output shape which performs some function. CAA (computer aided analysis) allows the user to model the function (e.g., stress or deformation) of a given shape. A true CAD (computer aided design) system allows the designer to specify a desired function, then determines a shape which provides that function, and ultimately obtains an input mask which evolves into the desired shape. True design works backwards from the desired outputs to determine the required inputs, while analysis deals with the forward path. In many cases what is termed CAD is actually the repeated use of CAA in an iterative fashion using the design knowledge of the designer. This iteration is used to converge on the desired output. This thesis will examine a subset of the general problem: the transition from input mask to output shape, while the highest level of this research is to produce masks that will create shapes that exhibit a desired function.

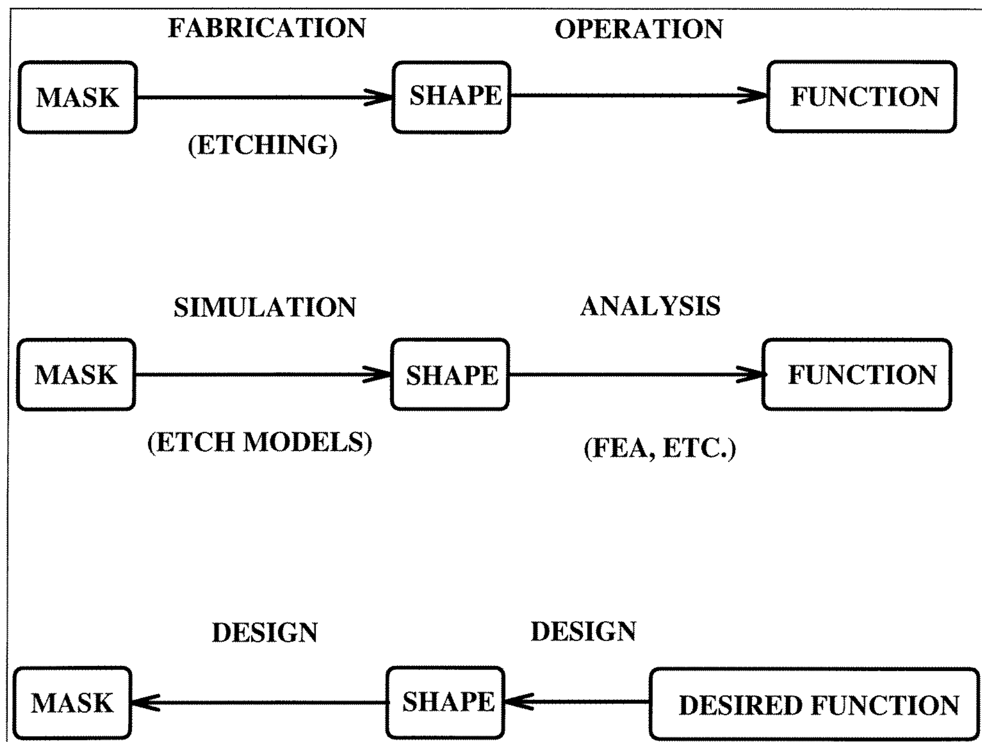

Figure 1-1: Manufacturing, Analysis, and Design.

Design methodology is dependent on the manufacturing technology, and this becomes especially true on smaller length scales. Large or macro scale objects can be built using many different techniques, each method having its advantages and disadvantages. Thin objects such as automobile body panels and tin cans can be made with sheet metal forming. Rotationally symmetric objects such as chair legs may be spun on a lathe. Other objects such as an engine block may be cast from a mold. Each of these technologies imposes limits on the possible output shapes, for example a square chair leg cannot be made on a conventional lathe without external cutting either before or after. In addition there are other trade offs; casting is cheaper than milling, but it is also less precise. No one technology is best suited for all applications, and a manufacturing process may involve many different steps in series.

Just as there are many fabrication methods for making macro scale objects, there are many ways to make MEMS [52, 55, 58, 70, 72, 79, 86]. In MEMS it is possible to make a wide variety of shapes, with a specific process being well suited for a specific set of shapes. A number of different fabrication technologies will be introduced later, but the focus of this thesis will be primarily on wet bulk etching. This process is well established and relatively inexpensive. More importantly it is often one of the steps in a multi step fabrication technology. Finally, the design methodologies developed here can be adapted to many other types of MEMS fabrication techniques.

In bulk wet etching, etched shapes evolve as a function of time in a complex fashion. Because the transformation from the initial two dimensional input mask to the final three dimensional output shape is quite complex, the design of MEMS is not straight forward.

1.2 Historical Perspective

This section presents a brief review of some of the important milestones in the history of MEMS. This summary is by no means complete, and only includes a portion of the work carried out in the field.

Both MEMS and micro electronics have seen dramatic improvements in recent decades, in fact many of the MEMS fabrication technologies were originally developed as micro electronic technologies. Micro electronics has progressed rapidly from the first transistor

(1948) [6] to the first integrated circuit(1959) [42] to the VLSI and ULSI systems of today. Throughout its history, micro electronics has been characterized by decreasing feature size and increasing density. MEMS on the other hand has no such universal figure of merit and its progress is measured not so much in terms of improving one specific parameter, but rather in terms of its diversity and the increasing range of possible applications. Thus the following summary is organized on a partly chronological, partly functional basis.

One of the earliest means of obtaining three dimensional shapes in mono-crystaline silicon was the use of anisotropic etchants. With these etchants the etch rate depends on orientation of the face being etched and the initial (two dimensional) mask is etched to become a three dimensional shape bounded by certain etch planes. Ethylene diamine pyrocathecol (EDP) was studied as early as 1967 [25, 62]. EDP etching has been used in a wide variety on applications. Early products included ink jet printer nozzles [8, 38, 57] and optical components [81, 80]. In addition EDP etches boron doped silicon very slowly [12]; doped etch stop layers provide a way of very accurately controlling the thickness of thin etched membranes and diaphragms. Another common etchant in potassium hydroxide (KOH) [85, 64]. KOH etching is very anisotropic and the ratio between fastest to slowest etch rate can be as high as 400 to 1. In addition KOH can produce vertical walls when etching a (110) wafer [39, 40]. This property has been used in a wide variety of applications [7, 9, 19, 41] including high capacity heat sinks for micro electronics [82]. While some measurements of the etch rate behavior have been done by a number of researchers [34, 44, 64, 65, 85], full three dimensional etch rate data is generally not available. More complicated wet etching techniques such as doping selective etching [46] have also been studied and newer etchants such as tetra-methyl hydroxide (TMAH) are being used [74].

Dry etching [1, 26, 71] involves a gas or a plasma in place of a liquid. Examples of dry etching systems include reactive ion etchers (RIE) and plasma etchers. Dry etchers can produce very small features, but are generally limited in etching depth [63].

Another fabrication technology, surface micromachining, takes a different approach to shape generation. Surface micro machining uses sacrificial layers to form thin, high resolution structures on the surface of the wafer. The sacrificial layer allows the generated parts to be freed from the wafer. Using this technology, very complex parts such as micro motors

can be manufactured [76, 75, 73, 23]. Pister [59] has demonstrated hinged structures that can be folded out of the plane of the wafer in order to create three dimensional shapes. Because of their high resolution and high density, surface micro machined parts show great promise.

A more recent development is the combination of existing etching techniques with directed energy sources. Two examples of this are laser assisted etching and LIGA. Laser assisted etching [3, 4, 10, 11, 13, 22, 54, 83] uses a laser to locally heat a sample in order to effect the etching. LIGA [32, 31, 33, 51, 84] uses a strong x-ray source to expose a pattern in x-ray sensitive resist. Both methods can produce detailed parts with small dimensions, but both have high cost per part [72].

A number of etch modeling methods have been proposed. Early shape modeling work included the Wulff-Jaccodine method of traveling planes [27, 36]. A number of computer implementations have been developed [18, 20, 21, 68, 69, 77] including ASEP (Anisotropic silicon etching program) [16]. Another important etching simulation tool is the Slowness method [67]. Both models are good simulators but do have some disadvantages, particularly in design. My research builds on these early etch modeling methods and resulted in several new etch simulation methods that improve on the previous methods, particularly for MEMS design. The new methods that I developed (Eshape, Cellular Automata, etch rate modeling, etc.) will be presented in detail below.

In addition, much work has been done on the broader picture of MEMS design concerning CAD architecture and the interface of shape modelers with FEA function modelers [15, 45, 48, 60, 66, 87].

Perhaps the most promising aspect of MEMS research is the integration of electronic and mechanical components into functioning systems. For example, applications such as pressure sensors have on-chip signal conditioning and processing [14, 53, 86, 52]. If any figure of merit is to be established to benchmark the progress of MEMS, it should be a measure of the number and different types of sensors and actuators and components that can be incorporated into a single system.

Modeling, wet etching and many of the other fabrication technologies will be reexamined later in Chapter 2.

1.3 VLSI vs. MEMS

Many of the fabrication techniques for MEMS are derived from the micro electronics industry. The introduction of VLSI (Very Large Scale Integration) design methodology (CAD) has led to a rapid growth in the micro-electronics sector [50]. It is hoped that a MEMS CAD system will lead to similar benefits in micro-devices. VLSI changed the way micro-electronic systems were designed, providing a design framework and a set of design rules. By separating the details of the fabrication technology from the electronic function, VLSI CAD freed designers from process knowledge and allowed them to think at a higher functional level, permitting large scale projects.

However, the logic gates of VLSI are essentially planar while a micro-machine may be fully three dimensional. The electronic function of a VLSI gate is essentially independent of its position and orientation on the wafer while the mechanical function of a micro-machine is usually highly dependent on its location and orientation. Thus there is a much more complicated relationship between input mask and output shape (and function) in MEMS. Because of the three dimensional nature of the shape-function relationship in MEMS, it may not be possible to fully separate the design process from the fabrication process.

1.4 MEMS CAD

Many useful micro-devices are now being built, but no structured formal design methods exist and automated design (in the VLSI CAD sense) awaits a strong foundation. Proposals for MEMS CAD systems have been made in recent years [15, 45, 48, 60, 66, 87] and as the complexity of devices rises the need for a coherent design system has been recognized. Considerable work has been done on establishing the best architecture for such a system. Some of the essential elements include: a user interface, a structure simulator, a materials database, a three dimensional modeler, a FEM package, along with the proper interconnections between elements. Implementation of this system has provided much information about both mechanical and electrical properties. For example stresses and deflections have been accurately predicted as have capacitance and resistance. Such systems have successfully analyzed MEMS devices and allowed for the higher level descriptions required for

complicated projects.

While much work has been done in other parts of CAD systems, there is much potential in an improved simulator/modeler. For some of the other elements it is logical to use existing software, however there are good reasons to reexamine simulators to ensure that the ones used are optimally designed for use with MEMS (as opposed to converted VLSI simulators). In fact Maseeh et al. recognized that "the critical block in this section is the Structure Simulator" [48]. Because the modeler occurs very early in the CAD architecture, it should be as general and flexible as possible in order to increase the scope of MEMS CAD applications. Finally, any simulator should have the capability for design in addition to simply analyzing MEMS behavior.

1.5 Thesis Overview

This thesis has four broad goals:

- To (empirically) explain why etched shapes change as they etch,
- To develop new methods to predict output shapes as a function of time,
- To develop new methods to perform MEMS design to obtain required input masks that will create desired shapes,
- To apply these design methods to real MEMS applications.

The first item is discussed in chapters 2, 3, and 4. Chapter 2 is an introduction to MEMS fabrication, explaining common processes and providing the necessary background for this work. Chapters 3 and 4 examine the effect of the crystal structure on the etching process. These two chapters show the link between crystal structure, etch rates, and etched shapes; they lay the foundations for constructing good design tools.

The remaining items are discussed in chapters 5, 6, 7, and 8. Chapters 5 and 6 present two different simulators which take two different approaches to modeling the etching. Chapter 7 examines broad design issues, including design inversion and model comparisons. Chapter 8 uses the previous methods in several real world applications. Finally, chapter 9 is a conclusion presenting a summary and an examination of possible future work.

1.5.1 Contributions

My research resulted in the creation of several new etch simulation methods that are aimed specifically at aiding MEMS design. These new methods are the Eshape method, the CA (Cellular Automata) method, and an etch rate modeling method.

While the foundation of the Eshape method is based on the same (empirical) method of traveling planes that the Wulff-Jaccodine method is based upon, the Eshape method recasts these calculations into a wholly new new etch simulation approach that has several significant advantages. The Wulff-Jaccodine method calculates the position of the traveling planes for each unique geometry for each time-step. The Eshape method is significantly more computationally efficient than the Wulff-Jaccodine method, because the calculations for the traveling planes are done once for all geometries far all time steps. This not only eliminates the many repeated calculations of the Wulff-Jaccodine method, it also directly aids MEMS design by graphically showing the designer which shapes are possible to etch (for a given silicon wafer orientation and etchant).

Because the underlying approach of the two methods is the same, they share limitations, most notably the difficulty in determining the presence and location of the intersections of one part of the evolving shape with another.

To surmount this difficulty, and to create an etch simulator that is robust for arbitrarily complex geometry, I developed the CA (cellular automata) method. This method applies the basic premise of all cellular automata to etching: to divide the spatial domain into small cells, provide each cell with simple and primitive (but appropriate) behavior, and the aggregate behavior of many cells will mirror the behavior of physical systems. Finite element analysis (FEA) and computational fluid dynamics (CFD) and other methods are all based upon this approach. The approach is simple to create conceptually and algorithmically (each cell is identical and the rules for each cell's behavior are simple), but the method is computationally expensive since a few simple calculations are repeated many times. Despite the computational limitation of the method (which imposes a trade off between the spatial resolution of the CA etch simulation technique and the simulation time) the approach's robustness to arbitrarily complex geometry and an unlimited number of etched shape intersections and interactions, provides a clear advantage for most MEMS design

problems.

The modeling of etch rates (in all directions within the silicon crystal) was limited. Since the most commonly used anisotropic etchants for silicon preferentially etch rectangles, and since most electronic structures are composed of rectangles, the etch rates for these etchants for the commonly occurring planes are well known. However for other directions, only a limited amount of data exists [34, 44], and no satisfactory model existed to calculate approximate rates in between well known rates. The etch rate model that I developed relies on etch rate data from the literature [64, 65], and can easily incorporate new data as it becomes available, however the modeling method itself is wholly new.

Finally, the underlying philosophy and approach of this research is a departure from other MEMS design work. The long-term goal of this research is to permit the designer to specify a desired MEMS function, and to have the design system automatically (or perhaps semi-automatically) determine the required silicon shape to exhibit that desired function, and further for the design system to automatically determine the mask and other processing instructions to fabricate that shape. This goal is motivated by the the desire to enable MEMS design to approach the level of automaticity present in VLSI design. Other contemporary MEMS design research is based on an analytic (rather than synthesis-based) view of MEMS design, namely: Given a mask what shape will be produced? [16, 20, 36, 67], and: Given a shape, what function will be exhibited? [15, 45, 48, 66]. The methods developed here were specifically developed for MEMS design (synthesis) rather than analysis, fundamentally based on the goal of developing highly-automatic MEMS design systems, on par with contemporary VLSI design systems.

1.5.2 Limitations

There are three principal limitations to the scope of this thesis. As previously mentioned, only part of the design problem is addressed: the transition between initial mask and final shape. Neither the relationship between shape and function, nor integration of shape modelers with function analysis tools such as FEA are examined. Both these issues are important, but the ability to predict and ultimately produce a shape is a prerequisite to any further study.

Secondly, while there are many fabrication techniques in MEMS (e.g. surface micromachining, LIGA, dry etching, laser micro machining, etc.), the thesis concentrates on wet bulk etching. Wet bulk etching is relatively easy to perform, is relatively inexpensive, and is commonly used in many applications. More importantly, wet bulk etching displays the fundamental behaviors found in many fabrication methods. While it is possible to do so, the design methods in this thesis have not been applied to other etching technologies.

Thirdly, the analysis of the etching of silicon has been empirical rather than theoretical. The question most commonly asked is "how?" rather than "why?". There are a number of reasons for this, primary among them are the complexity and diversity of silicon etching processes. Silicon and silicon etchants interact in a very complicated fashion, and much remains to be learned. Furthermore, the details of the etching can be very different for different etchants. Thus the thesis seeks to characterize etching in terms of experimentally measured quantities to form empirical relations describing the etching. The emphasis has been on distilling from the fabrication the important parameters, and using them in simple, efficient models. Nevertheless, this empirical approach must satisfy two requirements: (i) the results must be accurate (ii) the models must reflect the actual physics of the etching. To the extent that measurements are possible, the research presented in this thesis satisfies these two requirements. More work on a better theoretical understanding of the etching would be of great value.

1.5.3 MEMS design

The fundamental question this thesis set out to answer was

> What is the necessary input shape to get a desired output shape?

Unfortunately, the original question was superseded by another question:

> Does the necessary input shape exist to get a desired output shape?

One of the initial goals of this work was to develop a good etch simulator. There are a number of existing simulators, each having advantages and disadvantages, and the proper choice of modeler depends on the application. However, during the course of the research, it became apparent that even an "ideal" simulator is not an "ideal" design tool. The ability

to simulate the transition from input mask shape to final output etched shape is necessary for any MEMS CAD system, but it is not sufficient.

Because the transition from input to output can in general be very complex, the inverse process is very difficult and often impossible. In essence, since planes may disappear or appear, the forward path (mask to shape) and backward path (shape to mask) can be fundamentally different. In fact some shapes simply cannot be fabricated with some etchants. These issues are examined at greater length in chapter 7.

As MEMS design tools are developed, the need to differentiate between analysis and design must be addressed. The focus should shift away from the types of output shapes that can be produced to what types of output shapes can be inverted using design methods. Continuing MEMS CAD developments will increasingly permit designers to ignore fabrication details and concentrate instead on providing MEMS functions.

Chapter 2

MEMS Background

Micro Electro Mechanical Systems (MEMS) are silicon micro-structures produced by etching which exhibit valuable mechanical properties and can be readily integrated with microelectronics. The integration of micro pressure sensors (fabricated by etching a thin diaphragm) and processing electronics is only one of the recent applications of MEMS. Since these devices depend heavily on specialized fabrication methods, a brief review of several widely used methods will be presented.

2.1 MEMS Fabrication Techniques

2.1.1 Bulk wet micro machining process steps

There are many techniques for micro-machining silicon; this work will concentrate on bulk wet etching [7, 9, 40, 41]. Several other techniques will also be discussed, and the design methodologies developed will not be limited to bulk wet etching. Bulk wet etching is chosen because it is an established method that has been available for many years and it is relatively easy to perform and relatively inexpensive. The review article by Petersen [58] is an excellent summary of many MEMS fabrication methods.

The first step is to obtain silicon wafers cut along some orientation. The most common wafer orientation is (100) (the wafer is cut perpendicular to the x-axis), although other orientations such as the (110) are also available. Typical wafer sizes are one to four inches in diameter and 100 to 400 microns in thickness.

Next the wafer is cleaned and a thin masking layer is applied to the wafer (see Figure 2-1).

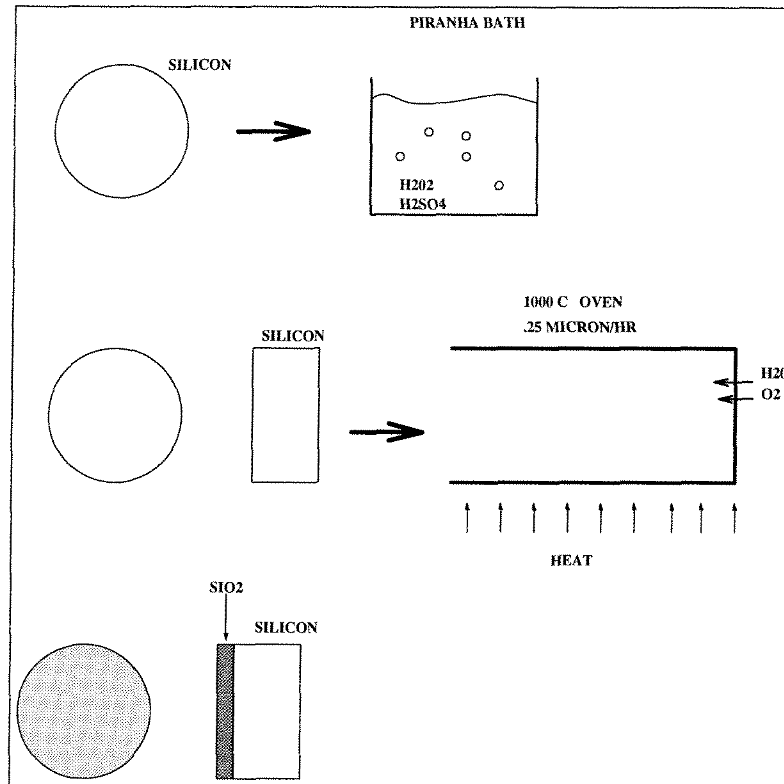

Figure 2-1: Oxide masking layer.

The masking layer used in these experiments is silicon dioxide. Silicon has the advantage that its oxide is grown easily and is lattice matched, which makes for low stress masking layers. The bare silicon wafers are placed in a furnace at approximately 1000 to 1100 degrees Celsius for several hours. The furnace contains water vapor to enhance the oxide growth. Thicknesses of up to a micron are readily attainable, the thickness in most of our experiments is roughly 8000 Ångstroms. Other possible masking layers include silicon nitride and evaporated metals such as gold or chrome.

Next a uniform layer of photoresist of roughly micron thickness is spun onto the wafer (see Figure 2-2). The desired input mask is used to selectively expose the photoresist. When exposed to ultraviolet light the photoresist is chemically altered and the exposed portions of the photoresist can then be removed with photoresist developer. With parts of the photoresist removed, the masking layer is now partially exposed. The exposed portions of the masking layer are etched away with an etchant which removes oxide but not photoresist

or silicon. Having done so, the remaining photoresist is removed, leaving a patterned oxide masking layer.

The wafer is then placed in a container of etchant as shown in Figure 2-3. The etchant may be KOH (potassium hydroxide), EDP (ethylene diamine pyrocatecol), TMAH (tetramethyl ammonium hydroxide), or some other etchant which attacks silicon but not the masking layer. A reflux system runs cold water through the top of the container to prevent evaporation of the etchant. Many etchants are used near their boiling point since the rate of etching tends to increase greatly with temperature. The container has both a temperature feedback to maintain constant temperature and a stirrer to ensure that the etching is homogeneous. The sample is etched for a set period of time then removed. The remaining masking layer can now be stripped, leaving a three dimensional shape in the silicon wafer.

Bulk wet etching may be done alone or in conjunction with other micro machining techniques.

Disadvantages

As mentioned above, bulk wet etching is an established relatively inexpensive method, but it does have many disadvantages. Many of the etchants are very hazardous and must be handled properly. The anisotropic nature of the etchants means that certain planes dominate others and that the etched shapes are distorted versions of the original masks [34, 37, 44, 65, 64, 85]. The anisotropy also limits the possible output shapes and the attainable height aspect ratios.

2.1.2 Other etching methods

A wide variety of other etching techniques also exists, a few are listed below. All these methods can be used either singly or in combination to manufacture micro machines.

Bulk dry etching

In bulk dry etching [63], the liquid etchant is replaced by a gaseous plasma or ions. Plasma etchers and RIE (reactive ion etchers) are two examples of dry etchers. The etching takes place by chemical means, by physical bombardment of the silicon, or by some combination

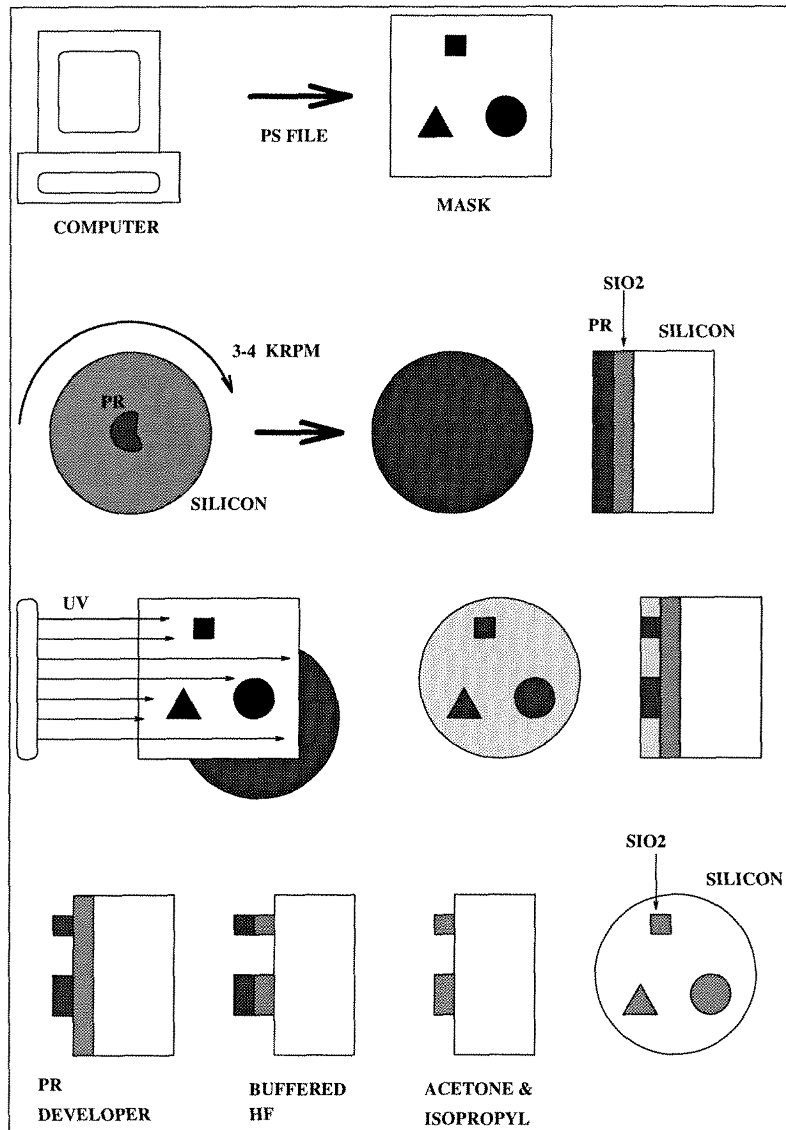

Figure 2-2: Patterning oxide masking layer.

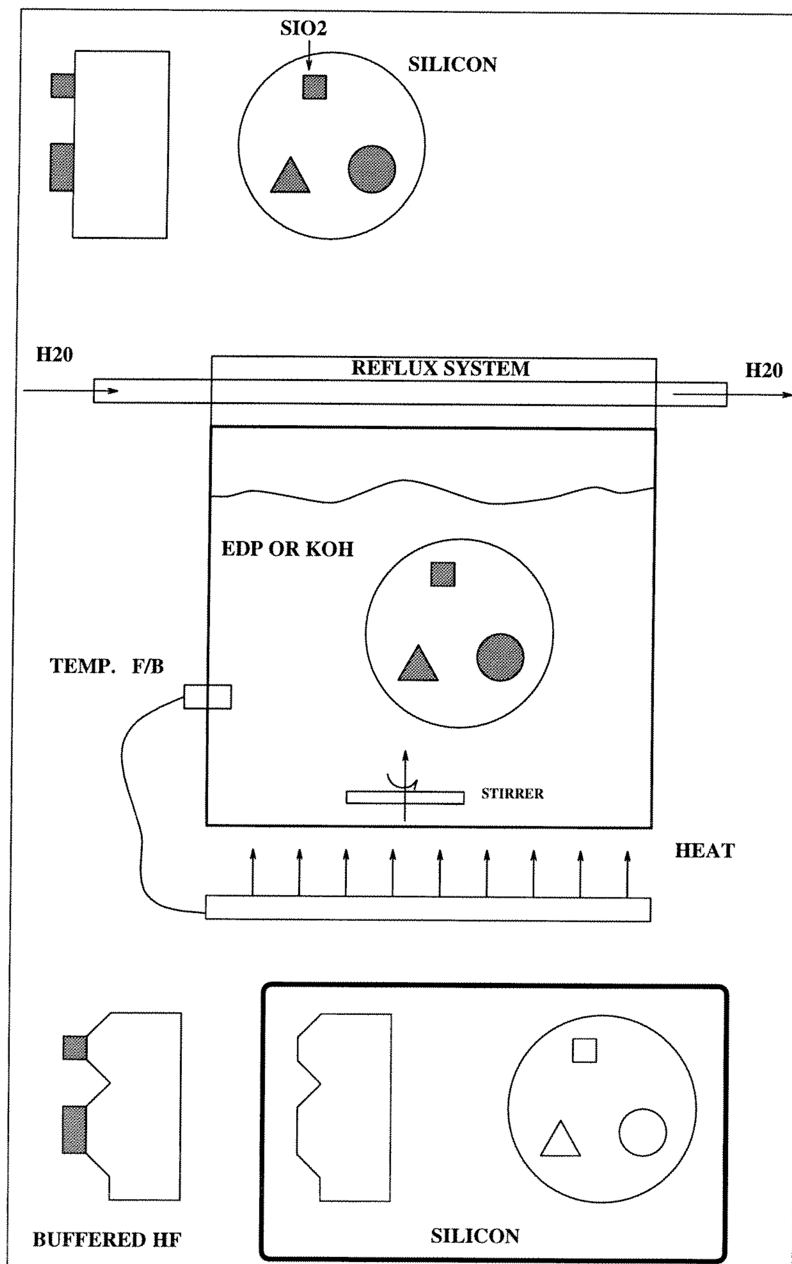

Figure 2-3: Wafer etching.

of both. A suitable mask which is resistant to etching must be chosen. By varying the gases in the etching chamber, both the etching characteristics and the mask selectivity can be changed. Dry etching advantages include high resolution (micron range) and wide variety of possible etching characteristics. Disadvantages include depths typically 25 microns or less (limited by masking material), loading effects (etch rate depends on amount of silicon etched), and changing side wall profile.

Surface micro machining

Surface micro machining [59, 76, 75, 73, 23] uses many masking layers to form thin structures on the surface of the wafer. Below each masking layer materials such as PSG (phospho-silicate glass) are used as sacrificial layers. After a masking layer has been patterned the underlying sacrificial layer may be removed. The resulting structures may be multi-layer and may be attached to the wafer or free to move. Surface micro machining has very high resolution (sub-micron is possible) but the output shapes are very thin (typically microns).

Laser micro machining

Laser micro machining [3, 4, 11, 10, 13, 54, 83] uses a laser to locally change the etching environment. Dry or wet etching may be used. The increased local etching may be due to photo-chemistry, higher local temperature, or a combination of both. Alternatively, local deposition can be performed in place of local etching. Laser micro machining can produce very complex shapes but it is a serial rather than parallel process so only one part at a time may be machined. This increases the price per part and decreases the throughput.

LIGA

LIGA (a German acronym) [32, 31, 33, 51, 84] uses an x-ray source to irradiate a radiation sensitive polymer. That polymer is then developed and a mold is formed. The mold is then used to make metal parts. The process is extremely accurate (sub-micron) and produces high aspect ratio structures (hundreds of microns deep) with vertical walls. Unfortunately, the required x-ray source makes LIGA very expensive, and limits the throughput.

2.2 Crystals and Shapes

In this section the effect of the crystal structure of silicon on the final output shapes will be discussed.

2.2.1 Why use silicon?

The vast majority of micro-machining uses silicon as a construction material. Silicon has several advantages: it is the basis of the semiconductor industry and as such has over thirty years of research into its production and use making it one of the best characterized materials. Silicon has the added advantage that its oxide is a good electrical insulator, is easily grown, and is lattice matched which makes for low stress. Also, surplus micro electronic equipment is usually sufficient for MEMS requirements and can be obtained inexpensively.

Silicon is one of the commonest elements (sand consists mostly of silicon dioxide) and huge quantities (Mkg/year) are produced so that the price is relatively low. It is one of the purest materials produced in bulk, almost free of defects (parts per billion purities) and has excellent mechanical properties including high strength and low density (see Table 2.1). Silicon will allow integration of micro mechanics and micro electronics. Unfortunately, silicon is a brittle material and will break rather than bend. In some applications this is desirable (for example a damaged part is obviously damaged and easy to separate from functioning parts so that no hidden defects arise), but generally more pliable materials such as steel are easier to use as mechanical design materials. This may be partly due to to the fact that much of the acquired design knowledge is concerned with non-brittle materials and brittle design is less well understood.

Many of the mechanical properties of silicon, such as Young's Modulus, are anisotropic and can vary by as much as a factor of two in different orientations.

Finally it is important to note that this work is not strictly limited to silicon but rather is applicable to any material. Non-crystalline materials may also be considered if a good characterization of the etching rates versus orientation is known. In many cases, non-crystalline materials have isotropic properties since all directions are equivalent.

Property	Steel	Aluminum	Silicon
Density (kg/l)	7.8	2.8	2.3
Young's Mod. (GPa)	200	70	130-200
Yield stress (GPa)	.2-1	.2-.5	2-7
Coeff. of Expansion ($/^{\circ}C * 10^{-6}$)	12	23	2.3-3.5
Hardness (kg/mm^2)	500	130	850

Table 2.1: Typical values for mechanical properties.

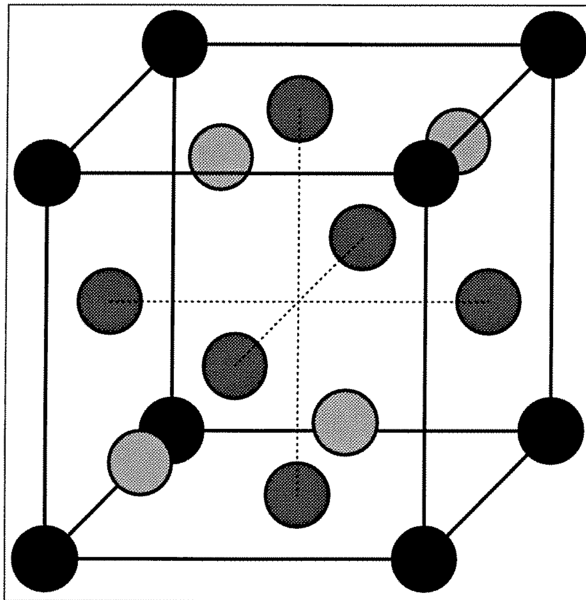

Figure 2-4: Silicon basis cell.

2.2.2 Crystal planes

Silicon has a diamond crystal structure which has atoms located at (0,0,0), (1/2,1/2,0), (1/2,0,1/2), (0,1/2,1/2), (1/4,1/4,1/4), and (3/4,3/4,3/4) (see Figure 2-4).

Crystallographic planes are characterized by their Miller indices (h,k,l) which are the inverses of the (x,y,z) intercepts for the planes. For example the (100) plane intersects the x axis but not the y or z axes. In MEMS etching, some planes appear more often than others. The most common planes in MEMS are the (111), (110), (100), and (311) planes. As different planes are cut, different atom densities are encountered as shown in Figure 2-5. Because of this, when silicon is etched, different planes are etched at different rates. In

general terms, the most dense planes are etched the slowest; the (111) planes are the most dense of all the planes. While each particular etchant has its own etch rate behavior, for many etchants the (311) planes are the fastest with the (100) and (111) planes somewhat slower. In addition to the density, another important factor is the symmetry. In general, the observed etch rate diagrams and the output etched shapes tend to have the same symmetry as the crystal structure of the wafer plane. For example (100) wafers tend to produce shapes with four-fold symmetry while (110) wafers tend to favor six-fold symmetry.

The actual etch rate behavior will depend on both the crystalline nature of silicon and on the particular etchant used. There are complicated chemical reactions involving the etchant and any two etchants can have very different etch rate behaviors. The crystal planes give the general behavior of etched silicon; further information can be obtained from experimental measurements.

The wafer itself can be cut along different planes and the experimental results show a two dimensional projection of the full three dimensional etch rate behavior onto the wafer plane. Cutting along different planes can produce very different results with different symmetry. Figure 2-6 shows an empirical fit to some etch rate data obtained for etchants such as KOH and EDP for the (100) plane. Both the experimental method used to obtain these results and some theoretical models will be discussed later.

2.2.3 Corner and shape classifications

There are two main classifications that describe how the two dimensional initial mask shape will evolve into the three diemsnional final etched shape:

Firstly, etched shapes may be classified as either pegs or holes. Holes are lower than the surface of the wafer and pegs are higher than the wafer (see Figure 2-7). Holes enlarge with time while pegs shrink. After long times, holes are dominated by slow planes, while pegs become dominated by fast planes.

Secondly, within a shape (be it a peg or a hole), there can be two types of corners in two dimensions: convex and concave (see Figure 2-8). The behavior of the two types of corners is very different. A square hole has four concave corners, a triangular peg has three convex corners, a general shape may have both convex and concave corners. For example, the hole

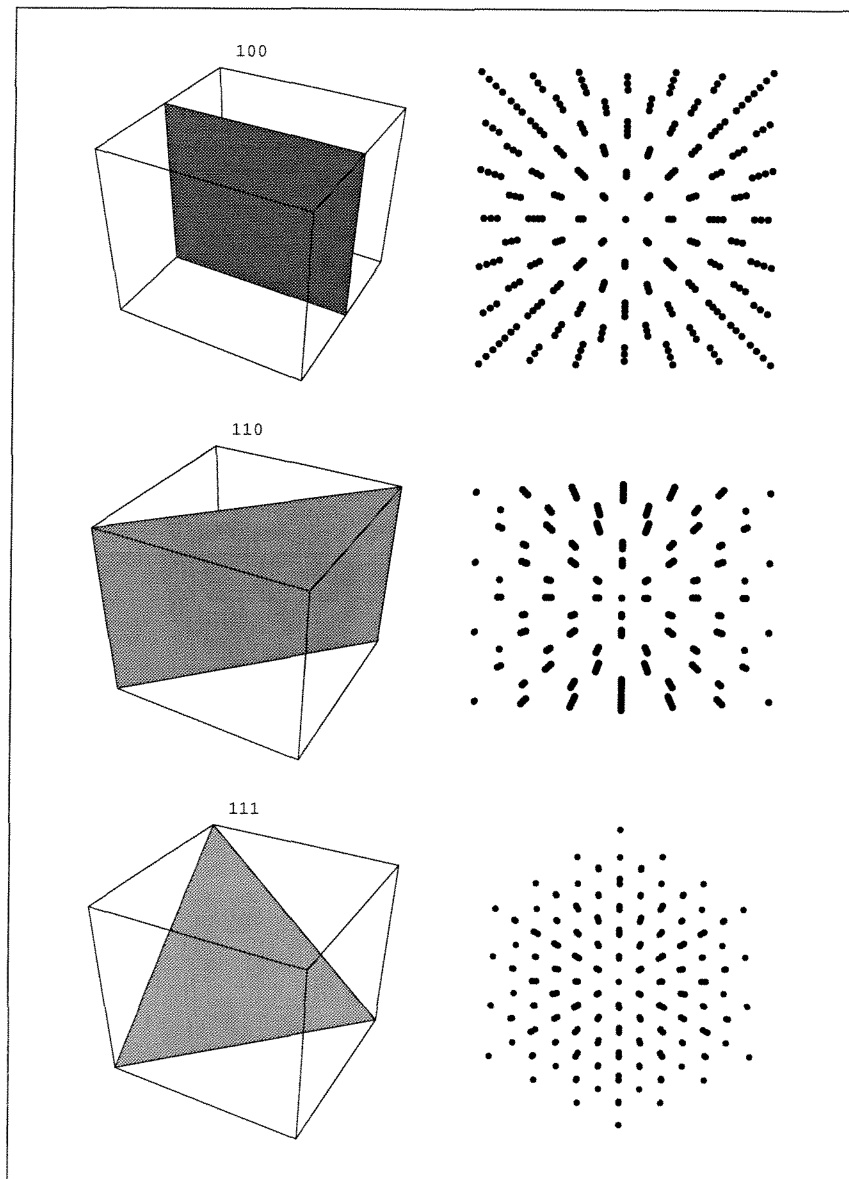

Figure 2-5: Silicon plane densities and symmetries.

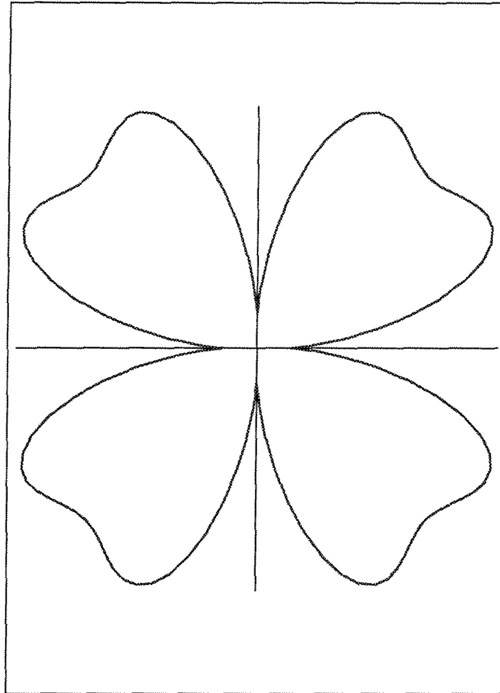

Figure 2-6: Qualitative (100) wafer etch rate diagram. The x axis is parallel to the wafer flat.

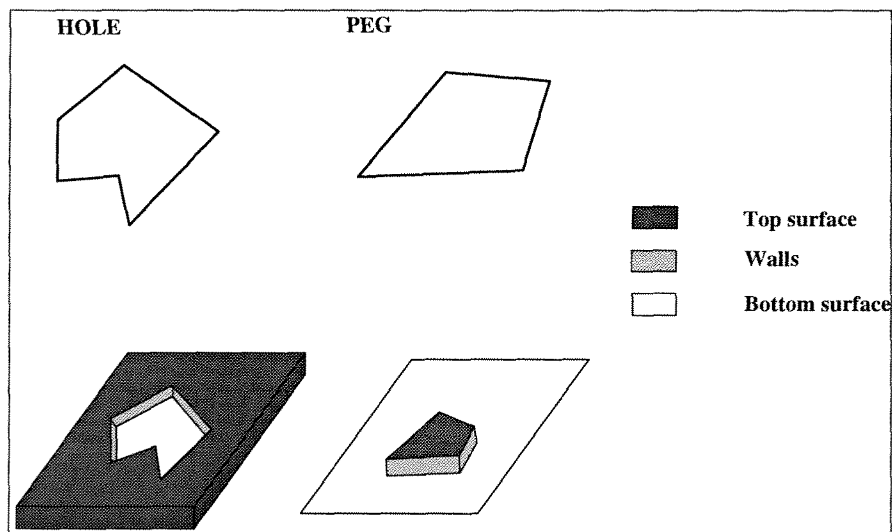

Figure 2-7: Definition of pegs and holes.

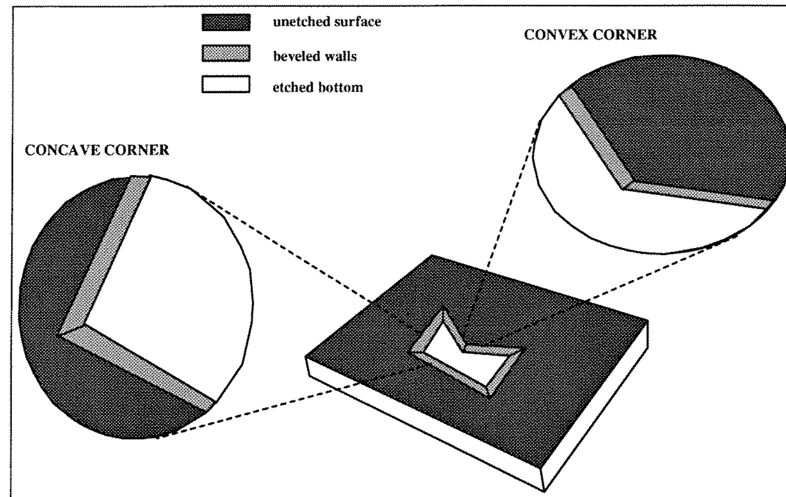

Figure 2-8: Definition of convex and concave corners. The unetched mask is dark, the etched bottom is light, and the beveled walls are grey.

in Figure 2-7 has five concave corners and one convex corner; the peg in Figure 2-7 has four convex corners. The inside of a corner is taken to mean the region defined by an angle smaller than 180 degrees. For a convex corner, the inside is unetched, while the inside of a concave corner is etched. While etching convex corners fast planes dominate: fast planes increase in length while slow planes decrease in length. For concave corners, slow planes dominate. The subjects of holes/pegs and convex/concave corners will reappear throughout this work.

2.2.4 Spoke patterns

There are a number of ways to experimentally determine the etch rate as a function of orientation. One method is to etch many long rectangular holes, with each hole at a slightly different angle. Then the small undercut along the long axis of the holes is measured with a microscope. This must be done for each hole. Long holes are required since the holes change shape with time and the corners of the holes are distorted. This method can produce accurate etch rate diagrams, but is time consuming since all the holes must be measured individually and a microscope is required.

Another, slightly less accurate method is to etch a spoke pattern of pegs. This method

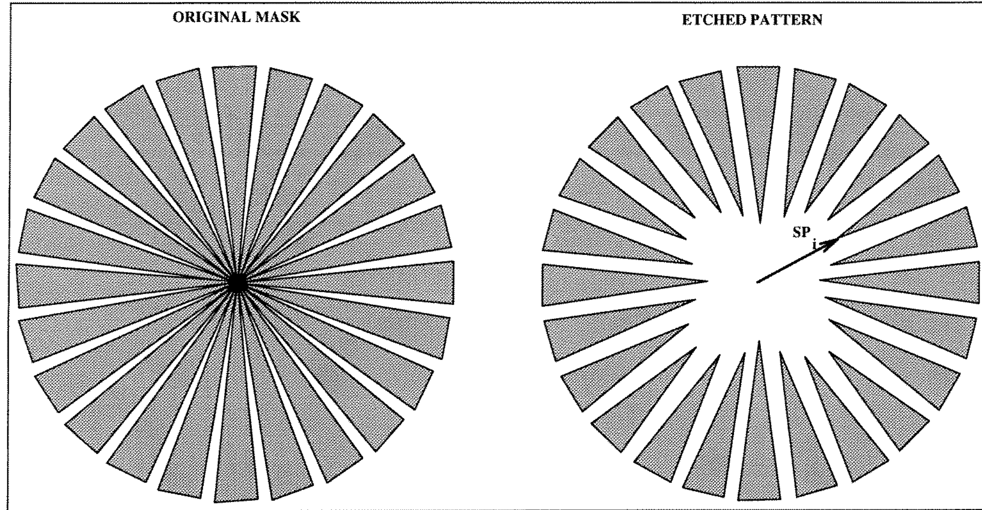

Figure 2-9: Spoke pattern geometry.

produces a macroscopic copy of the etch rate diagram which can be directly viewed or photographed. Seidel [65], for example has studied the etch rate behavior of KOH in both the (100) and (110) planes. The method works because the long thin wedges that make up the spokes retain their sharp endpoints and only the outer ends distort. This is true because the planes that make up the sides of the wedges are geometrically magnified while any new distorting planes are not.

Consider a spoke pattern consisting of a set of N radial thin triangular wedges (pegs) as shown in Figures 2-9 and 2-10. As each individual wedge etches, two things occur: the outer end of the wedge distorts slightly while the sharp inner end moves outwards. The outward motion of the sharp ends is primarily radial, at a rate proportional to the average of the two rates which make up the wedge sidewalls. These two rates are slightly different since the wedge has finite angular width.

In addition there is also a small lateral motion proportional to the difference between the two side rates, this motion is proportional to $1/N$ and is neglected for large N. Let the new radial position of the inner ends be a set of N points SP_i , then

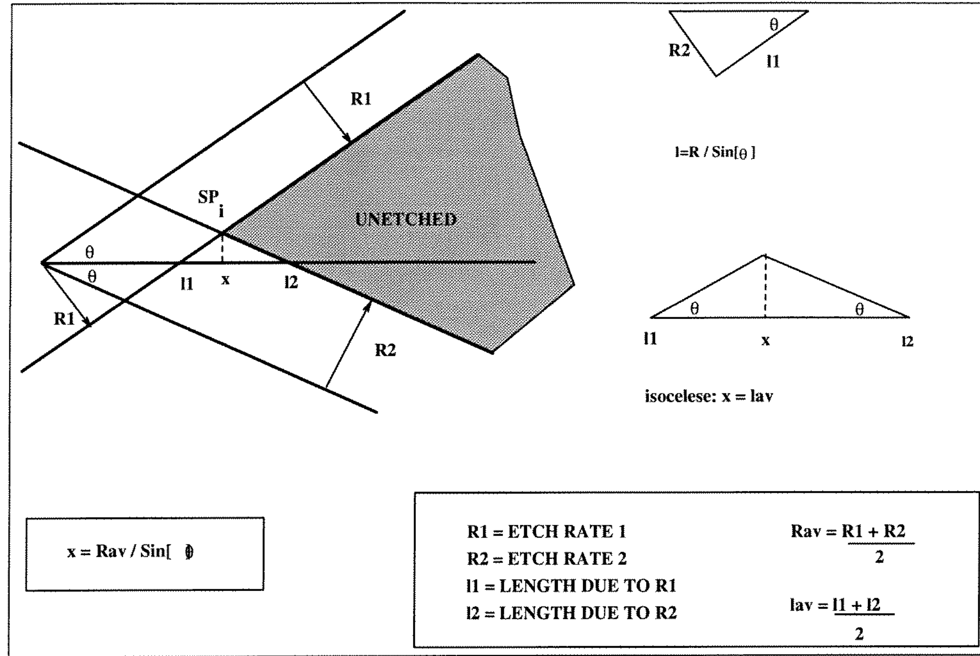

Figure 2-10: Spoke tip geometry.

$$SP_i = \frac{time}{\sin\frac{\pi}{2N}} * \frac{1}{2} * \left[R\left(\theta_i + \frac{\pi}{2} * (1 + \frac{1}{N})\right) + R\left(\theta_i - \frac{\pi}{2} * (1 + \frac{1}{N})\right)\right] \tag{2.1}$$

If N is large, the following approximation is valid:

$$SP_i = \frac{N time}{\pi} * \left[R\left(\theta_i + \frac{\pi}{2}\right) + R\left(\theta_i - \frac{\pi}{2}\right)\right] \tag{2.2}$$

Note that the position at an angle depends on the rate at the angle perpendicular to the wedge. The spoke pattern actually averages the etch rate diagram rotated clockwise 90 degrees with the etch rate diagram rotated counterclockwise 90 degrees. In addition the etch rate is geometrically magnified by the number of spokes, which allows a macroscopic output. The magnification is linear in N for large N.

For 2-fold symmetrical etch rates, rates at $\theta + \pi$ are equal to the rates at θ, thus

$$SP_i = \frac{2N time}{\pi} * \left[R\left(\theta_i + \frac{\pi}{2}\right)\right] \tag{2.3}$$

For 4-fold symmetrical etch rates (rates at θ, $\theta + \pi/2$, $\theta + \pi$, and $\theta + 3\pi/2$ are all equal) the rotation effect disappears:

$$SP_i = \frac{2N time}{\pi} * [R(\theta_i)] \tag{2.4}$$

Some etchants do not have 2-fold symmetry, and thus spoke patterns do not accurately model these systems.

Consider a 4-fold symmetric system (for example a (100) wafer): if N is not large the net effect is to blur the etch rate diagram by averaging over the width of the wedge:

$$SP_i = \frac{2N time}{\pi} * \left[R_{av}\left(\theta_i \pm \frac{\pi}{2N}\right)\right] \tag{2.5}$$

Figure 2-11 shows an etched spoke pattern for EDP.

The spoke method is also susceptible to lithography errors since all wedges converge at the origin and the pattern has some minimum feature size. The effect of lithography errors is to delay the etching time for some of the wedges, introducing error in the results. The error is diminished by using larger patterns so that the time error is smaller in proportion to the total etching time.

2.3 Shape Transformations

2.3.1 Examples of shape transformations

The fundamental process we will examine is the transformation from one shape to another. Such changes occur at all length scales, a few macro scale examples are listed below. These different examples all share the same mathematics.

- Painting:

  Consider a two dimensional curve defining the path of a paint brush. As the paint brush is swept along this curve the initial path is mapped to two output curves, an

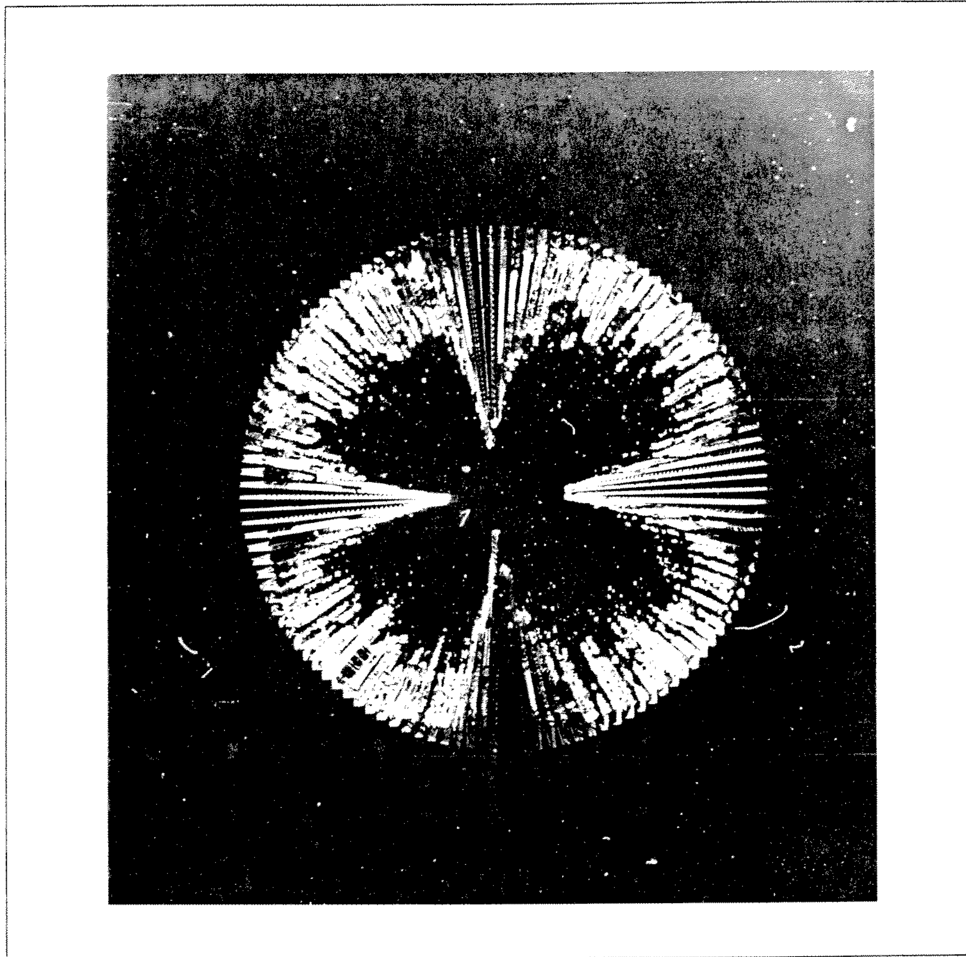

Figure 2-11: Experimental spoke patterns for (100) wafer in EDP.

inner and an outer path. (see Figure 2-12). By changing the shape of the brush we can model anisotropic transformations [28]. Note that some corners are rounded and others are sharp. This dichotomy of corner behavior is a fundamental part of shape transformation.

- Fonts:

  If the painting path is the outline of a letter, typographic fonts may be developed with a compact representation. By parametrically defining a brush which changes along the path, a wide variety of fonts may be generated [28].

- Milling:

  The ideal cutting path of a milling machine is enlarged by the finite size of the milling cutter. The output shapes are called offset surfaces. Offsets surfaces are difficult to calculate (because they often contain cusps) and are the subject of much research [24, 35, 78]. They are commercially important because NC (numerically controlled) milling machines must be able to predict the result of particular milling actions.

- Robotic Path Planning:

  Consider a circular two-dimensional robot in an obstacle filled room. Path planing algorithms attempt to move the robot from one location to another. If the obstacles are painted with a brush the same size and shape as the robot, the robot may be replaced with a point and the path planing done on this new system [29]. This method is valid for non-circular robots as long as rotation is not permitted.

- Profilers:

  One way to measure the surface profile of a sample is to drag a stylus across the sample (see Figure 2-12). One of the limitations of such a system is that the measurable height changes are limited by the shape of the stylus. In fact the output is a convolution of the actual shape and the stylus shape. This is a serious limitation at smaller scales.

- Optics:

  In most materials, the propagation of light is isotropic; a circular wave front remains circular. Birefringent materials have indices of refraction that depend on orientation.

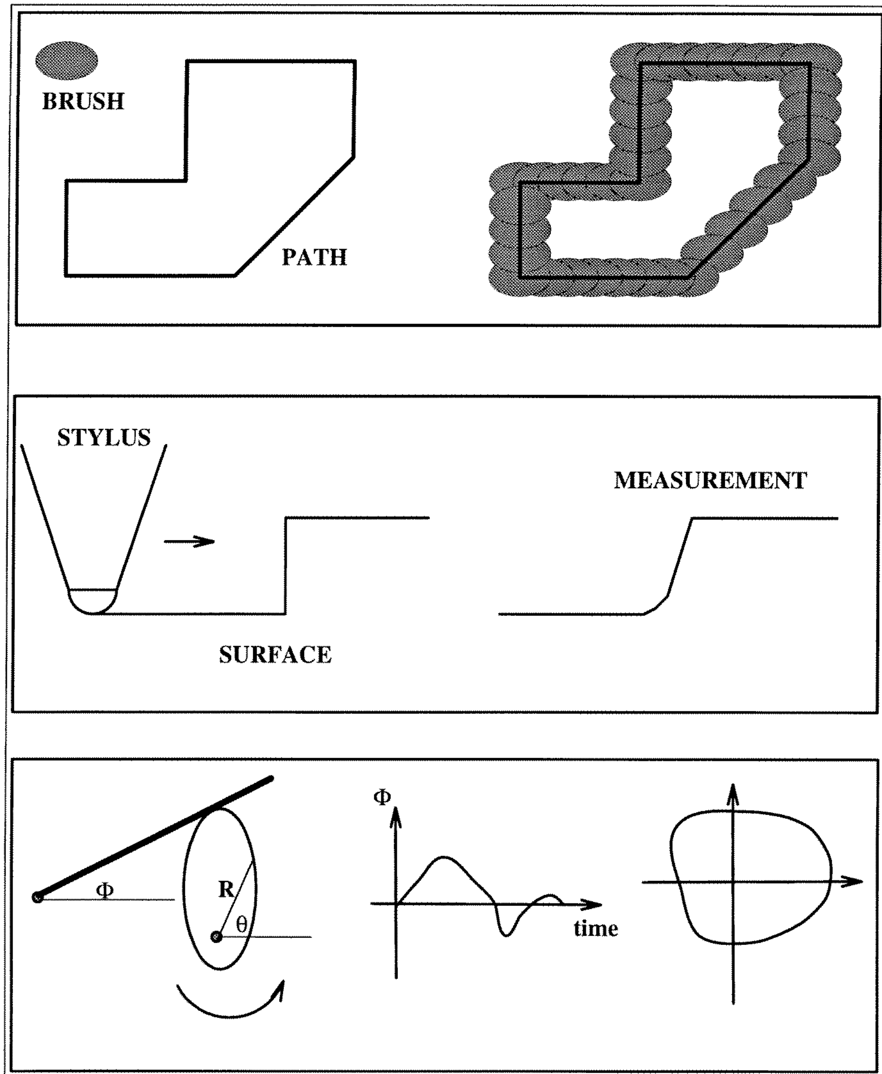

Figure 2-12: Shape transformation examples: (A) painting, (B) profilers, (C) cams.

The evolution of the wave front is anisotropic in this case and the wave front changes shape.

- Cams:

  When a rocker arm is in tangential contact with a cam the output motion of the arm depends on the shape of the cam [47] (see Figure 2-12). If the cam is defined by $R(\theta)$ and rotates at an angular rate ω, then the output as a function of time is Φ. This output can be expressed in Cartesian coordinates (Φ vs. time) or polar coordinates (radius: Φ, angle: time). In polar coordinates the motion of the cam is the transformation of the shape defined by $R(\theta)$ to a new shape $\Phi(time)$.

2.3.2 Minkowski transforms

Minkowski transformations [28, 29, 30] are a mathematical method of modeling shape transformations, some examples of which were given above. Minkowski algebra allows us to add two shapes represented by a list of vectors from one vertex of a polygon to the next vertex. If the polygons are both convex, then the Minkowski addition of two polygons is found by combining the two vector lists and slope sorting them (see Figure 2-13). Slope sorting means that the combined list of vectors is rearranged so that the vectors with the smallest slopes (with respect to the x axis) are the first vectors in the sorted list. The asterisks in Figure 2-13 represent the slope angles of individual vectors.

When one shape is nonconvex then the algorithm is more involved. Between two consecutive vertices of the nonconvex polygon perform the following steps:
i) if the rotation from one vertex to the next is counterclockwise (positive angle), insert into the nonconvex list the portion of the convex vector list that is between the two nonconvex vertices (this is the same as the convex/convex case).
ii) if the rotation from one vertex to the next is clockwise (negative angle), insert into the nonconvex list the negative of the portion of the convex vector list that is between the two nonconvex vertices (see Figure 2-14). Note that the output shape is non-simple and has self intersections. The final shape in the outer perimeter of the shape with the set of intersecting regions trimmed off. The finding of such self intersections is a non-trivial part of Minkowski transformations.

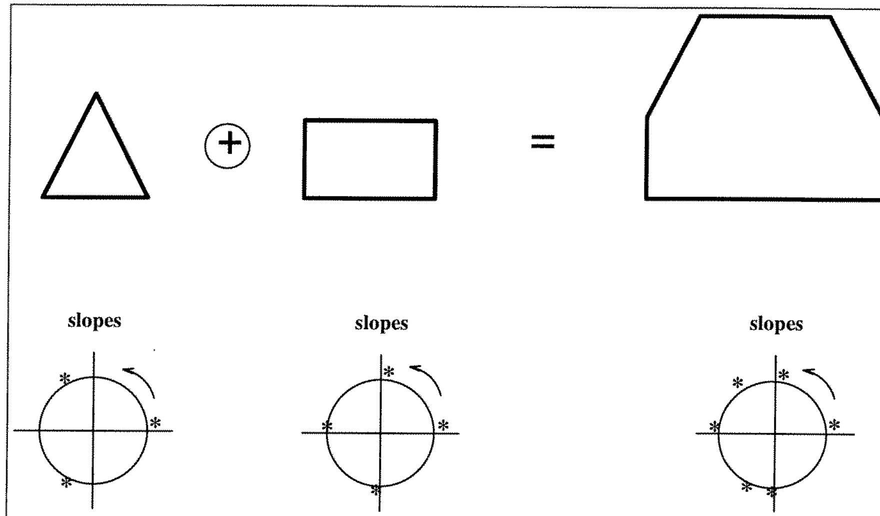

Figure 2-13: Example of Minkowski Addition (convex/convex). The slope diagrams are shown below.

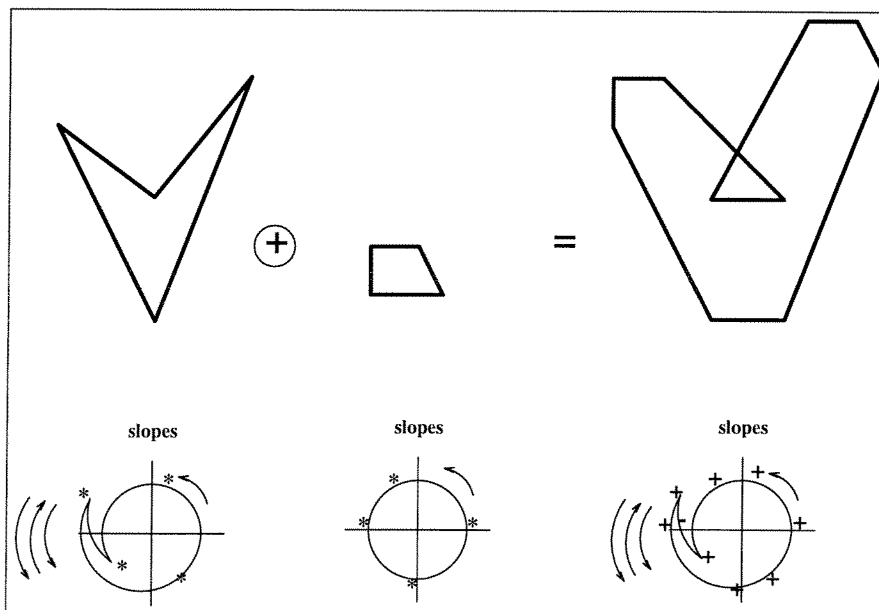

Figure 2-14: Example of Minkowski Addition (convex/nonconvex). + signs mean that the vector is used, - signs mean that the negative of the vector is used. The slope diagrams are shown at the bottom of the figure.

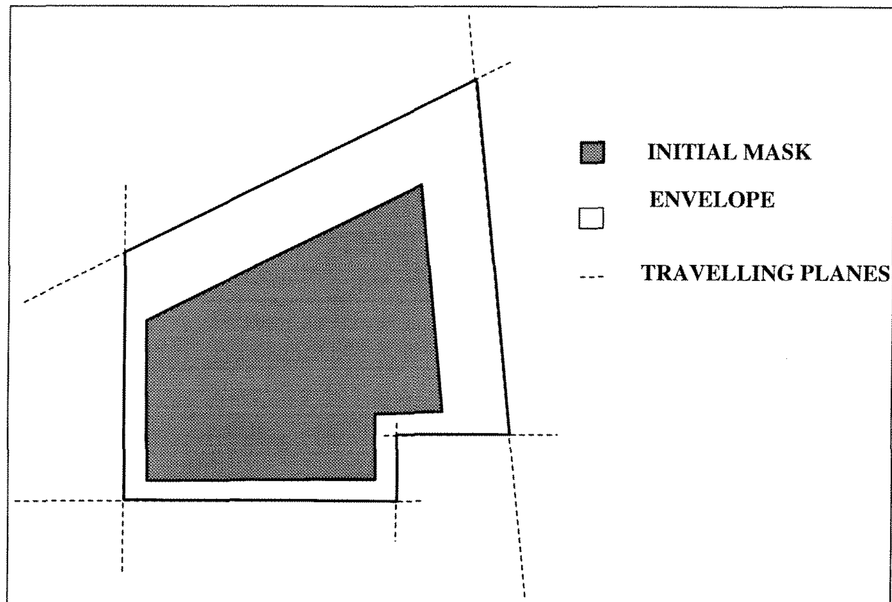

Figure 2-15: Wulff-Jaccodine method.

Minkowski subtraction is performed in the same fashion as addition but the negative of the vectors are used. Minkowski transformations will be revisited later.

2.3.3 MEMS shape modelers

There are a number of existing methods for predicting the output shapes in MEMS [16, 18, 20, 17, 21, 36, 67, 68, 77]. Two are listed below, each uses etch rate diagrams to give the etch rate as a function of orientation.

Wulff-Jaccodine

The Wulff-Jaccodine method [36, 20] uses plane waves that propagate outwards at a rate given by the etch rate diagram. At each point on the initial surface, a tangent plane is moved outward a distance equal to the appropriate rate multiplied by the time (see Figure 2-15). The final shape is the envelope of all these planes. This envelope is calculated by finding the intersections of adjacent lines. Planes may disappear and/or appear at corners and must be considered.

At corners there is a geometrical test to determine if new planes appear. Consider one

corner of a convex hole: a small intermediate plane is inserted and the evolution of this new plane is examined. As shown in Figure 2-16 fast planes soon disappear and slow planes tend to grow. For convex pegs the situation is reversed. A general shape may have both convex and concave corners. When etch rates differ greatly, only a few dominant planes appear. However as the etchant becomes more and more isotropic, more and more planes are relevant and must be considered. The major difficulty of this method is the computational cost of determining which planes appear or disappear at each time step.

Buser et al. [16] have developed a useful analysis tool called ASEP (Anisotropic Silicon Etching Program) which can predict the output shape based on traveling planes. These results have been verified experimentally. In addition the output can be linked to FEA modelers such as ANSYS. The model itself runs quickly.

However, much generality has been lost, and this approach is specialized. Only KOH silicon is being modeled in this implementation, although EDP is planned. The analysis is limited to a number of dominant plane families (111, 100, 110, 311) which tend to appear in crystal etching. In addition the permissible input masks shapes are limited: only 0, 45, 90, 135 degree etc. input walls are permitted.

Slowness

The Slowness method [27, 67] uses the inverse of the rate (the slowness) to calculate the trajectories of points or lines in the shape (see Figure 2-17). Using the slowness instead of the rate simplifies the mathematics.

The trajectory of a corner is given by a vector relation involving the slowness vectors of the two lines which form the corner. This relation states that the trajectory of the corner lies along the normal to the difference of the two line slowness vectors (see Figure 2-17). This ensures that the components of the trajectory vector in a basis defined by the normals to the corner lines are equal to the two line etch rates (see Figure 2-17). The Slowness method is equivalent to solving two simultaneous linear equations to find these two components.

In order to model appearing planes, many small lines are inserted at corners and left to evolve. The more isotropic the etchant, the more lines will be required. The trajectories of the corners are then used to determine when lines disappear; lines disappear when two

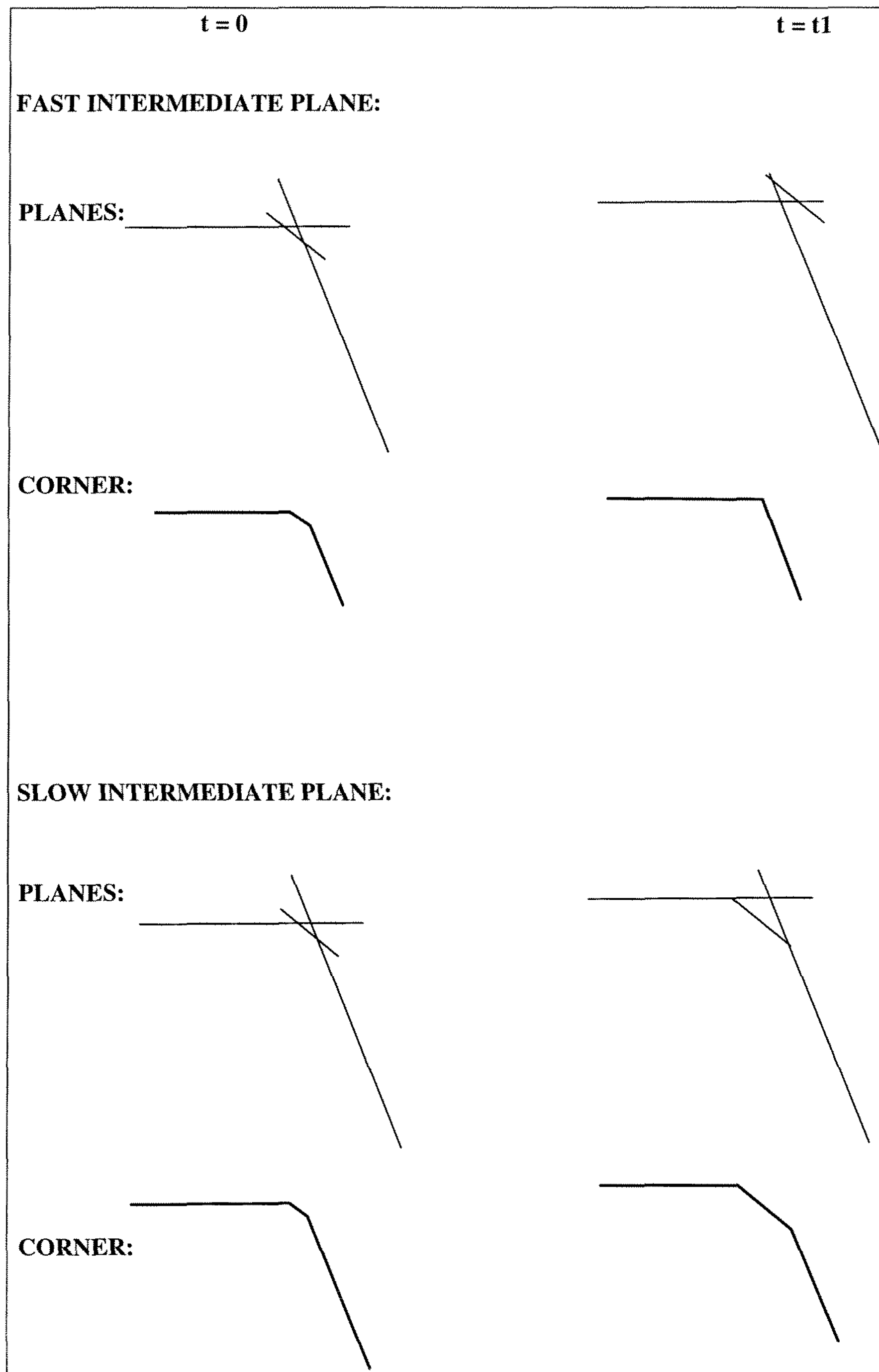

Figure 2-16: Corner evolution.

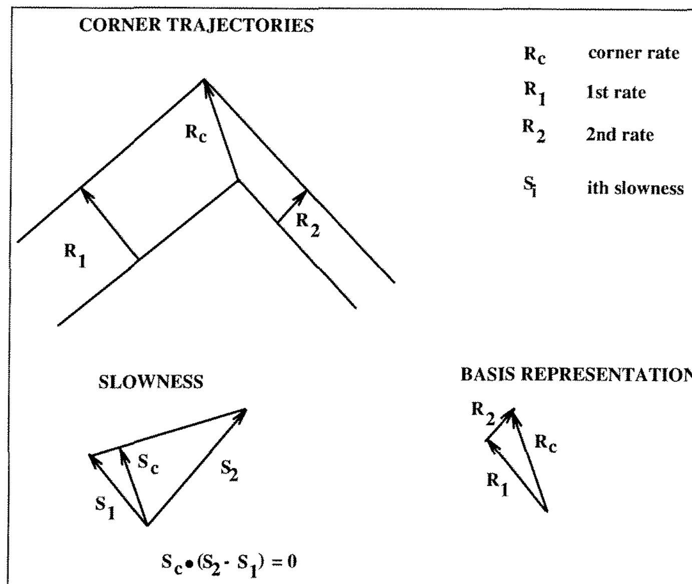

Figure 2-17: Slowness method geometry.

adjacent trajectories converge. The procedure is iterated to find the shape at any time. The method is extended to three dimensions by extending the vector relationship. The three dimensional case is more complicated because in two dimensions, a corner is always formed by two lines, while in three dimensions three or more planes may define a corner.

Sequin [67] has successfully used the Slowness method to model changing shapes, although experimental verification is not included in his publication.

Discussion

It can be shown that the two above methods are mathematically equivalent, but this does not imply complete redundancy. The two models each have their advantages; the Wulff-Jaccodine model is easy to interpret, while the Slowness method is easy to implement computationally.

These etch simulation methods have some disadvantages. The Slowness method is iterative and many time steps may be necessary, while ASEP is limited in its scope. In both methods, local calculations involving neighbors do not consider global effects. For example, when two separate shapes grow so that they intersect to form a new larger shape, all lines

in both shapes must be considered. A single complex shape may also have two parts that intersect. When such cases occur, the number of required calculations increases dramatically. Finally, both the Slowness and Wulff-Jaccodine methods cannot simply be reversed and run backward in time in order to perform design inversion. Because planes appear and disappear, such reversals do not give complete results and there is no general design framework inherent to either model.

Chapter 3

Rate Modeling

3.1 Introduction

Anisotropic etching of silicon is one common micro-machining technique. Anisotropic means, of course, that the rate of etching is dependent on the orientation of the face being etched in the crystal. These differing rates mean that most etched shapes change with time as will be discussed in considerable detail below. In order to simulate the time evolution of three dimensional etched shapes, it is essential that the full etch rates in all directions be well known. Any MEMS CAD system that will accurately be able to determine a mask shape for a given desired three dimensional fabricated shape will require well characterized and accurate three dimensional etch rate information. Similarly three dimensional etch simulators, such as the author's Eshape and Cellular Automata methods (chapters 5 and 6 respectively) as well as the Slowness method by Sequin [67] and ASEP by Buser [16] require accurate etch rate data.

Unfortunately, for most etchants etch rates for only a few major planes are known, notably the (100), (110), (111), and perhaps the (311) planes. Seidel [65], for example has studied the etch rate behavior of KOH in both the (100) and (110) planes. The (100) plane etch rate diagram has a characteristic four lobed rosette pattern while the (110) plane etch rate diagram is six-sided. These planes are chosen because they tend to dominate most etched shapes, but they do not give the full picture. In this chapter we will derive a model which supplies the full etch rate diagram given a few experimentally measured planes. The model requires a minimum of N planes to provide a N dimensional representation,

but more planes may be utilized if they are available, providing a more accurate etch rate diagram. The model will first be derived for two dimensions with two parameters, then with three parameters. The same approach will be used for the three dimensional models with three and four parameters. The models show excellent agreement with both experimental measurements and values reported in the literature.

3.2 Two Dimensions

We represent etch rates with vectors where, in polar coordinates θ is a given etch direction and $R(\theta)$ is the rate for the θ direction. Of course, this $\{R, \theta\}$ vector can also be represented by Cartesian coordinates: $\{x, y\}$. Because of silicon's symmetry, we need only examine 1/8th of the circle: $0 \leq \theta \leq \pi/4$ (or $0 \leq x \leq 1$ and $0 \leq y \leq x$). For example the (10),($\bar{1}$0), and (01) vectors have the same rate since they belong to the (10) family. This use of symmetry simplifies the derivation, but the model is in no way limited to symmetrical systems. For asymmetrical systems all regions of the plane must be modeled.

3.2.1 Two Parameters

In two dimensions, two independent vectors are needed to define a basis. In the two-parameter model there are two distinct rate vectors, the (10) vector at zero degrees and the (11) vector at 45 degrees. These vectors shall be called the principal vectors or principal rates.

These two dimensional rate vectors are the two dimensional projections of the three dimensional etch rates for different planes. The (11) vector is the projection of the (111) plane while the (10) vector is the projection of either the (100) or the (101) plane depending on the etchant being modeled.

In order to interpolate the etch rate of any arbitrary vector we wish to find its components not in terms of its Cartesian components but rather in terms of its (10) and (11) components. In other words we wish to transform from a representation in Cartesian space into a representation in the non-orthogonal basis of the two linearly independent principal rate vectors. We do this by multiplying the $\{x, y\}$ vector by the inverse of the basis matrix

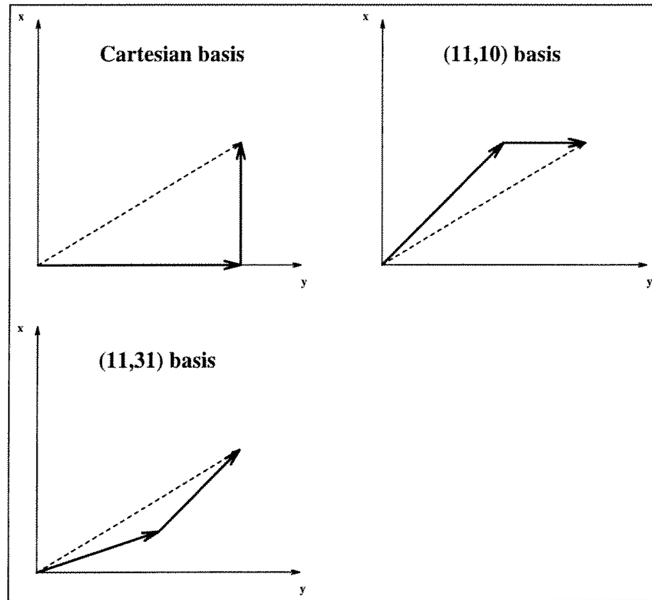

Figure 3-1: Two dimensional basis representations.

defined by the principal vectors. This is equivalent to solving two simultaneous equations to determine what magnitudes of the (10) and (11) vectors are required to construct an arbitrary vector (see Figure 3-1).

In addition we must satisfy the additional condition that the interpolated rates be isotropic when the (10) and (11) rates are unity. This is done with a diagonal scaling matrix which simply multiplies the result by two scaling constants. In the two dimensional two parameter model the scaling matrix is the identity matrix but this is not true in general. If this scaling matrix is not included the model is still valid but the model etch rates will differ from the experimental etch rates. The need for the scaling matrix arises because when the Miller indices are calculated, the numbers are scaled to be integers. The scaling matrix undoes this Miller scaling.

Every vector has a representation in the orthogonal Cartesian basis $\{x, y\}$. Let $\{a, b\}$ be the components of a vector $\{x, y\}$ in the non-orthogonal basis defined by the normals (Miller indices $\{h, k\}$) of two principal planes. Then:

basis vectors	*scaling matrix*	*component equations*	*normalization*
$\begin{bmatrix} 1 & 0 \\ 1 & 1 \end{bmatrix}$	$\begin{bmatrix} 1 & 0 \\ 0 & 1 \end{bmatrix}$	$a = x - y$ $b = y$	$1/x$

Table 3.1: 2D, two parameter model matrices and equations.

$$\begin{bmatrix} a & b \end{bmatrix} = \begin{bmatrix} x & y \end{bmatrix} \begin{bmatrix} h_1 & k_1 \\ h_2 & k_2 \end{bmatrix}^{-1} \begin{bmatrix} s_1 & 0 \\ 0 & s_2 \end{bmatrix} \tag{3.1}$$

where s is the scaling matrix. This relationship is valid within the triangular region defined by the two principal planes.

The etch rate along a vector $\{x, y\}$ is then given by a weighted sum of these components. By choosing the weights (W_i) to be the ratio of the ith rate to the (11) rate , it is possible to separate the shape of the etch rate diagram (ratio of rates) from the absolute size of the etch rate diagram ((11) rate). Thus $W_1 = 1$ and $W_2 = R_{(10)}/R_{(11)}$:

$$R(x, y) = N(a * W_1 + b * W_2) * R_{11} \tag{3.2}$$

where N is a normalization factor ($1/x$ in this case). N is necessary since R should be dependent on angle (ratios of x and y) and not on the magnitudes of x and y. This formula is valid for all possible symmetric etchants: isotropic or highly anisotropic. Table 3.1 displays the details of this model. Note that the equations are only valid when a and b are positive, since the weights cannot be negative.

Compared to other planes, the (111) planes are relatively dense. For many etchants they are the slowest etching planes. The ratio of the fastest to slowest planes ranges from 1:1 for the isotropic case to 400:1 for etchants such as KOH. For this reason it is not necessary to plot the etch rate diagrams for the cases where the ratio of (10) to (11) is less than unity, although the model would still be valid if small ratio etchants were available. Figure 3-2 shows an array of hypothetical ratios of the (10) etch rate to the (11) etch rate. Each

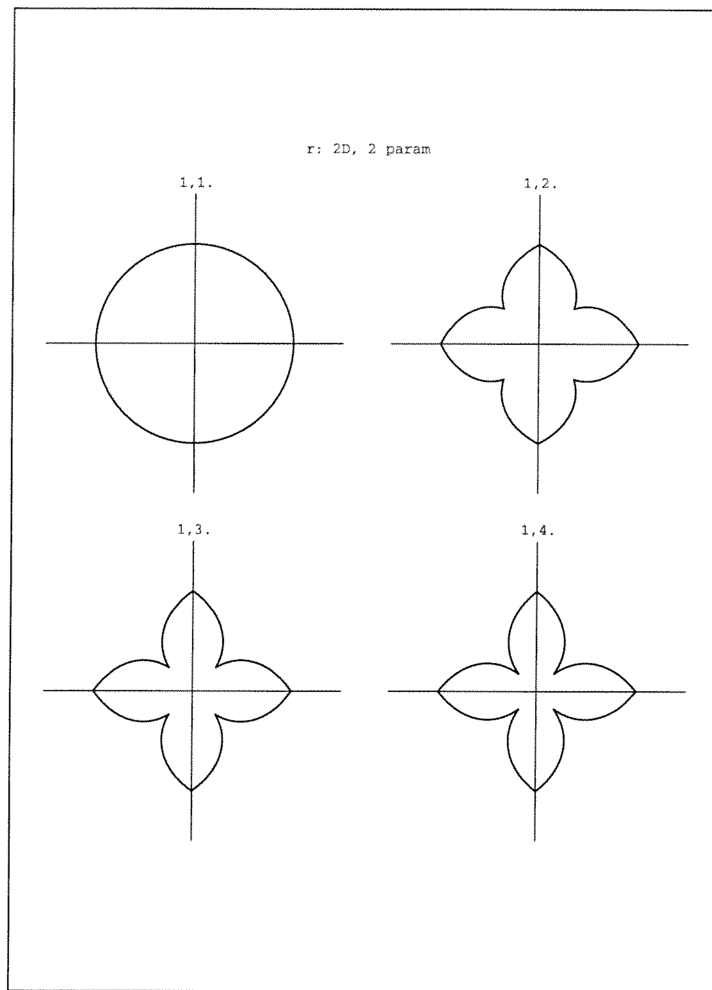

Figure 3-2: 2D, two parameter results.

element in the array has been scaled to fill an equal amount of space for display purposes. This has been done for all the arrays that follow.

Three Parameters

The effect of the (311) planes can be included by using a three parameter model. Again only the region $0 \leq \theta \leq \pi/4$ is considered, but there are now three principal rates (10), (11), and (31) where the (31) vector is the two dimensional projection of the (311) plane. The (10) and (11) rates appear in hole type shapes since they are slow compared to faster planes such as the (31) rates. Failure to include (31) rates will lead to peg type shapes that are correct

basis vectors	*scaling matrix*	*component equations*	*normalization*
$\begin{bmatrix} 1 & 0 \\ 3 & 1 \end{bmatrix}$	$\begin{bmatrix} 1 & 0 \\ 0 & 3 \end{bmatrix}$	$a = x - 3y$ $b = 3y$	$1/x$
$\begin{bmatrix} 1 & 1 \\ 3 & 1 \end{bmatrix}$	$\begin{bmatrix} 1 & 0 \\ 0 & 3 \end{bmatrix}$	$a = (-x + 3y)/2$ $b = 3/2(x - y)$	$1/x$

Table 3.2: 2D, three parameter model matrices and equations.

in form but incorrect in detail; the three parameter model eliminates this deficiency. The (31) vector lies at about 18 degrees (arctan(1/3)) with respect to the x axis. Because only two vectors at a time may be used as a two dimensional basis, two regions are examined: $0 \leq \theta \leq \arctan(1/3)$ with (10) and (31) as the basis and $\arctan(1/3) \leq \theta \leq \pi/4$ with (31) and (11) as the basis. The derivation for the two parameter model is carried out again for the two regions producing two separate weighted sums each valid within its associated region. In this case the scaling matrix is not the identity matrix but contains a 1 and a 3 along the diagonal. In general, the scaling matrix diagonal value is the maximum cartesian component of the associated plane. Note that the rates are continuous across the region interface. The net effect of the (31) rates is to produce secondary extrema. The results are rearranged to separate the size and shape effects as was done with the two parameter model. Furthermore by using the two parameter model we can find the default value for the (31)/(11) rate ratio required to collapse the three parameter model to two parameters:

default $R_{31}/R_{11} = (1 + 2 * R_{10}/R_{11})/3$

Rearranging, we obtain a weighted sum in terms of R_{10}/R_{11}, the R_{31}/R_{11} default rate ratio, and the scaling factor by which the default is multiplied. Table 3.2 displays the details of this model. Note that the equations are only valid when a and b are positive, since the weights cannot be negative.

Again the availability of etchants is used to limit the R_{10}/R_{11} rates and the scaling factor to be larger than or equal to unity. Figure 3-3 shows such plots.

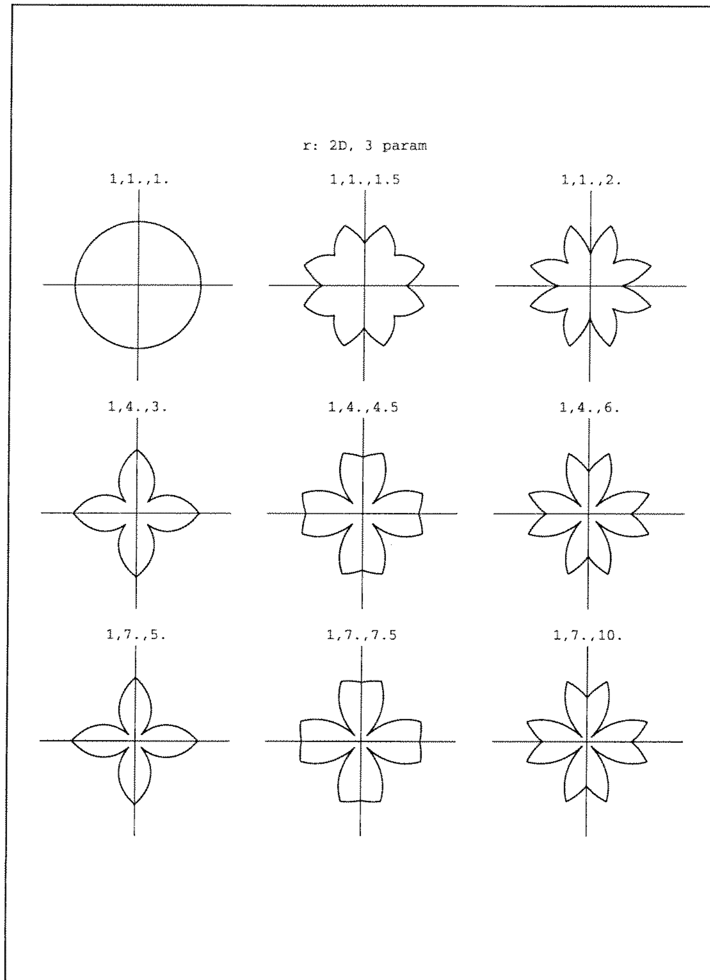

Figure 3-3: 2D, three parameter results.

3.2.2 Three Dimensions

Consider a vector in space defined by its cartesian components x , y, and z or in spherical coordinates R, θ, and ϕ. The magnitude of the vector is the three dimensional etch rate in the direction of the vector. Because of silicon's symmetry, we need only look at 1/16th of the sphere: $0 \leq \theta \leq \pi/4$ and $0 \leq \phi \leq \pi/2$ (or $0 \leq x \leq 1, 0 \leq y \leq x, 0 \leq z \leq 1$) .

Three Parameters

In three dimensions, three independent vectors are needed to define a basis. The three principal vectors for the three parameter model are the (111), (100), and (110) rates. In this section of the sphere there are 5 principal planes in 3 families: (100) family: (100) and (001) (110) family: (110) and (101) (111) family: (111) From symmetry, all planes within a family have the same rate. The five planes form three triangular regions on the sphere each bounded by three basis vectors: (100,111,110), (100,111,101), & (001,111,101) as is shown in Figure 3-4.

For each triangular section, the representation of any arbitrary vector is found in the non-orthogonal basis by multiplying the vectors cartesian components by the inverse of the 3 by 3 basis matrix. Again a scaling matrix is necessary. This is equivalent to solving three simultaneous equations to determine the magnitudes of the (100),(110), and (111) vectors required to construct an arbitrary vector. The required rate is a weighted sum of the components expressed in terms of etch rate ratios.

Every vector has a representation in a orthogonal Cartesian basis $\{x, y, z\}$. Let $\{a, b, c\}$ be the components of a vector $\{x, y, z\}$ in the non-orthogonal basis defined by the normals (Miller indices $\{h, k, l\}$) of three principal planes. Then:

$$\begin{bmatrix} a & b & c \end{bmatrix} = \begin{bmatrix} x & y & z \end{bmatrix} \begin{bmatrix} h_1 & k_1 & l_1 \\ h_2 & k_2 & l_2 \\ h_3 & k_3 & l_3 \end{bmatrix}^{-1} \begin{bmatrix} s_1 & 0 & 0 \\ 0 & s_2 & 0 \\ 0 & 0 & s_3 \end{bmatrix} \tag{3.3}$$

This relationship is valid within the triangular region defined by the three principal planes. The etch rate at a vector $\{x, y, z\}$ is then given by a weighted sum of these compo-

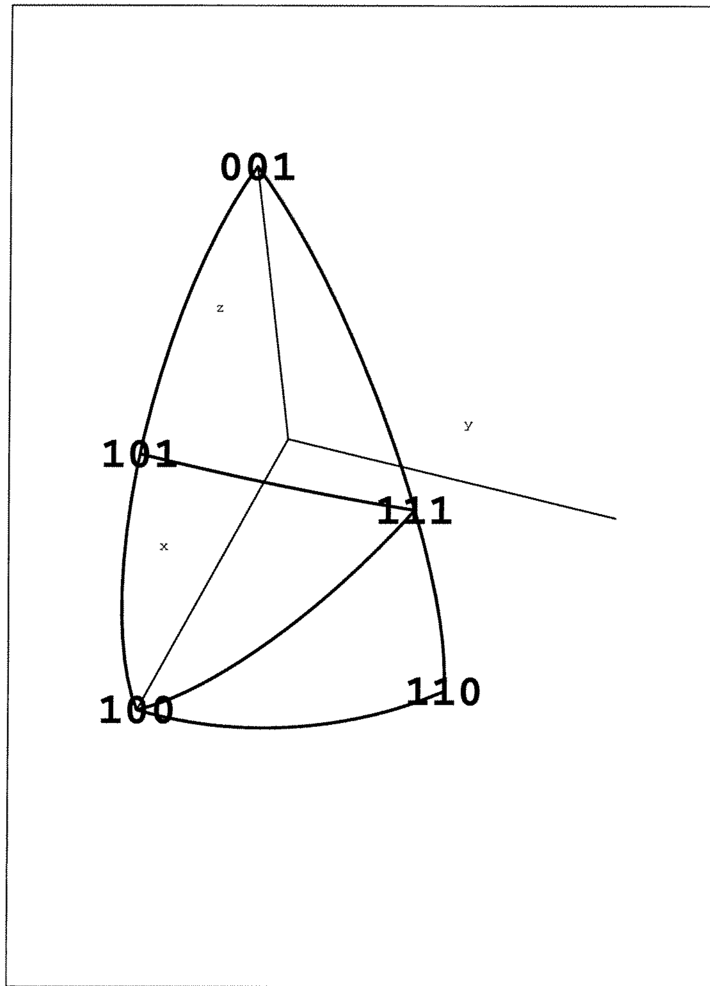

Figure 3-4: 3D, three parameter model regions.

basis vectors	*scaling matrix*	*component equations*	*normalization*
$\begin{bmatrix} 1 & 0 & 0 \\ 1 & 1 & 0 \\ 1 & 1 & 1 \end{bmatrix}$	$\begin{bmatrix} 1 & 0 & 0 \\ 0 & 1 & 0 \\ 0 & 0 & 1 \end{bmatrix}$	$a = x - y$ $b = y - z$ $c = z$	$1/x$
$\begin{bmatrix} 1 & 0 & 0 \\ 1 & 0 & 1 \\ 1 & 1 & 1 \end{bmatrix}$	$\begin{bmatrix} 1 & 0 & 0 \\ 0 & 1 & 0 \\ 0 & 0 & 1 \end{bmatrix}$	$a = x - z$ $b = z - y$ $c = y$	$1/x$
$\begin{bmatrix} 0 & 0 & 1 \\ 1 & 0 & 1 \\ 1 & 1 & 1 \end{bmatrix}$	$\begin{bmatrix} 1 & 0 & 0 \\ 0 & 1 & 0 \\ 0 & 0 & 1 \end{bmatrix}$	$a = z - x$ $b = x - y$ $c = y$	$1/z$

Table 3.3: 3D, three parameter model matrices and equations.

nents:

$$R(x, y, z) = N(a * W_1 + b * W_2 + c * W_3) * R_{111} \tag{3.4}$$

where W_i is the relative etch rate or weight for the ith plane. N is a normalization factor (either $1/x$ or $1/z$) which ensures that the rates are independent of the magnitude of x, y, and z. Two different normalizations are needed to provide continuity on the boundary between regions. Table 3.3 shows the details of this model. Again a, b, and c must be positive for the equations to be valid.

This formula is valid for all possible symmetric etchants: isotropic or highly anisotropic. Figure 3-5 shows the etch rates for ratios greater than unity.

Four Parameters

The (311) rates can be added to the model by redefining the triangular sections. In this case there seven vectors in the three principal families: (100) family: (100) and (001) (110) family: (110) and (101) (111) family: (111) (311) family: (113) and (311) The new vectors require that the triangular sections be properly chosen. The seven planes form six

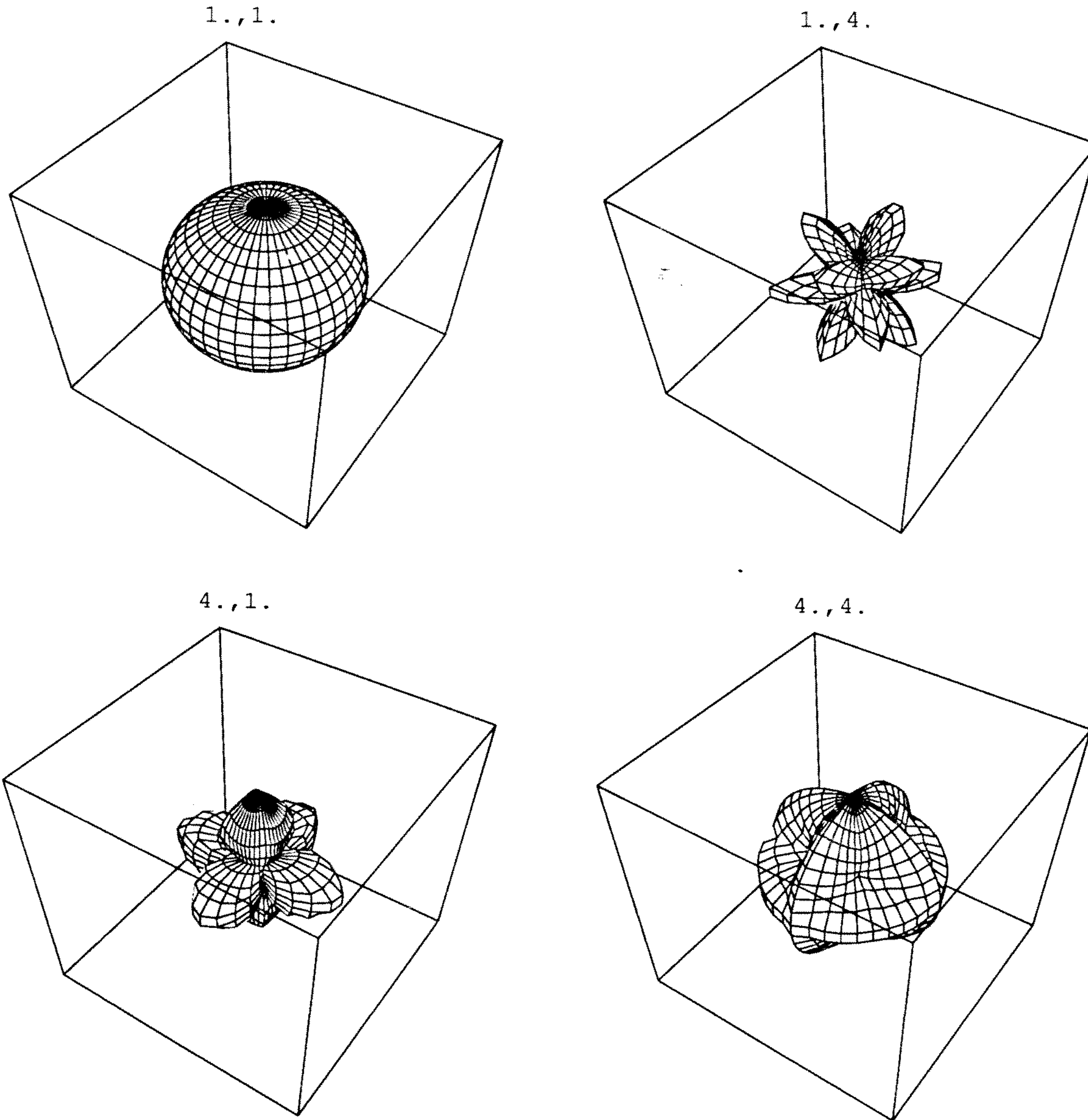

Figure 3-5: 3D, three parameter model results.

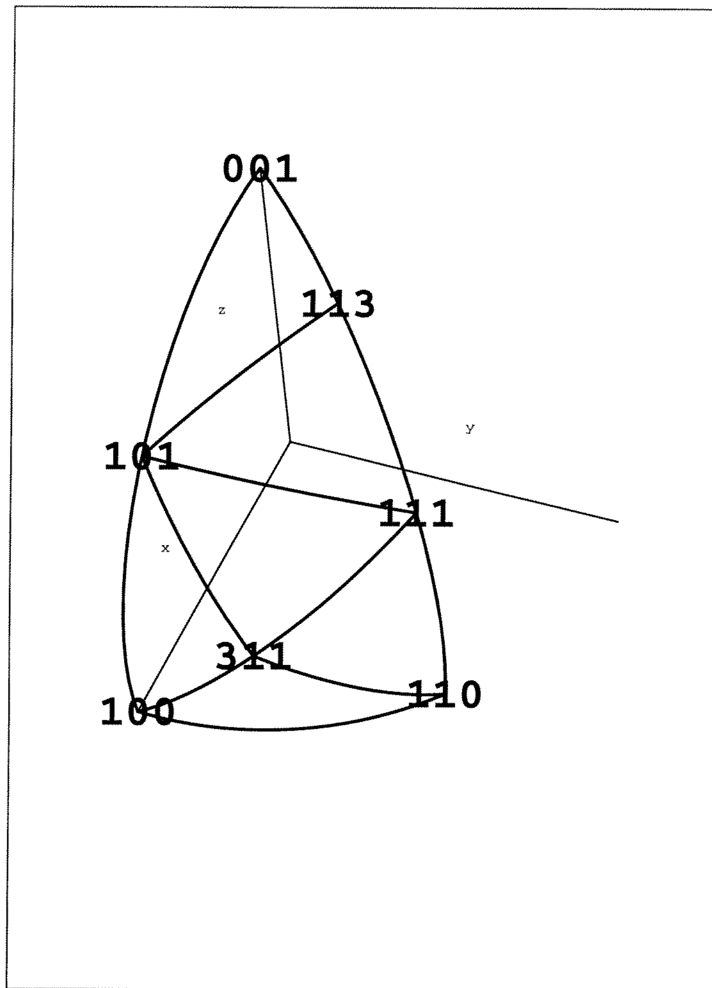

Figure 3-6: 3D, four parameter model regions.

triangular regions on the sphere each limited by three planes: (100,311,110), (100,101,311), (110,111,311), (101,111,311), (101,113,111), and (001,113,101) as is shown in Figure 3-6.

The etch rate at a vector $\{x, y, z\}$ is then given by a weighted sum of these components. Table 3.4 shows the details of this model.

Figure 3-7 shows the etch rates for ratios greater than unity.

basis vectors	*scaling matrix*	*component equations*	*normalization*
$\begin{bmatrix} 1 & 0 & 0 \\ 1 & 1 & 0 \\ 3 & 1 & 1 \end{bmatrix}$	$\begin{bmatrix} 1 & 0 & 0 \\ 0 & 1 & 0 \\ 0 & 0 & 3 \end{bmatrix}$	$a = x - y - 2z$ $b = y - z$ $c = 3z$	$1/x$
$\begin{bmatrix} 1 & 0 & 0 \\ 1 & 0 & 1 \\ 3 & 1 & 1 \end{bmatrix}$	$\begin{bmatrix} 1 & 0 & 0 \\ 0 & 1 & 0 \\ 0 & 0 & 3 \end{bmatrix}$	$a = x - 2y - z$ $b = z - y$ $c = 3y$	$1/x$
$\begin{bmatrix} 1 & 1 & 1 \\ 1 & 1 & 0 \\ 3 & 1 & 1 \end{bmatrix}$	$\begin{bmatrix} 1 & 0 & 0 \\ 0 & 1 & 0 \\ 0 & 0 & 3 \end{bmatrix}$	$a = (y - x)/2 + z$ $b = y - z$ $c = 3/2(x - y)$	$1/x$
$\begin{bmatrix} 1 & 1 & 1 \\ 1 & 0 & 1 \\ 3 & 1 & 1 \end{bmatrix}$	$\begin{bmatrix} 1 & 0 & 0 \\ 0 & 1 & 0 \\ 0 & 0 & 3 \end{bmatrix}$	$a = (2y - x + z)/2$ $b = z - y$ $c = 3/2(x - z)$	$1/x$
$\begin{bmatrix} 1 & 1 & 1 \\ 1 & 0 & 1 \\ 1 & 1 & 3 \end{bmatrix}$	$\begin{bmatrix} 1 & 0 & 0 \\ 0 & 1 & 0 \\ 0 & 0 & 3 \end{bmatrix}$	$a = (x + 2y - z)/2$ $b = x - y$ $c = 3/2(z - x)$	$1/z$
$\begin{bmatrix} 0 & 0 & 1 \\ 1 & 0 & 1 \\ 1 & 1 & 3 \end{bmatrix}$	$\begin{bmatrix} 1 & 0 & 0 \\ 0 & 1 & 0 \\ 0 & 0 & 3 \end{bmatrix}$	$a = -x - 2y + z$ $b = x - y$ $c = 3y$	$1/z$

Table 3.4: 3D, four parameter model matrices and equations.

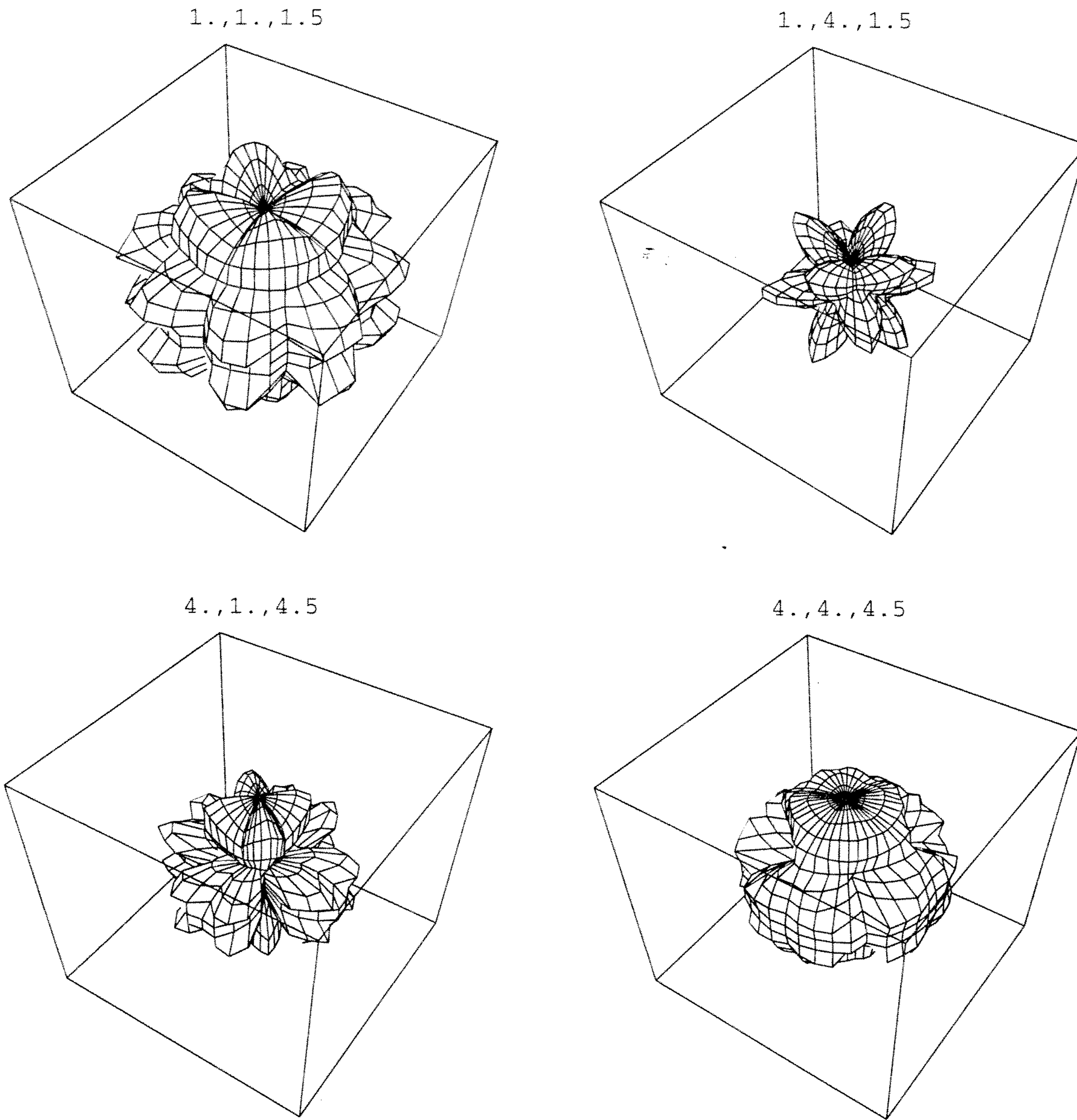

Figure 3-7: 3D, four parameter model results.

3.3 3D $\Rightarrow$ 2D (100) Projections

When etched shapes are produced, the three dimensional etch rate diagrams are transformed into two dimensional etch rate diagrams projected onto the plane of the wafer cut. This cutting of the wafer establishes boundary conditions at the wafer surface which limit the observed etch rates. At each θ value in the plane a minimization in ϕ is performed to find the minimum projection onto the plane. For a (100) wafer this is

$$R_{2d}(\theta) = MIN_{\phi}[proj(\theta,\phi)] \quad \Rightarrow \quad proj(\theta,\phi) = R_{3d}(\theta,\phi)/\cos(\phi - 90) \tag{3.5}$$

Figure 3-8 shows such a minimization performed graphically.

The plane of the wafer corresponds to a maximum ϕ of 90 degrees. It is possible to perform this minimization for other maximum ϕ values, in this case the projection is onto a cone (see Figure 3-9).

Three maximum ϕ values were examined, 90 (plane of wafer), 60 , and 30 degrees. The maximum ϕ=90 corresponds to the surface etch rate while the maximum ϕ=60 and 30 give information about the etch rate deeper into the crystal. Thus there are three contours to plot the etch rate behavior. Closely packed contours indicate sharply sloped walls while widely spaced contours indicate walls with smaller slopes. Note that each contour represents constant ϕ and not constant depth.

Figure 3-10 shows a modeled (100) projection while Figure 3-11 shows experimental data.

3.3.1 General Projections

This projection need not be limited to the (100) plane. In order to examine another plane the spherical coordinates in the new reference frame defined by the new wafer cut must be converted into the spherical coordinates in the (100) reference frame. If the old frame (ϕ,θ) is rotated by $\Delta\phi$ and $\Delta\theta$, the equations giving the new coordinates (ϕ_2,θ_2) are :

$$\cos(\phi_2) = \cos(\phi_2)\cos(\phi) - \cos(\theta)\sin(\Delta\phi)\sin(\phi) \tag{3.6}$$

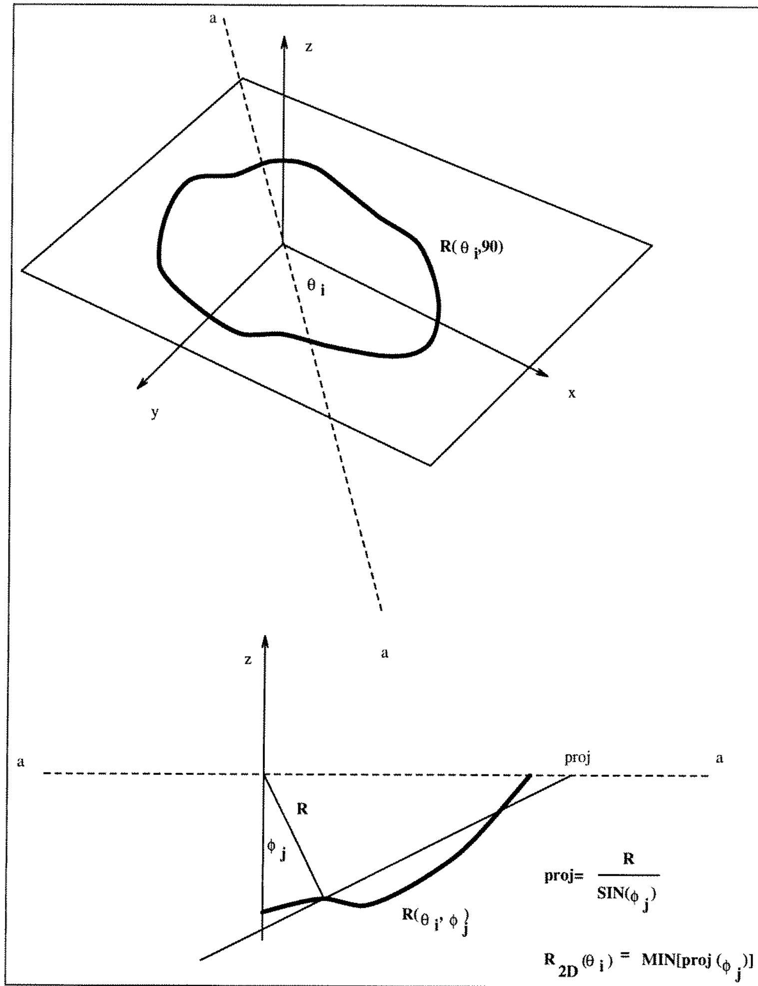

Figure 3-8: Minimum projection.

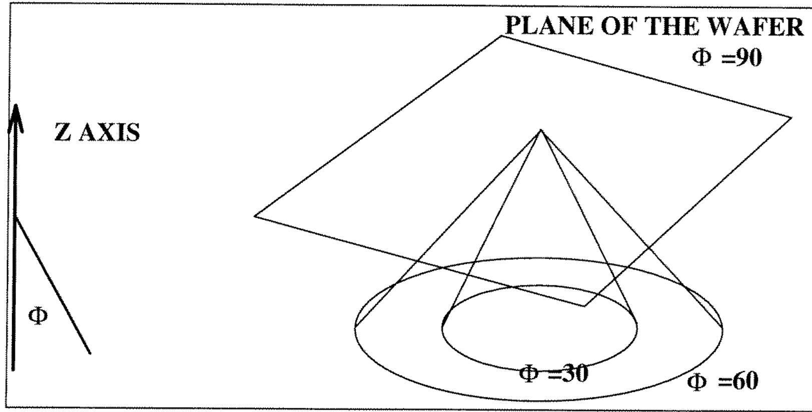

Figure 3-9: Projections onto cones.

$$\begin{aligned}\cos(\theta_2)\sin(\phi_2) &= \cos(\Delta\theta)\cos(\phi)\sin(\Delta\phi) \\ &\quad + \cos(\Delta\phi)\cos(\Delta\theta)\cos(\theta)\sin(\phi) \\ &\quad - \sin(\Delta\theta)\sin(\phi)\sin(\theta)\end{aligned} \tag{3.7}$$

where (ϕ_2, θ_2) defines the original frame.

For the (110) wafer $\Delta\theta = \pi/4$ and $\Delta\phi = 0$, while for the (111) wafer $\Delta\theta = \pi/4$ and $\Delta\phi = \pi/4$. The minimization is performed as before but the rate values used are those obtained from the new ϕ and θ. Figure 3-12 shows such a (110) projection. Figure 3-13 shows experimental measurements of the (110) projection (reproduced from a paper by Seidel [65]).

3.4 Generality

In this derivation the (111), (110), (100), and (311) rates have been chosen as principal planes. These planes were chosen because they appear quite often in the anisotropic etching of silicon. The model is in no way limited to such systems and any three principal planes may serve as a basis. More planes may be added to increase the accuracy of the model, in which case new triangular regions will have to be defined.

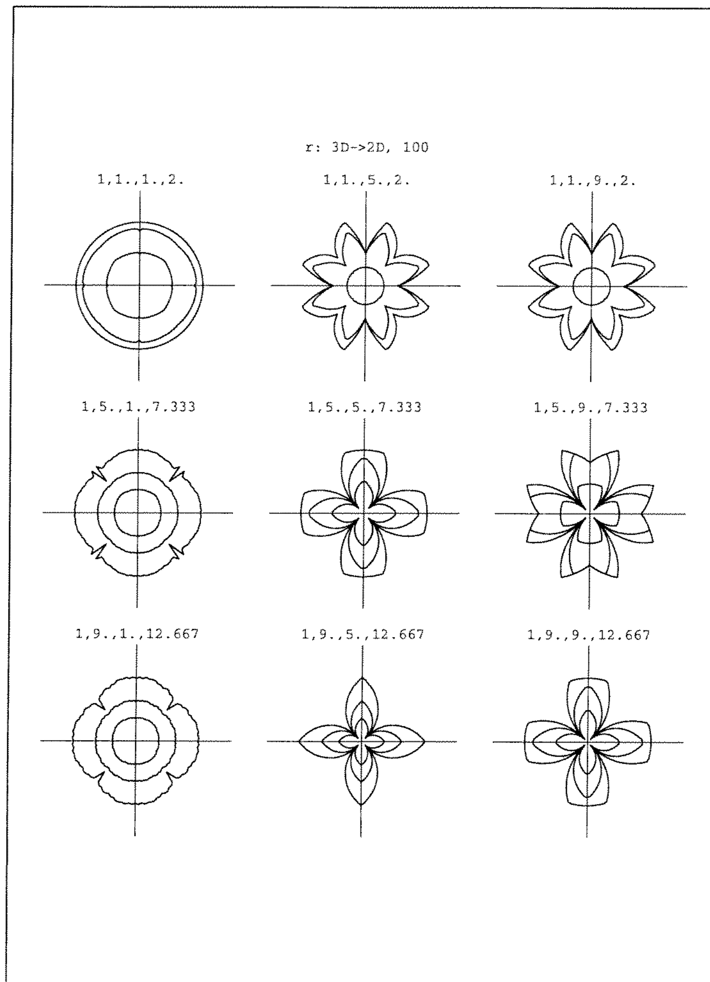

Figure 3-10: Modeled (100) projection.

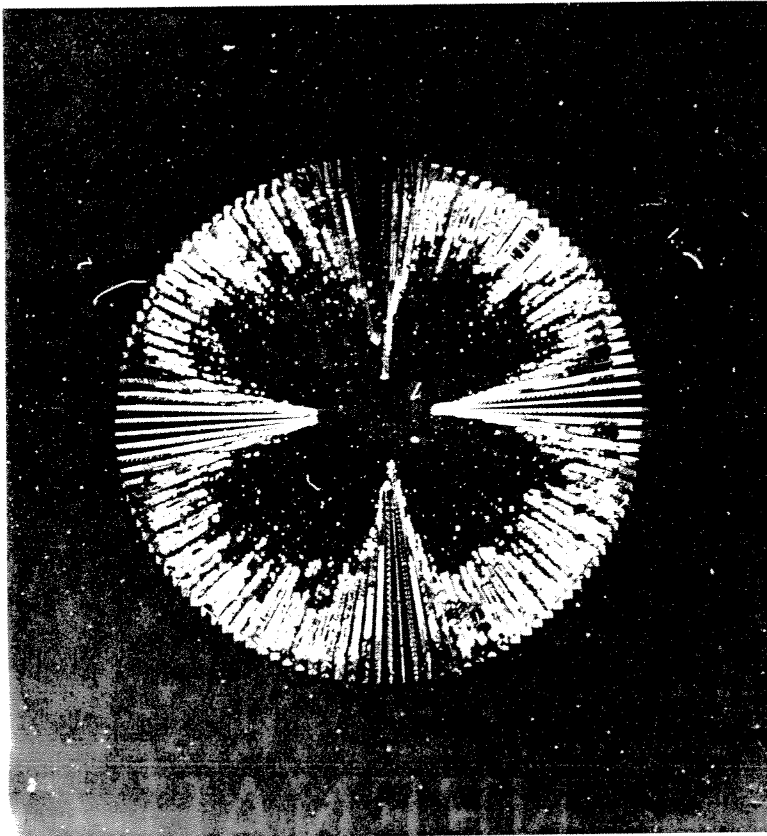

Figure 3-11: Experimental (100) projection.

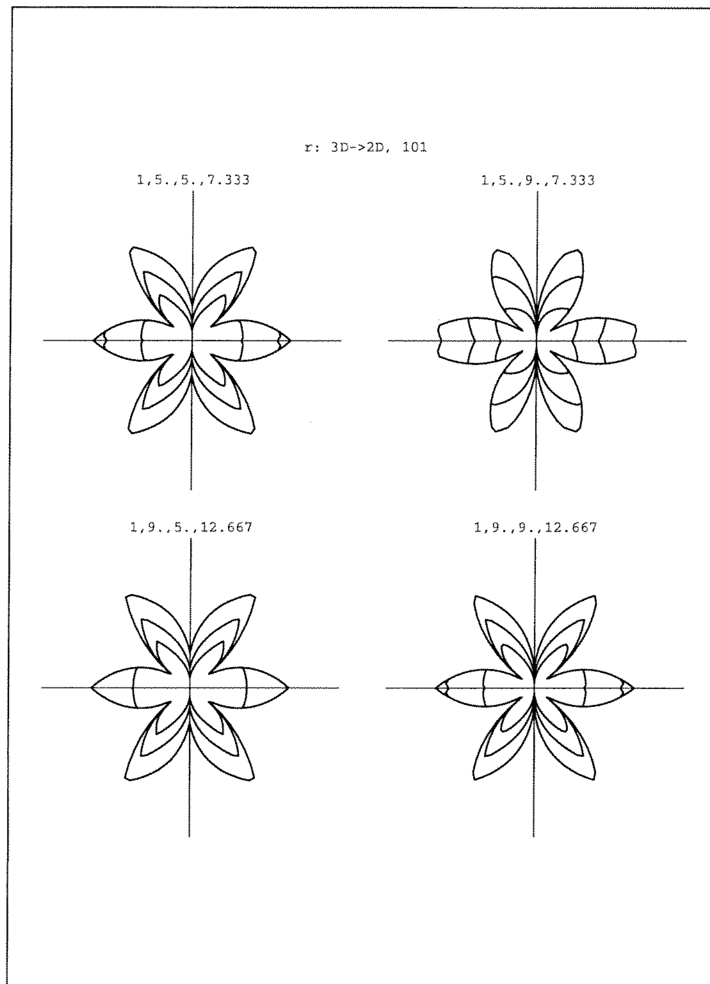

Figure 3-12: Modeled (110) projection.

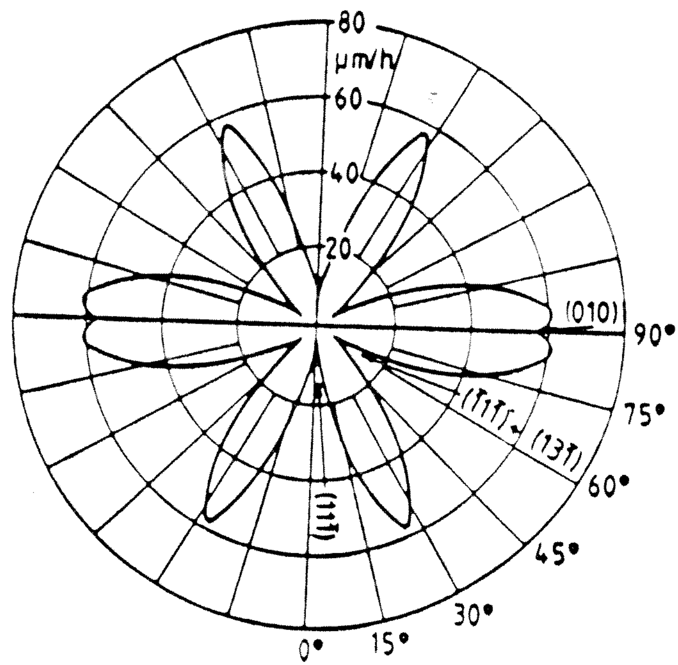

Figure 3-13: Experimental (110) projection from the literature [65].

3.5 Summary

A method for parametrizing the full etch rate behavior given a few known rates has been presented and found to agree with experimental measurements. The model does not seek to understand the reasons why etch rates differ, but rather uses the known available data to predict the results of differing etch rates. The method clarifies both the three dimensional nature of the etch rate diagram as well as the observed etch rates for different wafer planes. The predictions of any MEMS CAD tools can only be as good as the data it is provided. A standardized system for measuring and classifying different etchant based on their etch rate behavior is a much needed aspect of MEMS design. The model outlined above is a valuable part of such a system.

Chapter 4

Shape Modeling

4.1 Introduction

A wide variety of interesting shapes can be micro-machined from silicon using anisotropic etchants. Common etchants such as EDP and KOH are highly anisotropic and the transformation from two dimensional input mask to three dimensional output shape is quite complex in general. This chapter examines the output shapes that can be expected given specified etchant characteristics. While a number of techniques [16, 67] exist for predicting output shapes, the problem of inverting the design to find the required input mask for a desired output shape remains largely unresolved. A special class of shapes will be examined for which this kind of design inversion is possible. Uncertainties in design parameters will also be examined. The chapter uses as a starting point a full three dimensional etch rate diagram. In general etch rate diagrams are not well known, although some measurements have been made [65, 34]. For most etchants data is usually only available for a few planes and a few wafer orientations. This chapter uses a four parameter model to provide the three dimensional etch rate diagram. The model gives the etch rate diagram from the experimentally determined etch rates for four principal planes: (100), (111), (110), and (311). The following analysis is independent of the source of the etch rate diagram so other methods for obtaining the three dimensional etch rate diagram can also be used. The derivation assumes that the etching is linear and neglects non-linear effects such as diffusion.

4.2 Wafer Cuts

Given a three dimensional etch rate diagram $R(\phi, \theta)$ or $R(x, y, z)$, some planes will tend to dominate others in certain conditions. One important factor is wafer orientation. The wafer orientation refers to the crystal orientation along which the crystal is cut (the (100) orientation being the most common). This cutting of the wafer establishes boundary conditions at the wafer surface which limit the observed etch rates to a subset of the full three dimensional etch rate diagram. The observed etch rate within the plane of the wafer is the minimum projection onto the wafer at that orientation given by:

$$R_{2d}(\theta) = MIN_{\phi}[proj(\theta, \phi)] \Rightarrow proj(\theta, \phi) = R_{3d}(\theta, \phi)/\cos(\phi - 90) \tag{4.1}$$

Similar projections onto cones can also be found by replacing 90 degrees with another angle. These projections are combined to form a contour plot of the etch rate on a given wafer orientation. The surface etch rate is given by the planar projection and the conic projections give information about the etch rate deeper into the wafer. Figure 4-1 shows a variety of etchants on a (100) wafer). The outer contours show the etch rate at the surface and the inner contours show etch rates at conic angles of 30 and 60 degrees.

It is important to note that the transformation from three dimensions to two is a projection. The two dimensional etch rate diagram is not a shadow of the three dimensional diagram nor is it a slice through the three dimensional diagram.

Projections onto other planes such as the (110) are found by changing the reference frame of R before performing the minimization. In fact any arbitrary projection may be determined. Figure 4-2 shows nine different projections interpolating from the (100) to (110) wafer orientations. Again the contours indicate etch rates at different depth.

4.3 Limit Shapes

When EDP etches silicon, holes tend to converge to pyramidal pits bounded by four (111) planes. In general, the final shape to which a hole evolves depends only on the etchant used. In two dimensions consider an initial mask hole defined by a set of points in polar

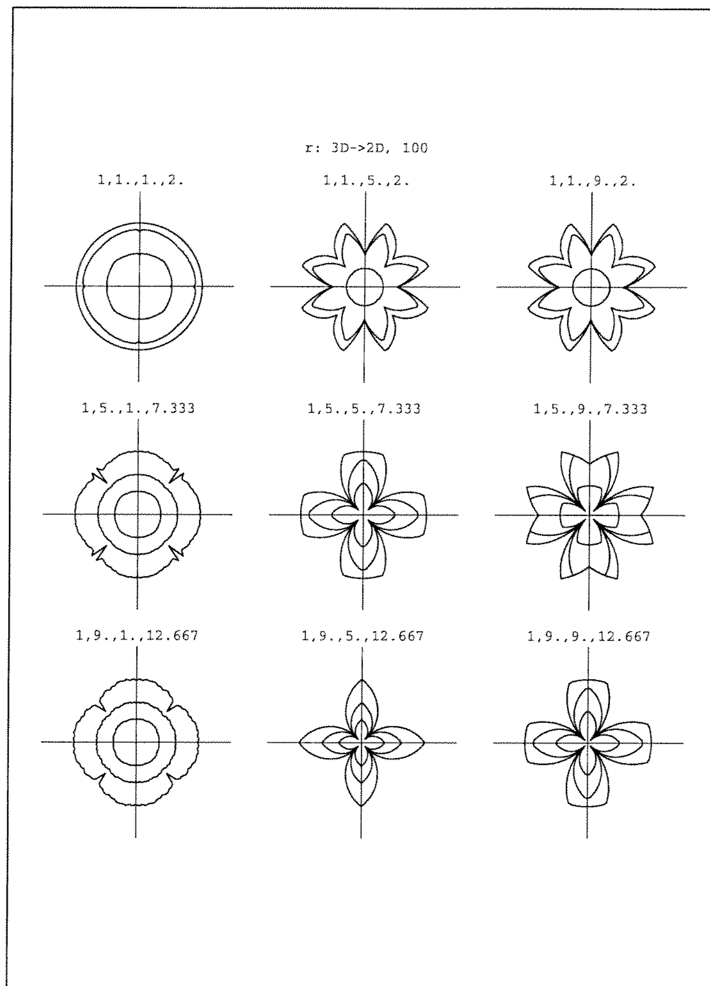

Figure 4-1: Different etchants for (100) wafer. Outer contours show etch rate at surface, inner contours show etch rate at greater depths.

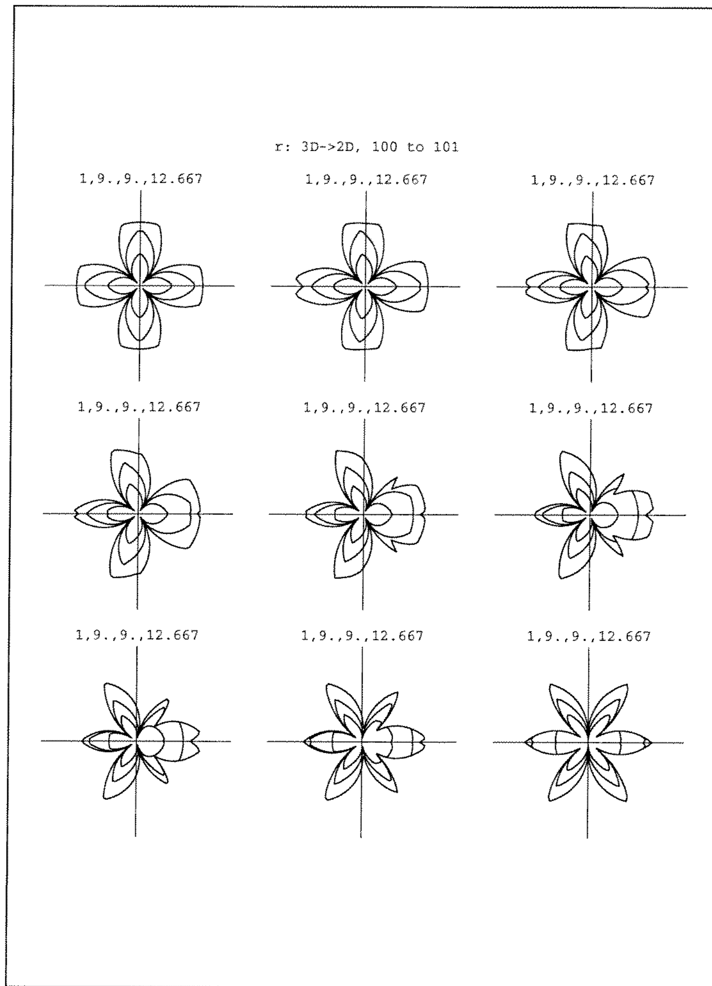

Figure 4-2: EDP/KOH-like etchant from (100) wafer to (110) wafer. Outer contours show etch rate at surface, inner contours show etch rate at greater depths.

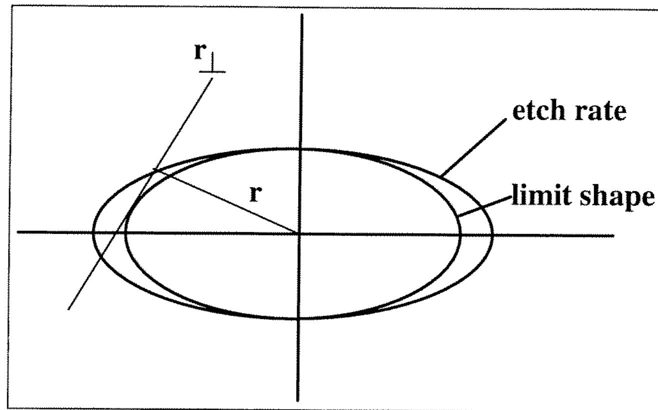

Figure 4-3: Limit shape (inner shape) for hypothetical elliptical etch rate diagram (outer shape).

coordinates. Each r_{0_i} is the initial radius at some angle θ_i. The output shape of the hole is the envelope of tangents of the shape; with each tangent displaced from its initial position by an amount which depends the tangent's orientation. The rate for any particular tangent is the rate which is normal to that tangent and the displacement is given by $Rate * time$. For large time, the r_{0_i} terms become negligibly small compared to the time dependent term. Thus the limiting shape for holes is the interior portion of the envelope formed by displacing a normal to θ by $R(\theta)$ for all θ values. Figure 4-3 shows an example of this process for a hypothetical elliptical etchant. This is termed the limit shape. As two examples, the two dimensional limit shape for isotropic etchants is a circle while for etchants such as EDP and KOH it is a square. The limit shape may be determined graphically as shown in Figure 4-3 or mathematically.

Let the two dimensional etch rate diagram be sampled at N θ values (see Figure 4-4). Consider a line at an angle θ with one endpoint of the line at the origin. Let the other endpoint of the line be given by its intersection with a displaced normal. The minimum length of the line determined from all possible intersections with all displaced normals is termed the radius of intersection for θ.

At each θ_i, $(N-1)$ lines have to be intersected to find the radius of intersection. Thus, $N*(N-1)$ calculations will have to be performed. Because, the limit shape is convex, (any non-convex part would be dominated by fast planes and etched away) a more efficient

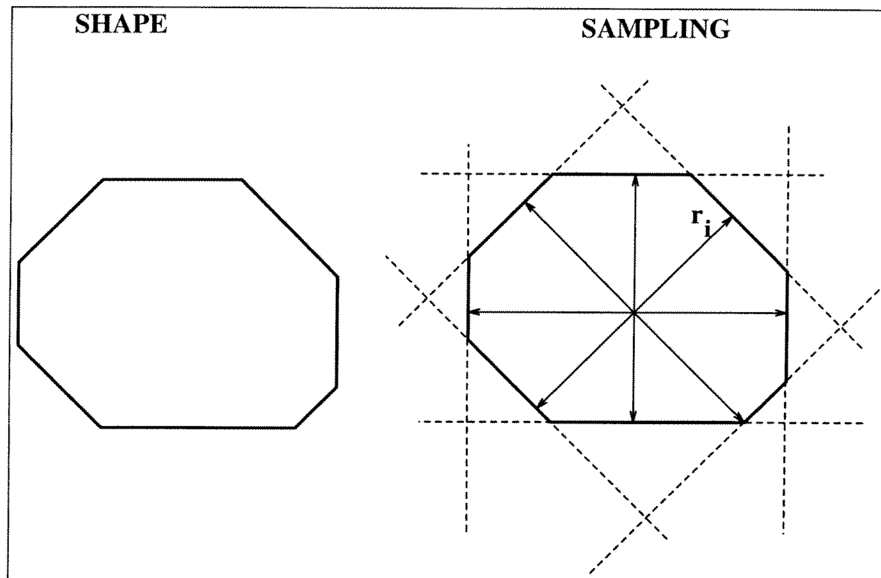

Figure 4-4: Sampling of a shape.

algorithm is possible. At each θ_i, adjacent normals at θ_{i+1},θ_{i+2}, etc. are intersected until the intersection radius increases. Normals any further away from θ_i cannot have a smaller intersection radius because the limiting shape must be convex. Note that the minimization must be carried out both in a clockwise and counterclockwise direction (θ_{i-1}, θ_{i-2}, etc. also must be considered). This improved algorithm performs on the order of N calculations, although the number of calculations does depends on the etchant. The improved algorithm is a type of gradient descent to find the minimum radius of intersection at every angle θ, using the convex nature of the limit shape to state that at each angle θ, there are no multiple minima in the radius of intersection.

Figure 4-5 shows the limit shapes associated with the etchants given in Figure 4-2. The outer contours show the limit shape at the surface and the inner contours show limit shape at conic angles of 30 and 60 degrees.

A full three dimensional limit shape could also be calculated from the three dimensional etch rate diagram if the radius of intersection minimization were performed in both the θ and ϕ directions. In this case the limit shape algorithm was applied to the surface etch rate diagram as well as the conic projections deeper into the wafer to obtain partial three

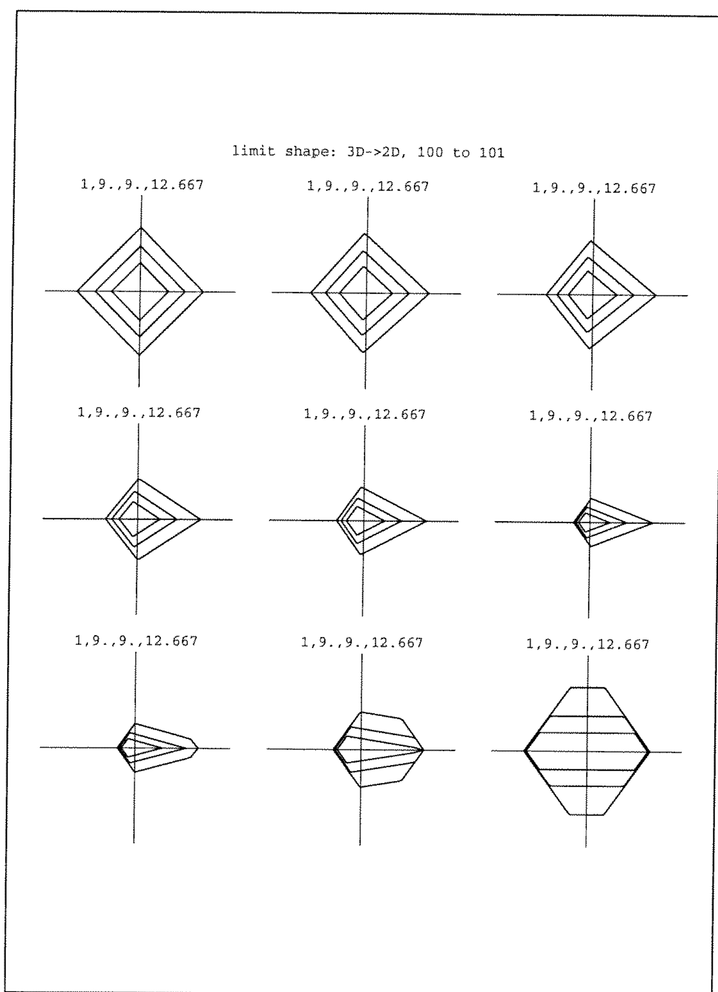

Figure 4-5: Limit shapes for Figure 4-2. Outer contours show limit shape at surface, inner contours show limit shape at greater depths.

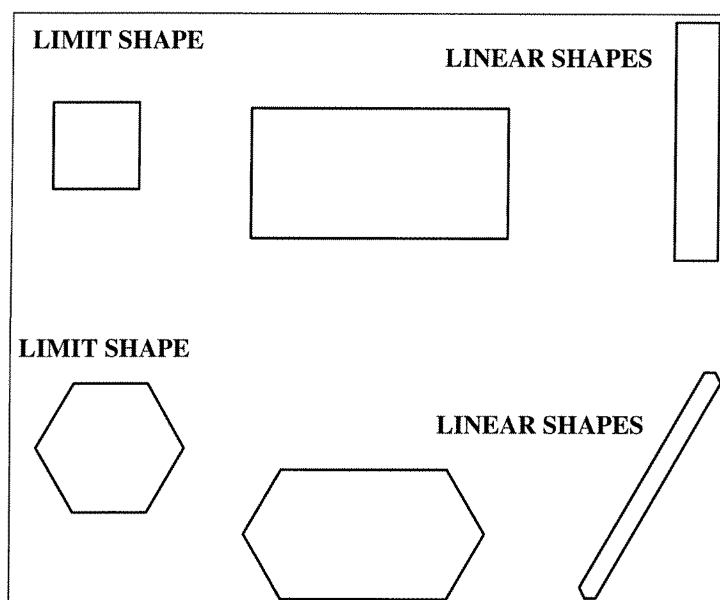

Figure 4-6: Limit and linear shapes.

dimensional information about the limit shape. Note that the limit shape is dominated by the slowest planes and has the same symmetry as the etch rate diagram. For this EDP/KOH-like etchant the (100) pyramidal pits (as shown in the upper left hand element of Figure 4-2) are obtained as expected.

While all holes converge to a limit shape independent of initial shape, the time required to converge increases as the initial shape differs from the limit shape.

4.3.1 Linear shapes

Closely related to limit shapes are linear shapes which change linearly from their present shape. A linear shape is obtained by stretching a limit shape along any two parallel lines. Figure 4-6 shows examples of linear shapes for KOH-like etchants for both (100) and (110) wafers. The linear shape for the (110) wafer is of great practical importance since it allows long thin vertical walled channels to be etched.

Planes appear at corners and since the linear shape has the same corners as the limit shape, no new planes appear in the linear shape. Similarly, no planes may disappear from the linear shape since it contains only planes found in the limit shape. While no planes

disappear in the linear shape, some planes will change length until the proportion of each plane is the same as the proportions of the limit shape.

4.3.2 Why are limit and linear shapes important?

The etching process transforms a two dimensional mask into a three dimensional shape. A general shape may change in a very complex manner. In the forward path (determining the final output shape given the initial mask) this does not pose serious difficulties. Simulation can still be performed on a general shape. However in the backward path, finding the necessary input mask in order to produce a desired output shape may be very difficult for a general shape. In some cases this design inversion is impossible.

In contrast to general shapes, limit and linear shapes change in a straigthforward fashion. Limit shapes, do not distort, they simply grow larger. Linear shapes "unstretch" and approach the limit shape. Because of this behavior, if the desired output shape is a limit or linear shape, the required input mask can always be found.The design implications of limit, linear, and general shapes will be examined in much greater detail in later chapters. Moreover, limit and linear shapes are not only easy to obtain and analyse, they are usually hard to avoid.

4.4 Shape Library

With the rate and shape tool thus far developed it is possible to build a library of shapes for use in design. While it is not possible in general to invert the design process to find the necessary initial conditions to obtain a desired output shape, an empirical inversion in some respects is possible. If the etch rates and associated shapes are tabulated, then the inversion can be performed by choosing the limit shape closest to the desired output shape. In effect we construct a library of limit shapes that point to the required initial conditions.

There are five important parameters to consider: the four major etch rates (111), (110), (110), and (311) as well as the wafer orientation. The values for the four principal planes are well suited to characterize the etched shapes since they appear quite often. By dividing all principal rates by the (111) rate, the size of the diagram ((111) rate) can be separated

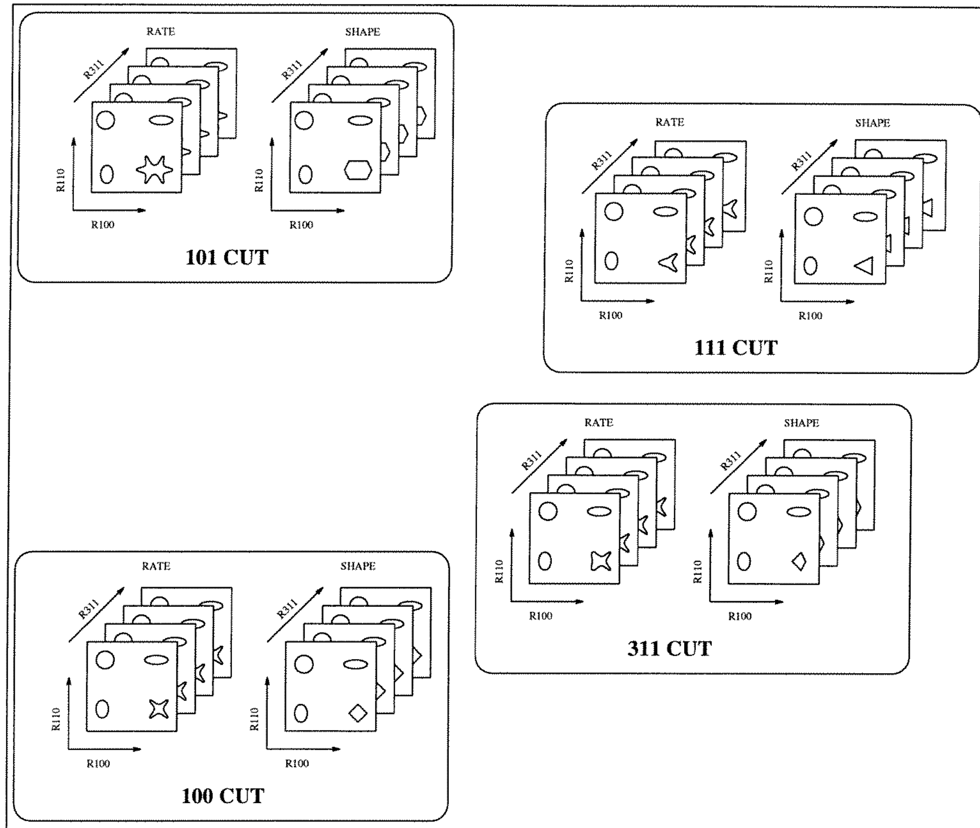

Figure 4-7: Shape Library.

from the shape of the etch rate diagram (ratio of the rates). Thus there are now four parameters. The effect of the (110) and (100) rates can be modeled by an array like that of Figure 4-5. This array is termed a page. Different pages with different values of the (311) rate are calculated to form a stack of pages.

For each element of each page in the stack, the associated limit shape is calculated to form a stack of shapes. This is repeated for different wafer orientations as is shown in Figure 4-7. The Figure only shows certain orientations and certain rates, but any arbitrary rate or orientation could be included.

The Shape Library is used in the following manner. The designer finds the linear shape closest to the desired shape. The linear shape has an associated limit shape which is found in the library. From the associated library rate entry, the designer now knows the requirements for etch rates and wafer orientation necessary to produce the linear shape. The initial mask

can be interpolated backward from the linear shape, as discussed above.

Movement within a page or within a stack is equivalent to being able to vary the etch rate behavior either by varying the temperature, composition, or chemistry. The ability to do this may be limited. Nonetheless, the required properties for a desired output shape are given by the Shape Library. Movement between stacks is equivalent to changing the wafer cut for a given etchant. While wafers are usually available in only a few orientations, if a particular application needs a specific shape, the Shape Library will show if it is possible. In general, a particular etchant and a particular wafer orientation may not always be available, but the Shape Library does indicate the type of etchant and initial conditions required to produce a desired shape.

4.5 Uncertainty

Often the etching parameters are not accurately known or measured. In this section the effect of error in both rate and wafer cut is examined

4.5.1 Noise

The idealized etch rate diagrams neglect such effects as error in rate measurements, nonhomogeneous etching, asymmetry in the etching, and defects in the crystal. All these possible sources of error are modeled by adding a random error to each $R(\phi, \theta)$. The new R is then used to calculate both projections and limit shapes. By repeating this process several times it is possible to obtain quantitative results on the effect of noise. Figure 4-8 shows such a simulation where a 3 x 3 array shows EDP-like etch rates with an error of 50 percent of the (111) rate. Again the contours indicate etch rates at different depth. From such Figures as Figure 4-9 it is possible to estimate both a maximum error and an average error in the limit shape expected for any given etch rate error.

4.5.2 Misalignment

Commercially available wafers are cut to a particular orientation with an accuracy of a few degrees. The effect of this misalignment, or mask misalignment, can easily modeled. The

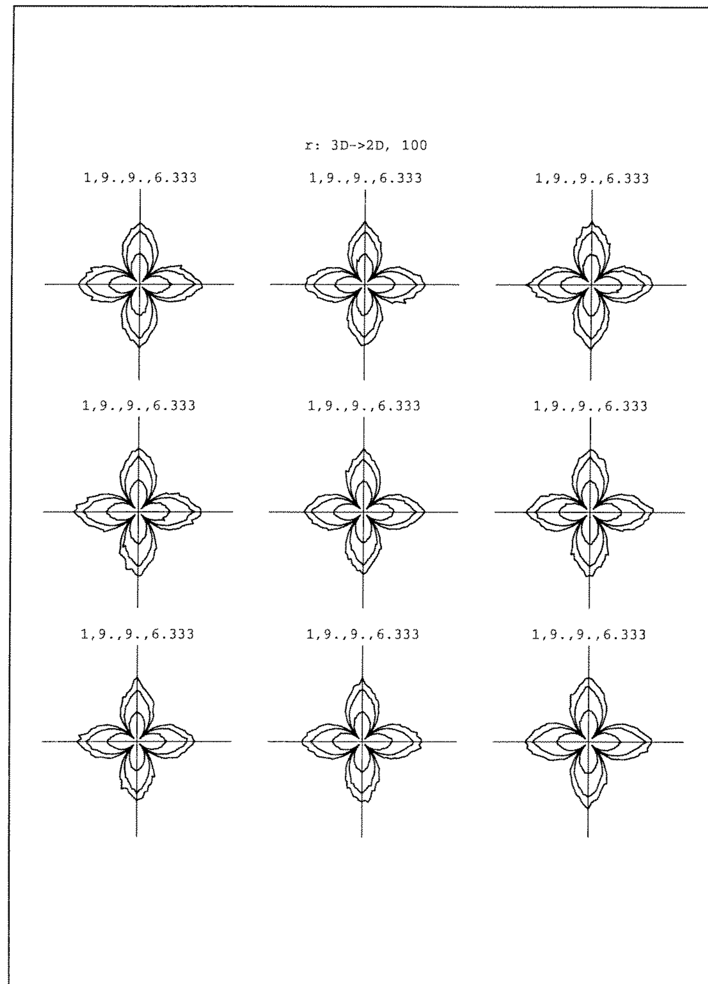

Figure 4-8: Rates with noise level of 50 percent of (111) rate. Outer contours show etch rate at surface, inner contours show etch rates at greater depths.

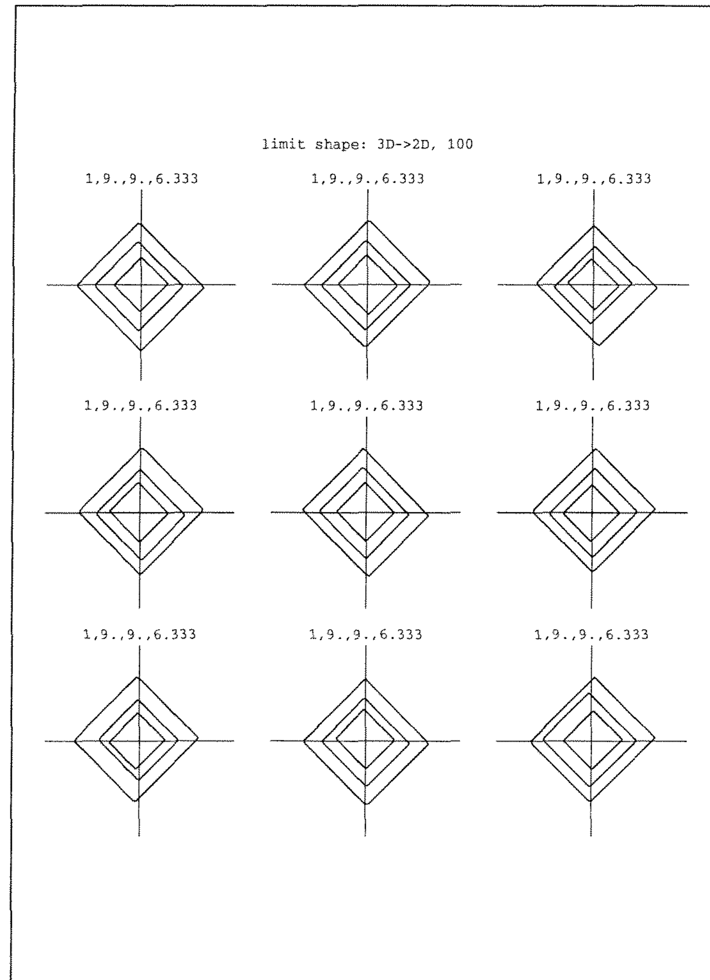

Figure 4-9: Limit shapes for Figure 4-8. Outer contours show limit shape at surface, inner contours show limit shape at greater depths.

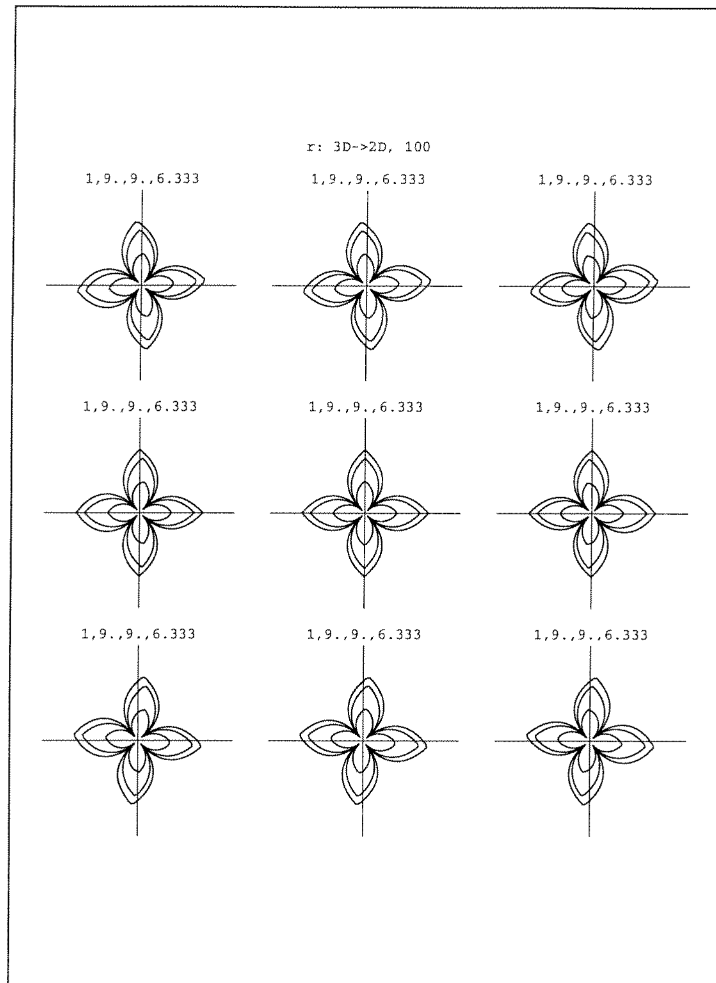

Figure 4-10: Rates with five degree misalignment. Outer contours show etch rate at surface, inner contours show etch rate at greater depths.

methodology for examining different wafer cuts is adapted to display an array of similar cuts that differ by some small misalignment. Figure 4-10 shows a three by three array for an EDP-like etchant where the center element is perfectly aligned and the surrounding elements have five degree misalignments in θ and/or ϕ. Figure 4-11 shows the effect of misalignment on the limit shape.

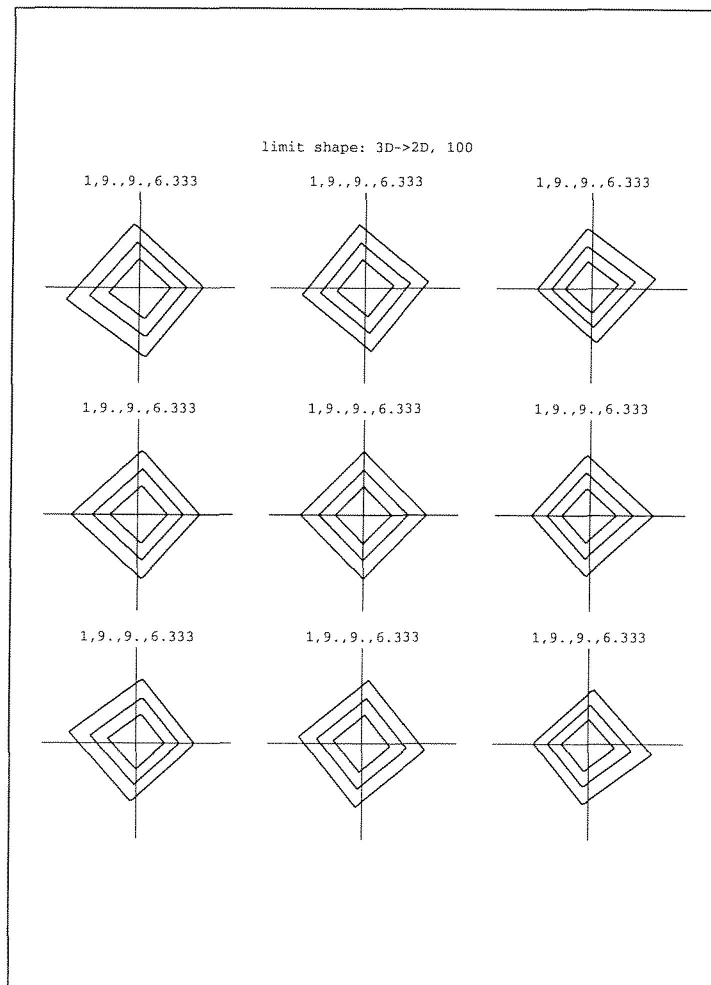

Figure 4-11: Limit shapes for Figure 4-10. Outer contours show limit shape at surface, inner contours show limit shape at greater depths.

4.6 Peg Limit Shape

It has been shown that for a given etchant any hole will evolve to some common limiting shape after a sufficient period of time has elapsed. The question arises, does there exist an analogue to the limit shape for concave shapes (pegs)? For example, EDP etched pegs tend to approximate an eight sided figure bounded by (311) planes. However, because pegs tend to get smaller with time, often the peg is completely etched away before sufficient time has passed to allow the peg to approach a limiting shape. This is especially true since pegs are dominated by faster planes. Thus the concept of a limiting shape to which all shapes evolving to some common limiting shape is not as universal as the hole limit shape concept. Nonetheless it may be possible to find a peg shape which is stable for a given etchant, that is for which a peg maintains its proportions as it becomes smaller.

4.7 Summary

The effect of the three dimensional etch rate diagram on the output shape was studied as well as the effect of uncertainties such as noise and wafer misalignment. The concept of limit and linear shapes was introduced as was the Shape Library design method.

Chapter 5

Eshapes

5.1 Introduction

This chapter introduces a new method for modeling the etching of single-crystalline silicon for arbitrarily complex MEMS fabrication, as a first step in developing comprehensive MEMS design methods approaching the level of development and automaticity in VLSI design.

This type of etching can be described by an etch rate diagram which indicates etch rate as a function of the orientation of the surface to be etched within the crystal. While full three dimensional etch rate diagrams are generally not available for most etchants, some two dimensional etch rate diagrams have been obtained [64, 65]. The (100) plane etch rate diagrams for KOH and EDP are of the form given qualitatively by Figure 5-1. Note that the etching is slowest along the (111) family of planes and faster on the (011) family. However the modeling of anisotropic etching is not straightforward because certain faces may appear while others may disappear [67]. This chapter will examine the modeling of emergent faces in crystal etching.

5.1.1 Prior work

There are a number of methods for predicting the output shapes. The Wulff-Jaccodine method [36, 20] uses plane waves that propagate outwards at a rate given by the etch rate diagram. At each point on the initial surface, a tangent plane is moved outward a distance equal to the appropriate rate multiplied by the time. At sharp corners there is a geometrical

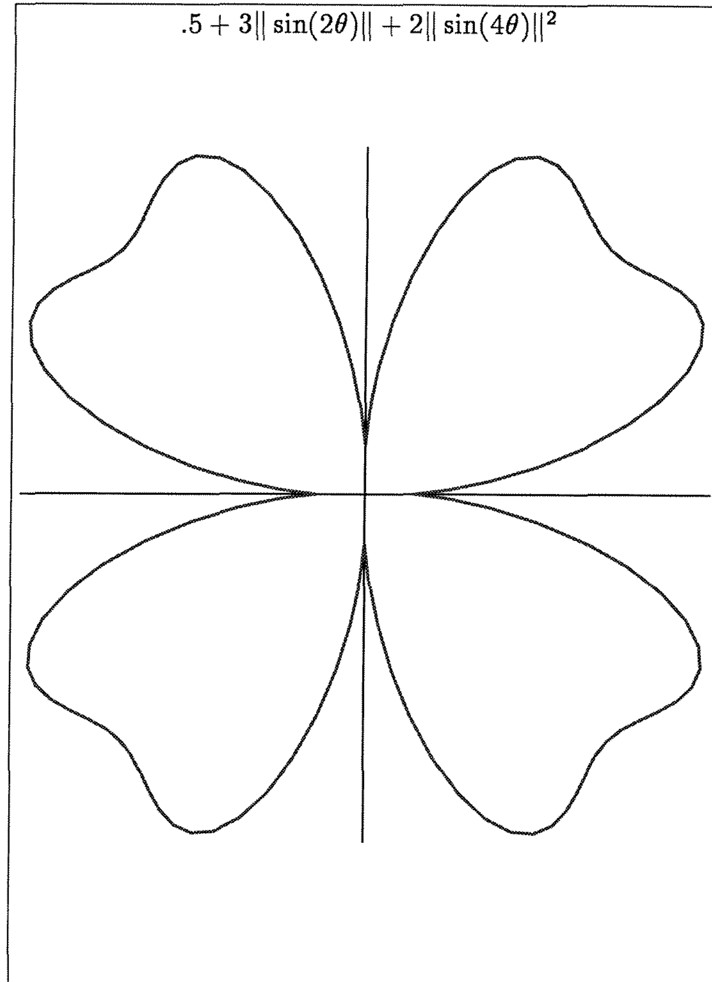

Figure 5-1: A qualitative example of an etch rate diagram. The formula for this rate in terms of angle θ is given above the figure. Etchants such as KOH and EDP have (100) etch rate diagrams which are very similar to the above figure.

test to determine if new planes appear. The final shape is the envelope of all these planes. Buser (*et al.*) [16] have developed a useful analysis tool called ASEP which can predict the output shape based on traveling planes. These results have been verified experimentally. However, their analysis is limited to a number of dominant plane families (111, 100, 110, 311) which tend to appear in crystal etching.

The Slowness method [67] uses the inverse of the rate (the slowness) to calculate the trajectories of points or lines in the shape. The trajectory of a corner is given by a vector relation involving the slowness vectors of the two lines which form the corner. This relation states that the trajectory of the corner lies along the normal to the difference of the two line slowness vectors. The trajectories of the corners are then used to determine when lines disappear and the procedure is iterated to find the shape at any time. Sequin [67] has successfully used the Slowness method to model changing shapes, although experimental verification is not included in that publication. Each method has its disadvantages and advantages and a more complete description of the above methods is given in Chapter 2.

In this chapter I present a third, geometric model which combines some aspects of the previous models, and various observations, to form a more complete and concise description of crystal etching. A comparison with previous work will be presented at the the end of the derivation. Idealized linear models including the one presented here do not consider non-ideal processes such as diffusion, however, such models do give accurate results where the effects of diffusion are small.

5.2 Mathematical Derivation

5.2.1 Shapes

The fundamental process that we are modeling is one of applying an etch-resistant mask to portions of a wafer of silicon, and exposing the non-masked portions of the surface to an anisotropic etchant. Anisotropic etchant refers to etchants whose etching rate depend on orientation. The etchant removes silicon and creates a depression in the surface which grows both in the direction normal to the surface of the wafer (down), and also laterally. Because the etchants of interest are anisotropic, the rates at which material is removed in

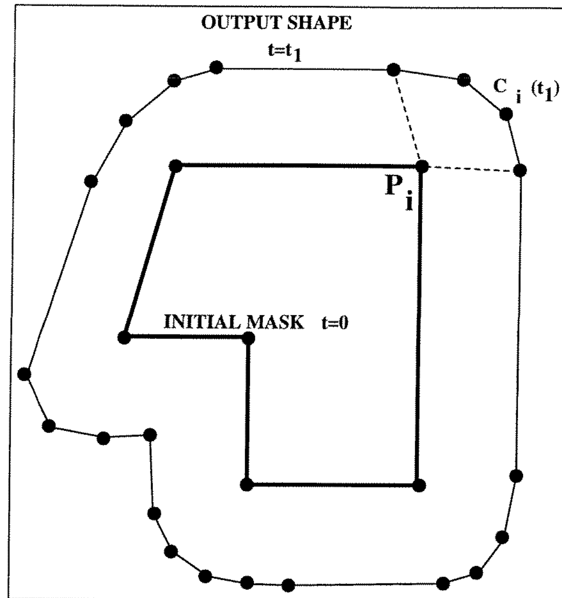

Figure 5-2: Evolution of corners.

the various directions are different.

We model the mask and etched shapes as (arbitrarily complex) polygons, and therefore our model of the etching process must properly account for the behavior of the sides of the polygons (planes, or tangents in 2-D) and the corners. We model the corners as a polygonal approximation to a circular curve with an infinitesimal radius. Thus each corner contains a very large number of nearly coincident planes or tangents. Our model focuses on the evolution of these planes as the etching takes place, with particular attention paid to the corners (since all planes or tangents in the entire polygonal shape appear at the corners).

Consider an arbitrary initial polygon defined by a set of m vertices $\{P_i\}$; we wish to find its shape at a later time. At each t the vertex P_i is mapped to a set of points $\{C_{i_1}(t), ...C_{i_{N_i}}(t)\}$ and these points are connected to form a piecewise linear curve (See Figure 5-2). The key lies in determining the set of points C_i which model the evolving corner shapes.

5.2.2 Envelopes

Consider the region near a corner P_i as shown in Figure 5-3A: the perpendicular distance from a local tangent plane to a local initial corner position is $R(\theta) * t$, where $R(\theta)$ is the etch rate as a function of orientation and θ is the orientation of the tangent. We wish to find the envelope of tangents displaced a distance $R(\theta) * t$ from the initial corner position as shown in Figure 5-3A.

The new evolved corner will be defined by the envelope of displaced tangents that move out at rates dependent on their orientation.

In order to understand the complete envelope formed by all the tangents, let us first examine one of the points on the envelope formed by the intersection of two adjacent tangents as shown in Figure 5-3B.

The algorithm we have developed makes the following assumptions: The etch rate is independent of time, is a function of orientation only, and is given by an etch rate diagram.

My nomenclature is as follows: in two dimensions, the x and y positions of a point define a vector [x,y]. A general vector is denoted by $\vec{V}$, its unit vector by $\hat{V}$ and its magnitude by V. If $\vec{V}$ is a function of some variable s, then $\vec{V}$(s) is used. t is time.

Let $\vec{E}$ be the vector per unit time from the initial corner to the intersection of two adjacent local tangents. From Figure 5-3B we see that in the (R, θ) reference frame (denoted by superscript $\star$)

$$\vec{E}^{\star}(\theta) = \left[R, \frac{dR}{d\theta}\right] \tag{5.1}$$

Transforming to the initial reference frame using a rotation matrix, we obtain

$$\vec{E}(\theta) = \left[R(\theta), \frac{dR(\theta)}{d\theta}\right] \; ROT_\theta \tag{5.2}$$

where

$$ROT_\theta = \begin{bmatrix} \cos\theta & \sin\theta \\ -\sin\theta & \cos\theta \end{bmatrix} \tag{5.3}$$

Interestingly, Equation 5.1 also appears in the study of disk cams with flat-faced followers where the follower maintains tangential contact with the cam [47].

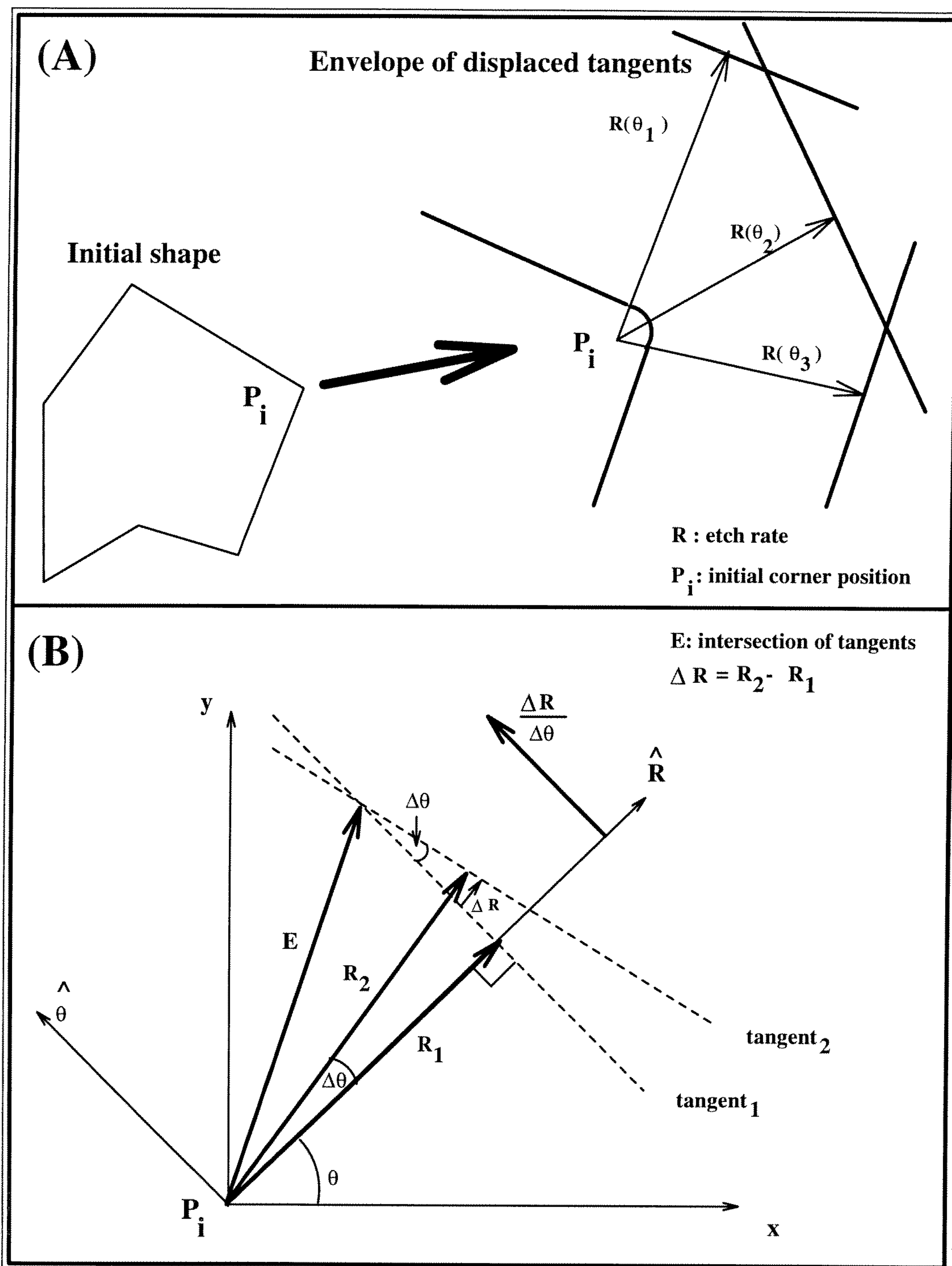

Figure 5-3: (A) Corner evolving to envelope of tangents. (B) Intersection of two adjacent tangents near a corner.

The local normal of the etch rate diagram is given by:

$$R_{\perp} = \left[1, -\frac{1}{R}\frac{dR}{d\theta}\right] \tag{5.4}$$

Thus $\vec{E}$ is the local normal of $R(\theta)$, (here denoted by $R_{\perp}$) multiplied by R then reflected about the R axis:

$$\vec{E}(\theta, t) = R\ R_{\perp} \begin{bmatrix} 1 & 0 \\ 0 & -1 \end{bmatrix} ROT_{\theta} \tag{5.5}$$

From Equation 5.4, it can be seen that the E differs from the etch rate diagram in that an individual point on the etch rate diagram at an angle θ is rotated in the θ direction an angle equal to the local derivative of the rate at that point with respect to θ.

5.2.3 Eshapes

Plots of $E(\theta)$ that cover the entire range of θ are termed Eshapes (envelope, equilibrium, or eigen shapes). Because the complete Eshapes contain all possible envelopes, they also contain all possible evolving corners. The evolving corners (where the ith corner is denoted C_i as shown in Figure 5-2) are found by extracting a subset of the Eshape termed an Esection. If $(\theta_1)_i$ and $(\theta_2)_i$ are the angles of the two line segments forming the ith vertex, C_i is obtained from the section of the Eshape, $E(\theta)$, lying between $(\theta_1)_i$ and $(\theta_2)_i$. C_i may consist of from one to N_i points and the jth point is denoted C_{i_j}. For each corner, a set of points is taken from the Eshape region and this set is translated to the initial corner position and then scaled with time:

$$C_{i_j}(t) = \{P_i\ + t\ *\ E(\theta_{ij})\} \tag{5.6}$$

where the angle of the jth point in C_i is given by $\theta_{ij} = (\theta_1)_i + j * ((\theta_2)_i - \theta_1)/N_i$

The map $t \mapsto \{C_{i_1}(t), ...C_{i_{N_i}}(t)\}$ has the property:

$$\{C_{i_1}(\alpha t) - P_i, ...C_{i_{N_i}}(\alpha t) - P_i\} = \alpha\{C_{i_1}(t) - P_i, ...C_{i_{N_i}}(t) - P_i\}$$

Thus individual evolved corners obtained from the Eshape do linearly change size but do not change shape as a function of time (hence the name: equilibrium).

The evolved shape S is given by a set of evolved corners $C_i(t)$ which themselves are a combination of the original polygon P and the Eshape E:

$$S(t) = \{C_1(t), C_2(t), ...C_m(t)\} \tag{5.7}$$

Figure 5-4 shows two hypothetical etch rate diagrams and the resulting Eshapes.

By differentiating E with respect to θ, we obtain the following test to determine the location of cusps in the Eshape,

$$\frac{d^2R(\theta)}{d\theta^2} + R(\theta) = 0 \tag{5.8}$$

If Equation 5.8 is satisfied by any θ, then the Eshape will be non-simple.

Eshapes and Esections will be examined further below.

5.2.4 Corners

There are two types of corners in two dimensions: convex and concave (see Figure 5-5). A square hole has 4 concave corners, while a triangular peg has 3 convex corners. The inside of a corner is taken to mean the region defined by an angle smaller than 180 degrees. For a convex corner, the inside is unetched, while the inside of a concave corner is etched.

To determine the shape of an etched corner at a later time, begin at each corner of the initial polygonal shape, and locate the two lines forming the corner.[1] The appropriate Esection can be determined by finding points on the Eshape that are tangent to these two lines. The etched corner shape corresponds to the region of the Eshape between the two points of tangency. Figures 5-6 and 5-4 show the use of the Eshape method for predicting output corner shapes. Note that hypothetical, asymmetrical, etchants have been used to demonstrate the model. The predictions for these figures are correct for these two

[1] We approximate all shapes as arbitrarily complex polygons, hence the shapes are composed of straight line segments and corners. For a curve approximated with many chords, the line segments will be short, and the angle between them near 180 degrees.

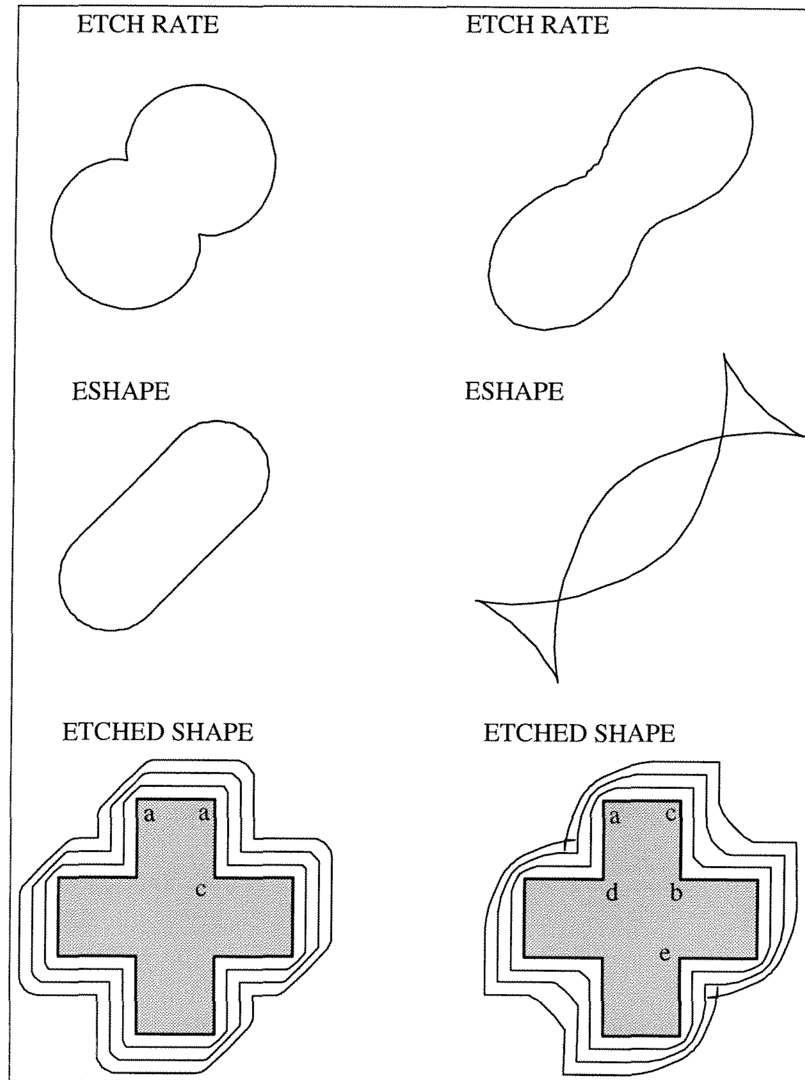

Figure 5-4: Hypothetical two dimensional etch rate diagram (top), corresponding Eshapes (center), and Etched shape (bottom). Note that the two etchants are not real etchants. The initial mask shape was the cross shaped hole shown at the bottom of the Figure.

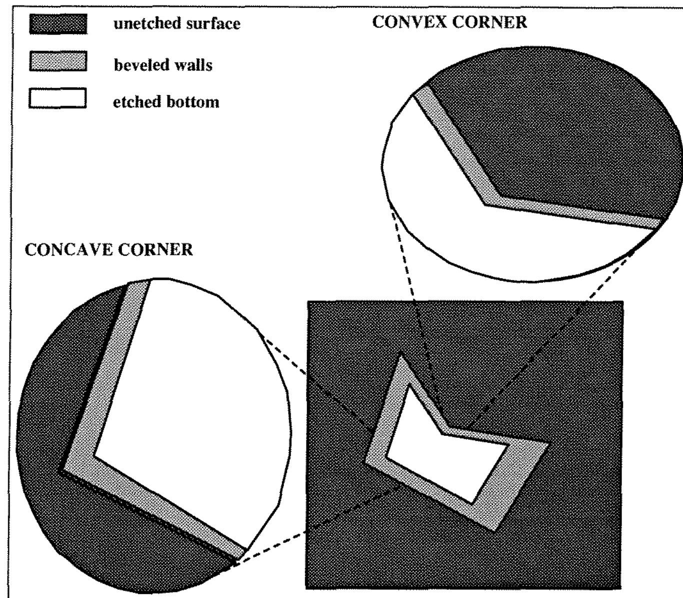

Figure 5-5: Definition of convex and concave corners.The unetched mask is dark, the etched bottom is light, and the beveled walls are grey.

hypothetical etchants but may differ from the results expected with actual silicon etchants.

When using the Eshape model, there are three different corner types that must be considered:

Concave corners: If the original corner is concave then the resultant corner is the Esection which lies within the two lines which enclose the origin (see Figure 5-4, corner a).

Convex corners: If the original corner is convex then the resultant corner is the Esection which lies in the quadrant opposite the two lines which enclose the origin (see Figure 5-4, corner b).

Static corners: If there are no Esections in the appropriate area, the corner remains a sharp corner. The corner is located at the intersection of the two lines and its trajectory is along the radius from the origin to the intersection (see Figure 5-4, corner c).

Figure 5-6 shows a further example of the Eshape method.

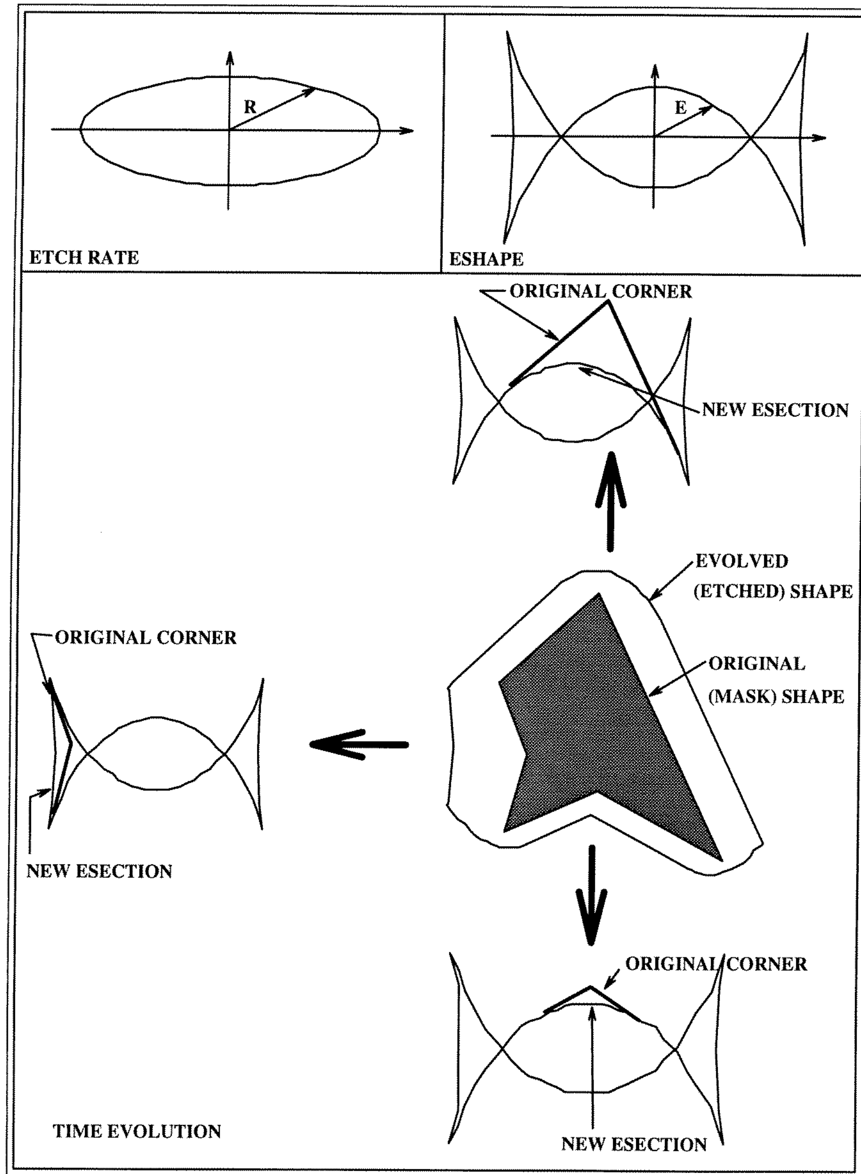

Figure 5-6: Summary of Eshape analysis: The etch rate is first transformed into an Eshape diagram. Then each corner is tangent-matched to the Eshape, and the appropriate Esection is extracted. The initial mask (shaded region) evolves to the surrounding curve. Concave corners use interior Esections, while convex corners use exterior Esections. The three corners shown are, starting at the top in counterclockwise order, concave, convex, and convex.

5.2.5 Time Evolution

A polygon evolves in the following manner: The etched shape at any time is formed by connecting each corner, determined by the method above, to its neighboring corners as shown in Figure 5-4. At each corner the extracted Esection is scaled (magnified) by the time. However as time increases, corners commonly intersect (see for example corners d and e in Figure 5-4) and some faces may disappear. The segments of corner sections that lie beyond the intersection of two corner sections do not appear in the final shape. Determination of the etched shape involves finding all such intersections, or cusps, and removing the non-physical segments.

The finding of such intersections has been extensively studied in the field of computer aided geometric design. Specifically, the etching process can be viewed as the generation of an offset curve with an orientation-dependent offset distance. Such offset curves [78] appear in applications such as numerically controlled machining.

In addition, new corners may appear and new Esections may have to be inserted when through-cut occurs (for example when two separate polygons merge into one larger polygon). After these new Esections have been added, the analysis proceeds as before.

5.3 Limit Shape

Etchants produce characteristic etched shapes, shapes that tend to appear after long etch durations. For example, KOH and EDP produce pyramidal pits on a (100) wafer. These characteristic shapes (which do not further evolve in time, though they grow in size) are limit shapes and are produced by the following process. Consider some initial polygon which is closed, then the corner angles must cover the range 0 to 360 degrees at least once. Therefore all parts of the Eshape are present in the etched shape, but each section is translated from the origin by the initial corner positions. As time goes to infinity, this initial translation becomes negligible compared to the size of the Esections, and the shape converges to Esections all centered at the origin. Using the rules for intersections stated above we see that the etched shape at large time converges to the interior of the Eshape, termed the limit shape.

5.4 Time Scaling

Etchants exibit a relationship between time, size, and shape. Two geometrically similar polygons, one large and one small will evolve into different shapes if etched for the same time. However, if the etch times are proportional to the polygon sizes, the geometric similarity is preserved.

The exact relationship between size and time can be found by considering two initial polygons where the second polygon is a scaled version of the first:

$$\{poly_2\} = \{poly_1\} * k \tag{5.9}$$

From Equation 5.6 ,

$$(C_{i_j}(t))_1 = \{P_i \ + t \ * \ E(\theta_{ij})\} \tag{5.10}$$

$$(C_{i_j}(t))_2 = \{P_i * k \ + t \ * \ E(\theta_{ij})\} \tag{5.11}$$

therefore $(C_{i_j}(k * t))_2 = k * (C_{i_j}(t))_1$ and

$$S_2(k * t) = k * S_1(t) \tag{5.12}$$

Thus, if a second polygonal mask twice as big as a first is etched, the shape of the second at time $2t$ is the shape of the first at time t, enlarged by a factor of two. Time scaling has a very important consequence: if several scaled versions of a mask are placed on a wafer and that wafer is etched for one value of time, then each of the evolved shapes will present a scaled version of the output shape at *different* values of time (see Figure 5-7). The smaller masks will represent the evolved shapes at larger time, with the effective time going as the inverse of the scale. This allows the entire time history of a shape to be etched in one experiment. This result has been verified by simulation and experiment as shown in Figure 5-11B.

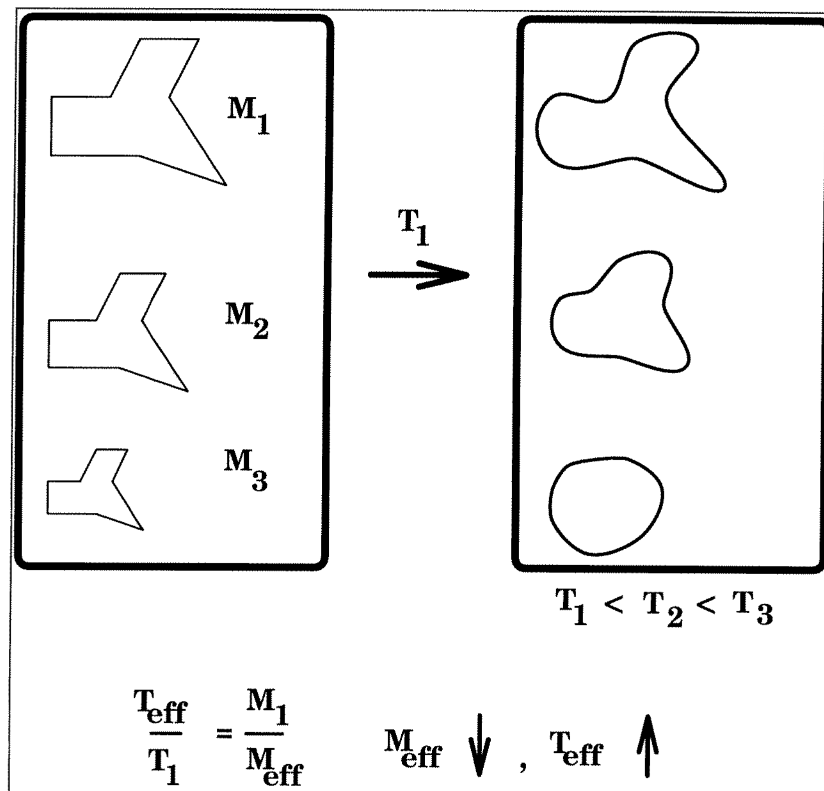

Figure 5-7: Time evolution of a shape in a single etch. The initial mask on left is repeated at different scales. The output shapes are on the right. The effective etch time is inversely proportional to scale.

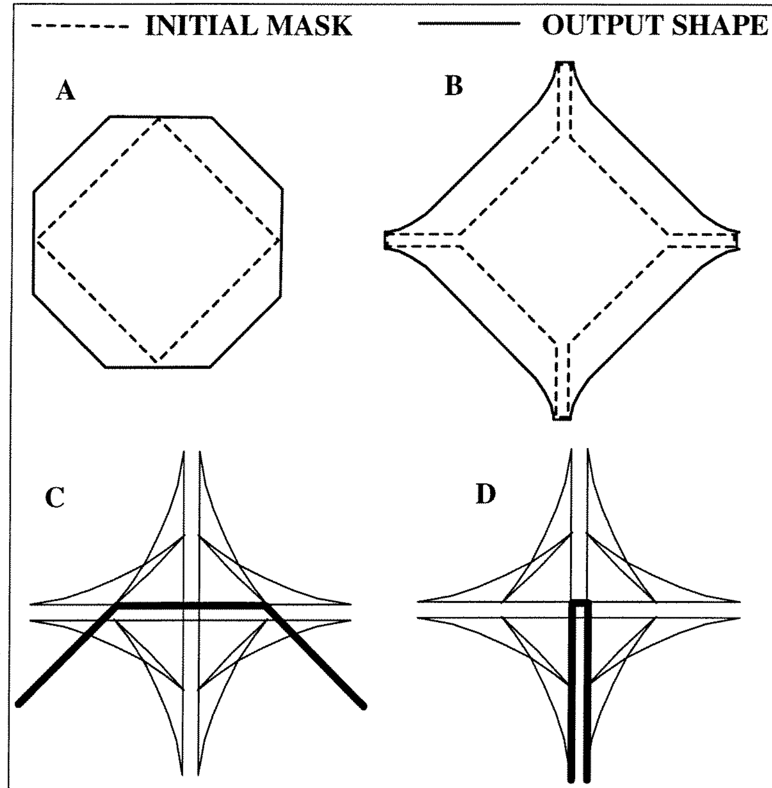

Figure 5-8: EDP or KOH etching: (A) diamond mask evolves to octagon. (B) modified diamond evolves to approximate diamond. (C) Eshape for (A). (D) Eshape for (B).

5.5 Design Inversion

The most general and most powerful form of design inversion is: given a desired final etched shape and a particular etchant, what initial mask is necessary to produce the desired output? This is a very difficult problem to solve in general and there are some shapes for which it is impossible to design an input mask, however it may be possible to closely approximate the desired shape. For example in EDP or KOH etching, a diamond shaped hole tends to evolve into a octagonal shape (see Figure 5-8A). If we desire a diamond we can approximate it by using the initial mask shown in (see Figure 5-8B).

This shape evolves into something which more closely resembles a diamond. The reason is immediately clear if we examine the Eshape. Consider the top corner: The first mask has a corner defined by the thick line (see Figure 5-8C). The second mask because of different

tangent matching conditions, has a much sharper outline (see Figure 5-8D). This particular example has also been verified experimentally.

Another type of inversion is as follows: Given a desired output shape, what type of etchant is needed to etch this shape? Since the tangent of the Eshape is perpendicular to the rate, the normal of the Eshape is parallel to the rate and thus the inversion formula is given by

$$R(\theta) = (\vec{E} \cdot \hat{E}_{\perp})\hat{E}_{\perp} \tag{5.13}$$

where $\hat{E}_{\perp}$ is the unit normal of the Eshape.

To verify this capability, the Eshapes shown earlier were inverted and the original etch rate diagrams were obtained. This process is independent of desired output and because of the limit shape theorem is also independent of initial mask. Of course this second form of inversion is limited by our ability to tailor the behavior of etchants. Nevertheless it provides information on the desired etchant behavior for any desired output specification.

5.6 Comparison with Experiment

5.6.1 Test patterns

A two dimensional model was used to model the surface outline of etched shapes. Tests were performed with both KOH and EDP, and although only the KOH results are presented here, the results from both etchants agreed with experiments. Samples were etched from one to two hours in a reflux system with temperature feedback. The temperatures for the KOH and EDP were 60 and 95 degrees Celcius respectively. In both cases the masking layer was silicon dioxide (approximately 0.8 microns in thickness).

The etch rate diagram in Figure 5-1 was used to generate the Eshape shown in Figure 5-9.

A test pattern was designed to verify different aspects of the model. The pattern included squares, circles, diamonds, and crosses of various sizes. In addition, both positive (holes) and negative (pegs) images were used. The Eshape of Figure 5-9 was use to generate the predicted shapes of Figure 5-10B. The model shows very good agreement with experiment as shown in Figure 5-11A. Note that both the pegs and the holes are accurately rendered as

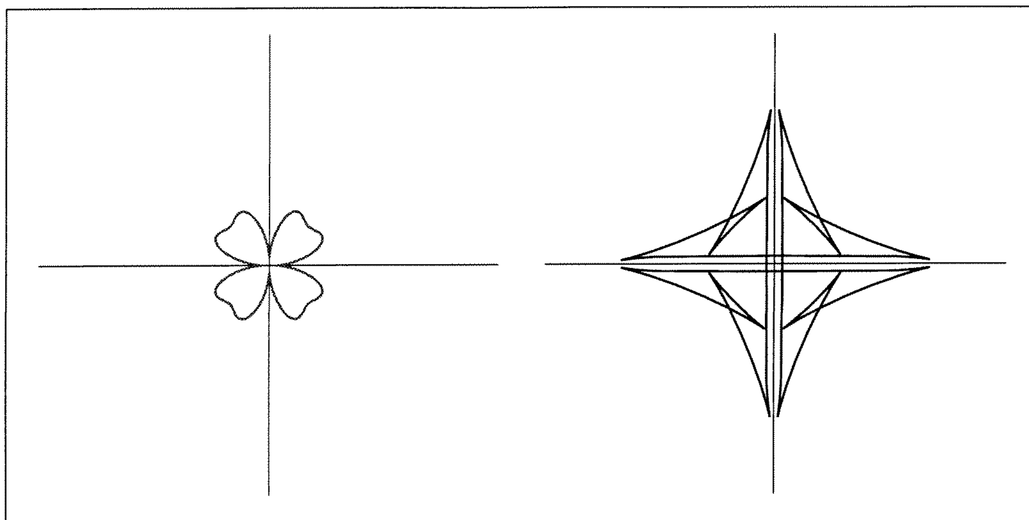

Figure 5-9: Etch rate diagram for (100) silicon in KOH and associated Eshape.

are both the convex and concave corners. In general it was found that the ability to predict output shapes is most limited by rate diagrams. Given that the Eshape model is a linear model, the error between the output shapes and the predicted results is on the order of the error between the actual etch rate and the etch rate used by the model.

Figure 5-11B shows another etch of half the duration of Figure 5-11 A. Comparison of the two figures confirms that the time scaling rule is valid.

5.6.2 Spoke patterns

One way to experimentally obtain the etch rate as a function of orientation is to etch a spoke pattern constisting of many radial wedges (see Figure 5-12 A). These spoke patterns are discussed more completely in Chapter 2.

Simple geometry shows that for N spokes each centered about angle θ_i, the pattern SP formed is given by:

$$SP_i = \frac{time}{\sin\frac{\pi}{2N}} * \frac{1}{2} * \left[R\left(\theta_i + \frac{\pi}{2} * (1 + \frac{1}{N})\right) + R\left(\theta_i - \frac{\pi}{2} * (1 + \frac{1}{N})\right)\right] \tag{5.14}$$

where SP_i is the radial position of the tip of the spoke at angle θ_i. This formulation

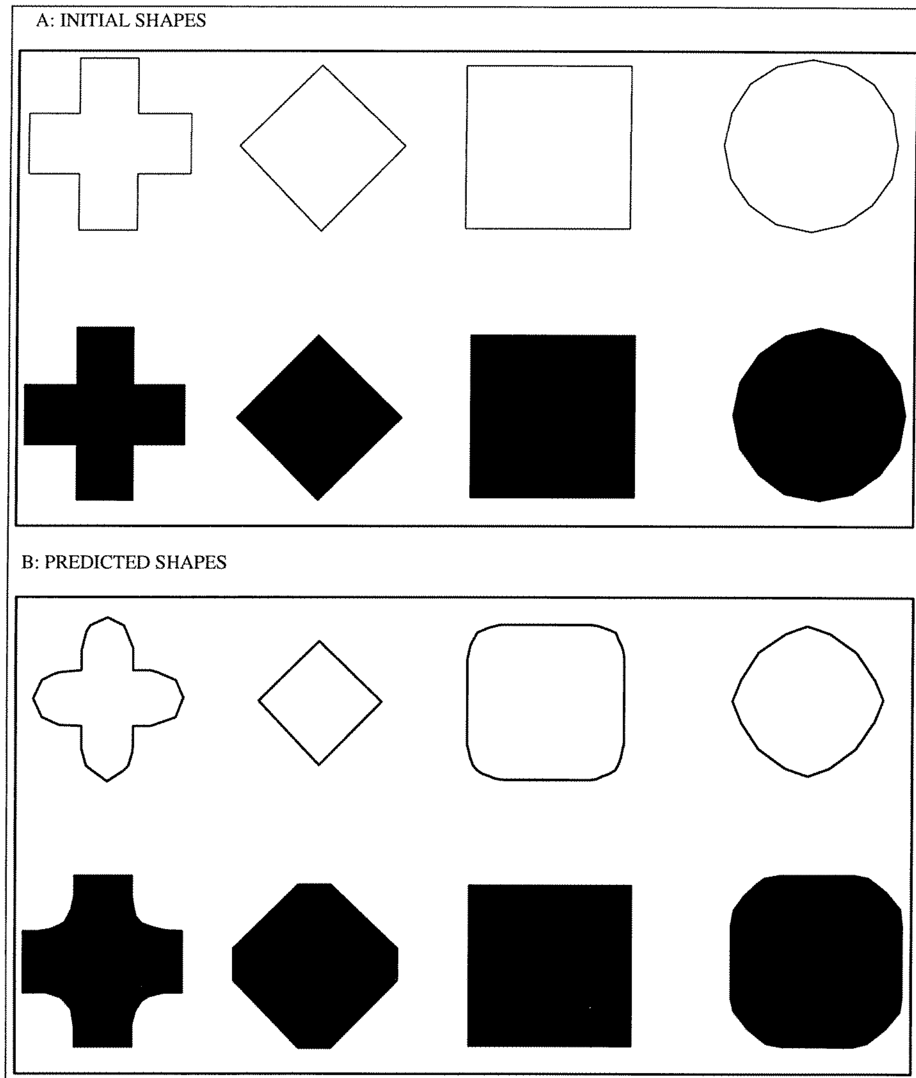

Figure 5-10: (A) Initial mask shapes; the squares are 0.8 mm across. (B) Predicted shapes derived from Figure 5-9. Compare with Figure 5-11. In both A and B, The top row of figures represents "pegs" while the bottom row represents "holes".

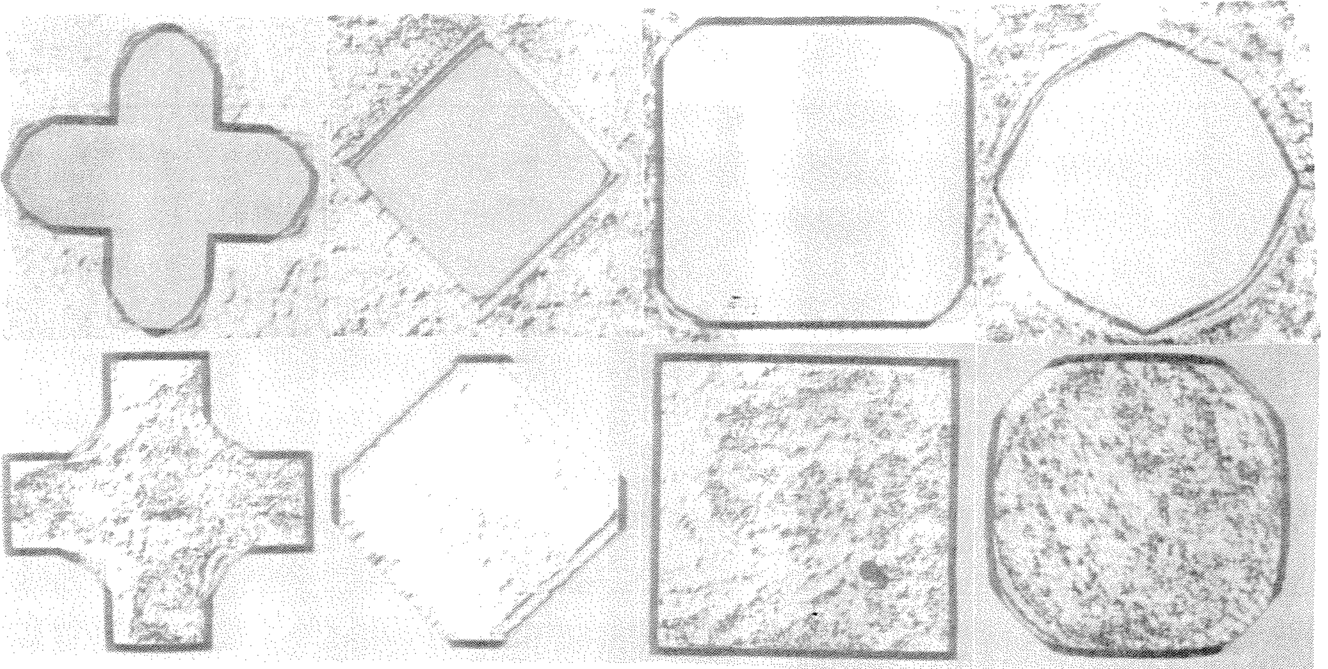

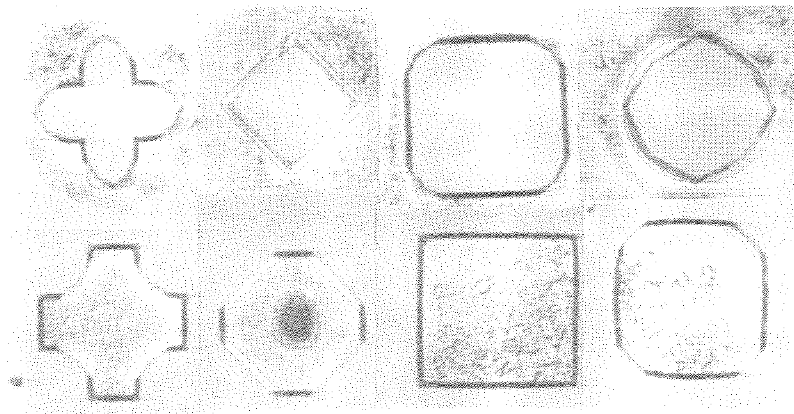

Figure 5-11: (A) (100) silicon etched with KOH at 60°C for two hours. The largest square is 0.8 mm across. (B) (100) silicon etched with KOH at 60°C for one hour. Compare any shape in this figure with the corresponding shape in Figure 5-11 A. In both A and B, The top row of figures represents "pegs" while the bottom row represents "holes".

illustrates four phenomena: (1) the pattern grows linearly in time; (2) the etch rate is magnified: as N increases, the effective etch rate (the rate at which SP_i moves radially) increases; (3) the etch rate is averaged over the width of the spoke; (4) the pattern depends on the rates perpendicular to the spokes;

For etchants that have four-fold symmetry and for the number of spokes N large, the formulation reduces to:

$$SP_i = \frac{2Ntime}{\pi} * [R(\theta_i)] \tag{5.15}$$

Figure 5-12 B shows the Eshape simulation of the etching of the spoke pattern. Compare this both with Figure 5-1 and Figure 5-12 C & D. Figure 5-12 C & D show experimental etches in both EDP and KOH. The experimental patterns suffer from lithography problems at the center where all lines meet and the lithography resolution is exceeded. However, these problems may be minimized by increasing the size of the pattern which reduces the relative effect of the center region.

Finally a comparison of an enlargement of the wide ends of the spokes (Figure 5-12 C & D) to the simulation of this region (Figure 5-12 B) shows good agreement in modeling the etch rate pattern as well as the changing shape of the spoke ends.

5.7 Extension to Three Dimensions

5.7.1 Exact solution

The extension from two dimensions to three dimensions can be very complicated [67, 20]. Many different geometries can arise and have to be considered individually. Because of its intuitive nature, the extension of the Eshape method introduced above allows us to observe which corner types are possible, and to classify those types by inspection.

In three dimensions, consider a vector [x,y,z]. As in two dimensions we have a reference frame and a rotated frame. The rotated frame is located at some angle ϕ from the z axis and rotated from the x axis by an angle θ.

Repeating the derivations for Equations 5.1 through 5.4 in three dimensions we obtain

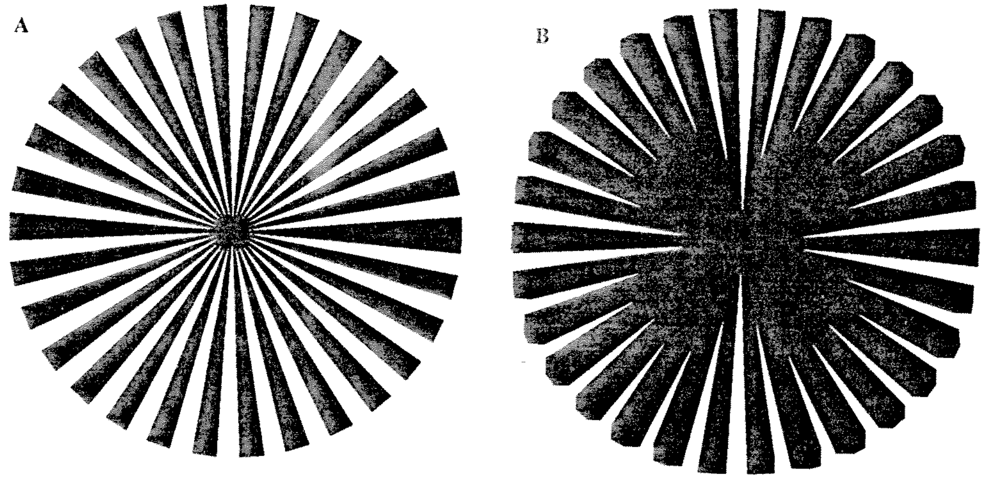

Figure 5-12: (A) Initial spoke pattern. (B) Simulated etch using Eshape method with KOH etchant. Compare with Figure 5-1. (C) Spoke pattern etched in KOH. (D) Spoke pattern etched in EDP. Both patterns are approximately 1.5 centimeters across and both were etched for several hours. Note that the end regions on the simulations agree with the observed experiments.

(compare with Equation 5.5):

$$\vec{E}(\theta,\phi,t) = \left[R(\theta,\phi), \frac{\partial R(\theta,\phi)}{\partial \theta} * \frac{1}{\sin\phi}, \frac{\partial R(\theta,\phi)}{\partial \phi}\right] ROT_{\theta\phi} * t \tag{5.16}$$

or

$$\vec{E}(\theta,\phi,t) = R\ R_{\perp} \begin{bmatrix} 1 & 0 & 0 \\ 0 & -1 & 0 \\ 0 & 0 & -1 \end{bmatrix} ROT_{\theta\phi} * t \tag{5.17}$$

Here:

$$ROT_{\theta\phi} = \begin{bmatrix} \sin\theta & 0 & -\cos\theta \\ 0 & 1 & 0 \\ \cos\theta & 0 & \sin\theta \end{bmatrix} \begin{bmatrix} \cos\phi & \sin\phi & 0 \\ -\sin\phi & \cos\phi & 0 \\ 0 & 0 & 1 \end{bmatrix} \tag{5.18}$$

and $R_{\perp}$ is the local normal of $R(\theta,\phi)$ in spherical coordinates.

Hypothetical three dimensional etch rate diagrams have been formulated (since full 3-D etch rate information is not available in the literature) and the corresponding three dimensional Eshapes have been constructed using Equation 5.16.

The results for limit shapes and time scaling can also be extended to three dimensions.

5.7.2 Approximate three dimensional solution

Three dimensional etch simulation using the method described above can become quite complex, however, in many common situations an approximation is sufficient. Rather than examining the three dimensional evolution of corners, a two dimensional outline (as a function of time) can be used to simulate the three dimensional evolution of the edges which make up the shape. Two assumptions are necessary: (1) the etching is anisotropic, thus the cross section of any edge perpendicular to the (100) plane is a straight line inclined at some angle; (2) the depth is shallow, such that three dimensional corners do not intersect.

The shape is given by the two dimensional outline extended into the (100) plane at the appropriate angles. In order to calculate this, the inclination of planes (with respect to the z axis) as a function of orientation within the (100) plane must be obtained. This may be done from the spoke pattern described earlier.

EDP and KOH have similar etch rate diagrams in the (100) plane but they differ out

of the (100) plane. Both produce 54.7 degree z-inclined planes for lines inclined at 0 or 90 degrees in the (100) plane. However, for planes inclined 45 degrees in the (100) plane, EDP produces a z-incline of 45 degrees while KOH produces vertical walls (90 degrees). Using this data and intermediate values, we can add to the two dimensional outline and produce three dimensional images. This was done for the experimental test patterns as shown in Figure 5-13 A. The results agree very well with the data.

The three dimensional representation allows us to view the shape from any direction we choose as shown in Figure 5-13 B.

5.8 Summary

Several models for analyzing MEMS exist and accurately model the future output shape given the initial conditions [16, 20, 27, 67]. The Eshape model also accurately predicts the output shapes, but offers some additional advantages. It provides a simple mathematical description of the etching process as well as a framework for inverting the design process to determining the required input mask for a desired output shape. Thus it is closer to CAD (Computer Aided Design) than to CAA (Computer Aided Analysis). The disadvantages of the Eshape model are shared by many other models. For example, a model is only as good as the etch rate information that is available. Additionally, when two or more etched shapes intersect to form new shapes, more detailed global calculations are required.

A new method for modeling the time development of emergent faces in crystal etching. This modeling is fundamental to MEMS fabrication simulations and design. The two dimensional Eshape method was presented, which is both intuitive and easy to implement manually or by computer. The concepts of equilibrium sections, equilibrium shapes, limit shapes, and time scaling were introduced. The predictions of the model agreed well with experiments performed with KOH and EDP. The Eshape etch model presented here is a first step in developing the ability to represent and manipulate complex (mechanical) shapes to be fabricated in silicon, and in developing comprehensive MEMS design methods which we hope will approach the level of development and automaticity in VLSI design.

The next chapter will introduce another etch simulator which complements the Eshape method.

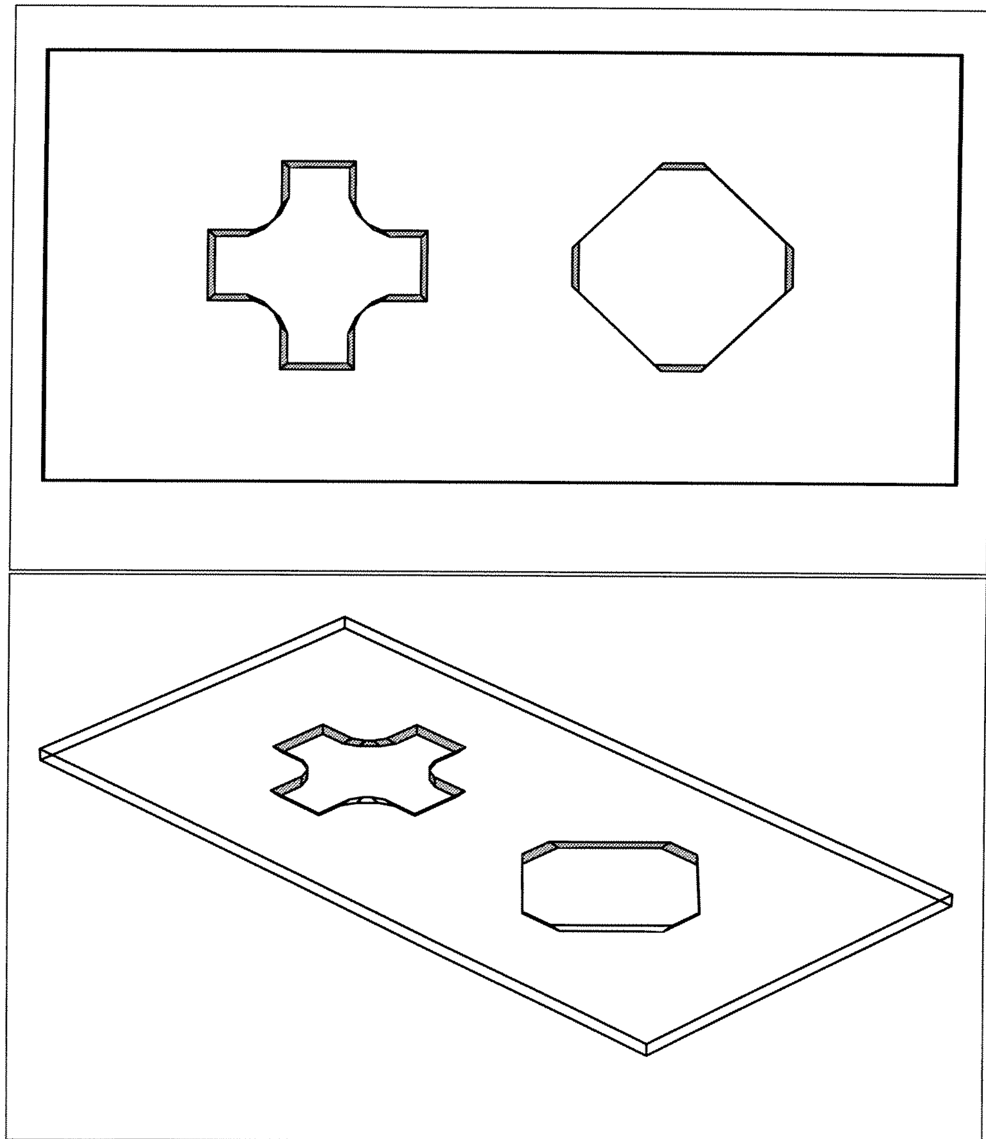

Figure 5-13: Cross and diamond shaped holes. (A: top) KOH etch simulation extension to three dimensions (B: bottom) View from an oblique angle. Compare with Figure 5-11.

Chapter 6

Cellular Automata

6.1 Introduction

As discussed above, when silicon is etched with anisotropic etchants, the etched shape changes as a function of time. A number of different approaches exist to accurately predict the etched shape given an initial mask. The ASEP program by Buser [16] uses traveling planes and the intersections between them to define the shape as a function of time. The Slowness method of Sequin [67] examines the corners of a shape and predicts the trajectory of those corners. This is done using a vector expression involving the inverse of the rate (the slowness) of the planes which make up the corner. These models deal very well with most basic shapes. In both of these cases however, complex shapes are more difficult to deal with. For example when two distinct shapes merge to form a new shape (termed through-cut), much more computation must be done.

This chapter presents a robust cellular automata model which predicts the three dimensional etched shape as a function of time for arbitrary etchants and arbitrary initial mask shapes. The fundamental idea is to use many small cells, each with simple empirical rules of behavior, but whose aggregate behavior is an accurate simulation of anisotropic etching. Some preliminary work has been done on atomistic approachs [67]; this chapter will focus on cellular automata and address, at greater length, issues such as generality, efficiency, and speed. The model can deal with very complicated structures and has moderate computational requirements.

6.2 Modeling Methods

The above methods and others like them are high level; the fundamental modeling unit or primitive is defined in terms of endpoints with an associated interior. The intersection points between two or more units are calculated and new endpoints delimiting new interiors are defined. In two dimensions the units are line segments while in three dimensions they are planar polygons. For example a sharp two dimensional corner is defined by the changing intersection point of the two segments that make up that corner.

The advantage of this approach is that each unit is defined at a relatively high level of abstraction. Thus relatively few units are needed to define shapes. The disadvantage of this approach is the difficulty of calculating interactions between etching primitives. In general as the etched shapes are modeled by fewer, more complex primitives the computational intensity required to calculate the change in primitives increases. When only local calculations are performed, the number of computations is low since only only a few neighbors may interact. Unfortunately, the most interesting phenomena (through-cut, shape intersections, compensation, etc.) require global calculations. This means that all primitives must be checked for interactions. There are hierarchical testing schemes that narrow the possible interactions using efficient tests, then examine only those that pass the first tests, but the computational cost is still high. Thus the attributes of models such as Slowness are only fully utilized for simple cases. For more complex cases the methods incur disadvantages.

The Cellular Automata model is a low level representation, each shape is represented by a sequence of cells. Each cell interacts *only* with its neighbors, there are no global interactions. Moreover all interactions are computationally efficient. Thus cellular automata always perform many calculations, but the individual calculations are small and only the net cost (number of calculations $\times$ cost of one calculation) is important.

Higher level methods *may* do much better but they are only faster when they do not have to do global calculations. In other words by doing a few large calculations, the other methods are superior in simple cases because the cellular automata always does many small calculations. However cellular automata excel at complex cases where heavy computation is required regardless of method.

6.2.1 Scaling

The Cellular Automata method is based on the principal of scaling. For a given mask shape, the form of the etched shape does not change if the initial mask size is scaled, although the output size and effective etch time do change. Thus the mask can be reduced to smaller and smaller sizes until the crystal nature of silicon becomes important. In effect, the cellular automata replaces many atoms in a shape with one atom. Another way of thinking about the model is to say that within the shape, groups of atoms behave as if they were only one atom obeying crystallographic laws. In this way the number of required primitives is minimized. Linearity is necessary for this to be true, linearity in the sense of scaling, but the etching itself may be nonlinear in space. Through-cut and compensation are inherently non-linear, but they scale linearly with size.

6.2.2 Empirical vs. theoretical

As mentioned in the introduction to the thesis, the analysis of the etching of silicon has been empirical rather than theoretical. The theoretical approach would involve the study of the chemistry of both the silicon and the silicon etchant. However such chemical reactions are very complex and are not fully understood. Furthermore, such a "pure" approach is beyond the scope of this thesis and is perhaps better suited to separate, independent study.

The empirical approach of this thesis is more empirically oriented. The emphasis has been on using experimental data and experimental observations to formulate empirical rules that accurately model the etching. The use of such rules allows for the efficient implementation of modelers which would otherwise be very computationally intensive. In formulating these etching rules two guidelines must be followed: (i) the rules must produce accurate results (ii) the model rules must agree with the microscopic chemical behavior.

The empirical rules used in the Cellular Automata model reduce the complexity of the interactions between cells while still producing accurate predictions of the changing shapes as a function of time.

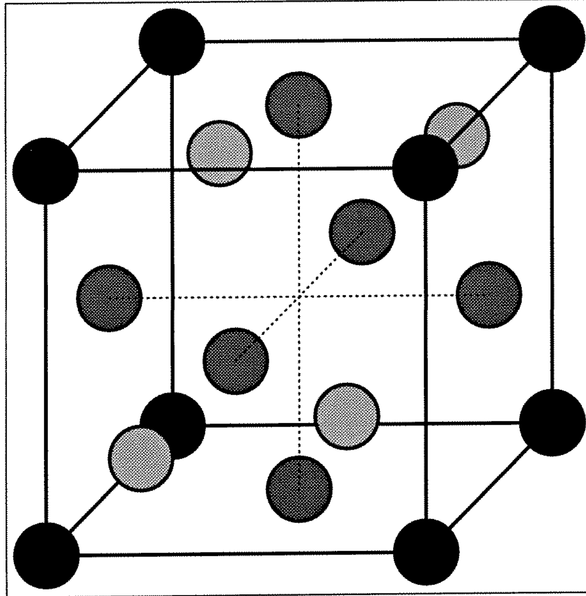

Figure 6-1: Silicon basis cell.

6.3 Two Dimensional Algorithm

The cellular automata model will first be developed in two dimensions then extended to three dimensions.

To begin developing a two dimensional cellular automata etch simulation, consider the diamond lattice crystal structure of silicon as shown in Figure 6-1. For the purposes of simulation the diamond structure of the lattice is converted into an array of cells. If we examine an x-y plane of atoms, one lattice unit cell deep, from above we see the pattern shown in Figure 6-2 and Equation 6.1 (the depth within the page is not shown). An array of cells is constructed such that it contains a 1 when an atom is present and a 0 (or is empty) when no atom is present. Each two dimensional unit cell resembles the number 5

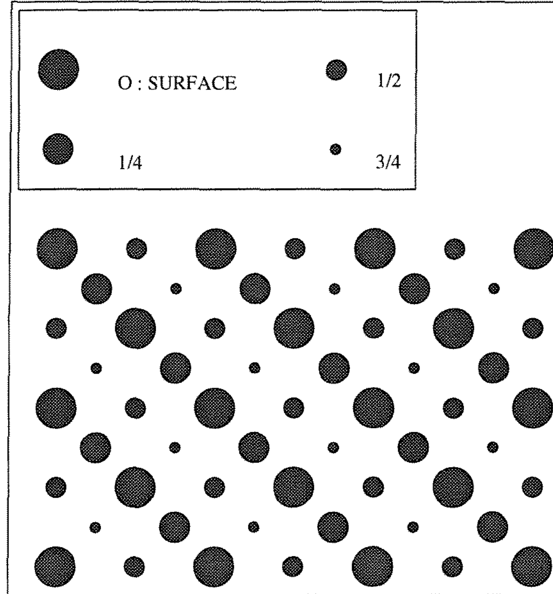

Figure 6-2: Silicon basis cell viewed from above, size indicates depth.

on a throwing die, and has four nearest neighbors, as shown in Equation 6.1.

$$\textit{cell array} = \begin{bmatrix} 1 & & 1 & & 1 & & 1 & & \cdots \\ & 1 & & 1 & & 1 & & 1 & \\ 1 & & 1 & & 1 & & 1 & & \cdots \\ & 1 & & 1 & & 1 & & 1 & \\ 1 & & 1 & & 1 & & 1 & & \cdots \\ \vdots & & \vdots & & \vdots & & \vdots & & \ddots \end{bmatrix} \qquad \textit{unit cell} = \begin{bmatrix} 1 & & 1 \\ & 1 & \\ 1 & & 1 \end{bmatrix} \tag{6.1}$$

At each cell in sequence, the number of nearest neighbors is counted along with the number of next nearest neighbors. From this information, the local plane is classified as either (111), (101), or (311). For example, the (111) plane has three nearest neighbors while the (101) plane has only two (see Figure 6-3).

As would be expected, the fastest planes (as measured experimentally) have fewer neighbors. Table 6.1 shows the neighbor conditions for the different planes. These planes were chosen since most etched shapes can be accurately modeled using these three planes.

At each time step a certain percent of the cell is removed, the larger the etch rate of the

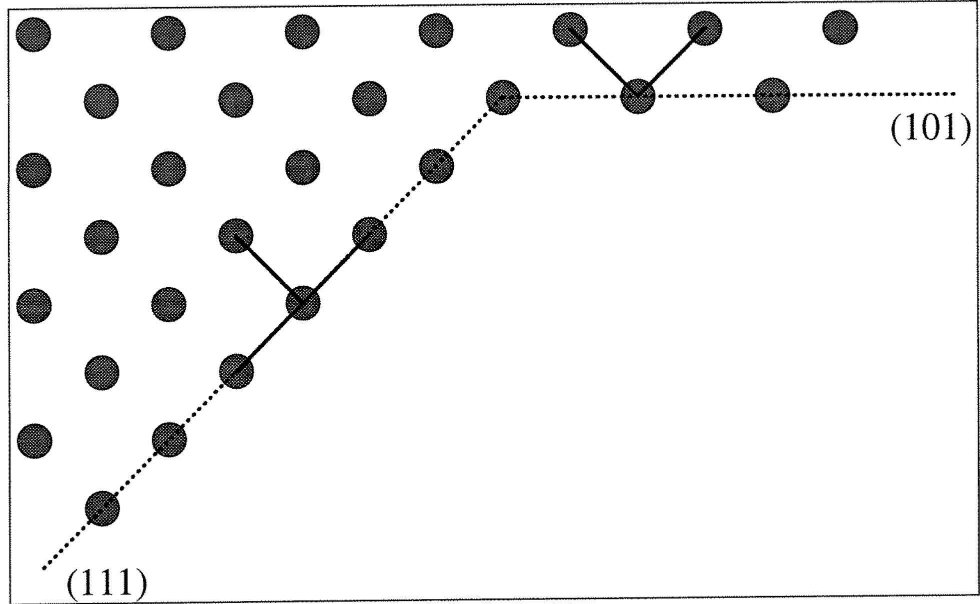

Figure 6-3: Classification of planes based on neighbors.

plane	*nearest neighbors*	*next neighbors*	*speed*
(111)	3	2	*slowest*
(100)	2	3	*varies*
(110)	2	3	*varies*
(311)	2	2	*fastest*

(6.2)

Table 6.1: Number of neighbors for etching planes.

plane the more is removed. The behavior of any etchant can be modeled by appropriate choice of etch rate for each major plane. The etch rate diagram can be varied from isotropic to highly anisotropic. When the fraction of a cell falls to zero it is removed. These steps are then repeated to find the etched shape at each time step. The algorithm uses the anisotropicity of the etchant to automatically introduce new planes.

6.4 Three Dimensional Extension

This method can easily be extended to three dimensions when a vertical stack of cell arrays is used. Once the topmost array has been calculated for a particular time, it is used to calculate the next lower array. To calculate each succeeding array, at each cell in the lower layer, examine the five nearby cells above it. If any of these cells are present, the lower cell is protected and kept, otherwise it is removed. This lower array is then used to calculate the one beneath it. This process is repeated for each time step. The final section of this chapter lists a pseudocode implementation of the Cellular Automata method.

The above extension algorithm is valid for etchants modeled by (111), (100), (101), and (311) planes. This is the case for a (100) wafer etched with EDP. Different etchants have different dominate planes; with KOH etching, the (101) planes (45 degree walls) are replaced by the (010) planes (vertical walls). If a different etchant is to be modeled, a slightly different three dimensional extension algorithm must be used.

A sample of the Cellular Automata simulations (EDP etchant) is shown in Figure 6-4. Figure 6-5 shows the result of the Cellular Automata simulation for an initial cross shaped mask. The simulation shows good agreement with the experimental results (see Figure 6-6). Note that the bounding planes for long times are the (111) planes.

6.5 Full Three Dimensional Algorithm

In addition to the two dimensional model extended to three dimensions, a full three dimensional algorithm was developed. In this case the actual diamond lattice is modeled with a three dimensional array having elements at each atom location. In three dimensions, each atom has four nearest neighbors. Referring to the five atom unit cell of two dimensions

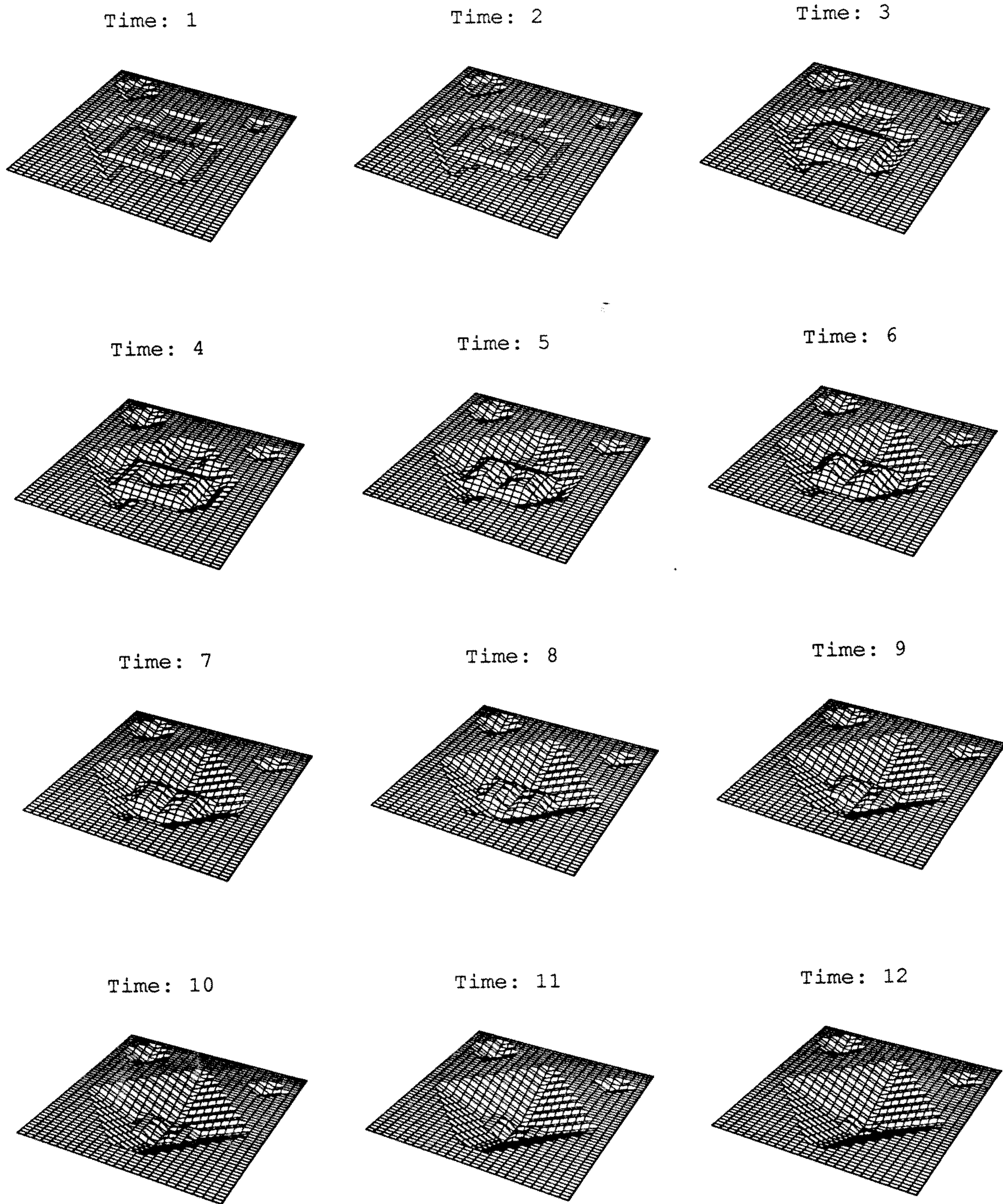

Figure 6-4: Sample of Cellular Automata algorithm output.

OUTPUT

Time: 0

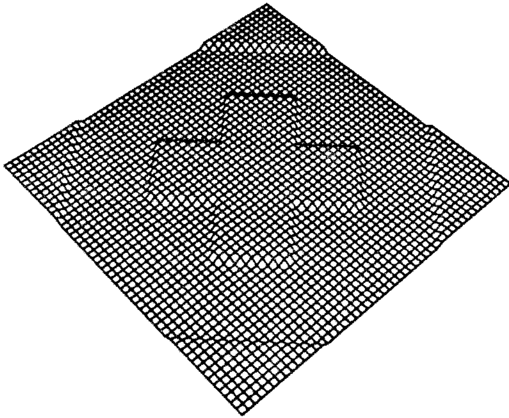

Time: 2

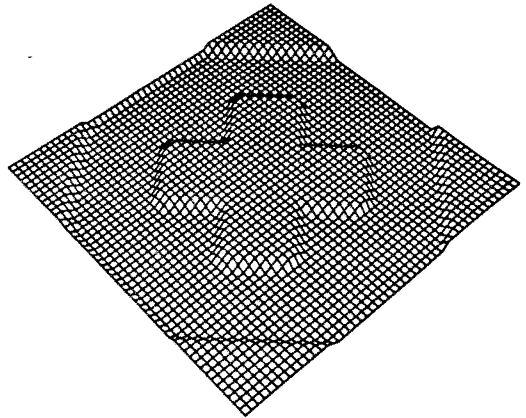

Time: 4

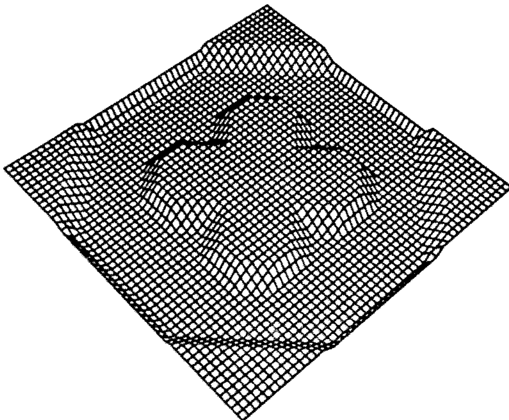

Time: 6

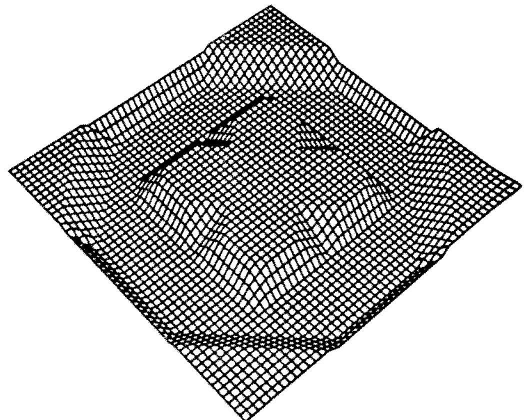

Figure 6-5: Cellular automata algorithm output for initially cross shaped pegs.

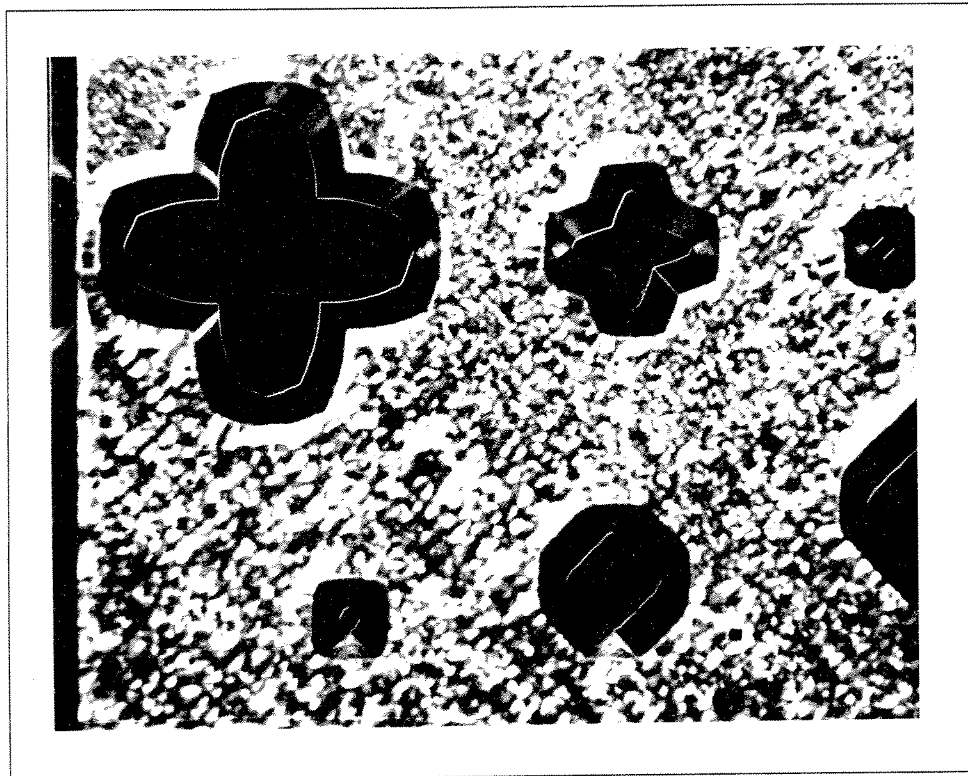

Figure 6-6: Experimental output shapes for initially cross shaped pegs.

(see Equation 6.1), the central atom remains the same but the northeast and southwest atoms are one atomic level higher while the southeast and northwest atoms are one atomic level higher. Each cell also has twelve next nearest neighbors. As with the two dimensional case, a classification scheme is developed based on the the number of nearest and next nearest neighbors. This algorithm has been used to predict output shapes with results similar to those for the extended two dimensional case. However this algorithm is slower. One reason for the slowness is that this array is not symmetric. Planes at +45 degrees (along the southeast/northwest line) will differ in height from planes at -45 degrees (along the southwest/northeast line) by two atom heights. Thus the results have to be averaged over two heights steps, and the number of calculations needed is doubled. The two dimensional extension above in effect removes this asymmetry.

6.5.1 Two dimensions vs. Three dimensions

Both the two and three dimensional algorithms produce similar results, and both classify planes according to the number of neighbors with more neighbors meaning a denser plane. However it is important to note that they do so by using two different classification schemes. The three dimensional algorithm is a general approach, while the extended two dimensional algorithm is a specialized subset of the full three dimensional case which uses certain conditions ((100) wafer) to reduce the complexity of the rules.

The choice of classification rules involves a trade off between accuracy of modeling and speed of implementation. A very complex rule system involving many neighbors will provide a more detailed model of the etching, but at the price of increased computation. The extended two dimensional algorithm was chosen over the full three dimensional algorithm since it provides a sufficiently accurate modeler in a faster, more efficient implementation.

6.6 Computational Cost

Consider an area divided into N by N cells. Most higher level approaches scale on the order of N in two dimensions, but Cellular Automata fair less well. They scale as N^3, N^2 cells are needed and the effective time scales with N; if the size of the array is doubled, then

twice as many time steps are required. In three dimensions, all models add an extra factor of N in the scaling. Note that the scaling only relates to the number of calculations, not to the net cost of calculation, and may be misleadingly biased against Cellular Automata.

Computer time is required for calculating the Cellular Automata, storing the data, and displaying the data. For three dimensional Cellular Automata, the actual calculations for twenty time steps of a 50 by 50 cell input mask, required several seconds on a Unix work station. A 100 by 100 array for 40 time steps would require a few minutes, a 200 by 200 for 80 time steps would require on the order of half an hour. Despite the rapid rise in processing time, there are measures which improve the situation greatly.

6.6.1 Area vs. volume calculations

The speed of the algorithm can be increased if the model only looks at the boundary of shapes and not at the entire shape. In two dimensions this means modeling the perimeter and not the area of a shape; in three dimensions, the surface area and not the volume is considered. This can lead to a marked increase in performance, but this increase is only seen at larger sizes since there is a cost overhead associated with keeping track of the perimeters. It is vital to update the changing perimeter since through-cut may create or destroy individual shapes and their perimeters. This approach can make the Cellular Automata model much more competitive with some higher level models.

6.7 Cellular Automata Advantages

Cellular automata models were designed and tested and were found to be useful tools for in MEMS design. The algorithm used is very efficient, is easy to implement and requires little computational time. Cellular automata have the added benefit of being extremely robust since only local calculations are performed. Cellular automata excel at complex cases where heavy computation is required regardless of method. For instance, the most interesting phenomena in MEMS design (through-cut, intersections, compensation, etc.) have been successfully analyzed with the Cellular Automata algorithm reported in this chapter.

6.8 Implementation

Listed below is a pseudocode implementation of the extended two dimensional Cellular Automata method. Comments are denoted by (* comments *).

```
1)    Create (N x N x depth) array
      Create (N x N x depth) temporary array
2)    Transfer mask in array level 1
3)    Input percentages to be removed for each plane
4)    (* Two dimensional algorithm *)
      For each (i,j) element in level 1:
          count occupied nearest cells: (i+1,j-1), (i+1,j+1), (i-1,j-1), (i-1,j+1)
          count occupied next nearest cells: (i,j+2), (i,j-2), (i+2,j), (i-2,j)
          use Table 6.1 to classify plane
          remove proper percentage of cell (i,j) in temporary array
      Switch level 1 of array and temporary array
5)    (* Three dimensional extension *)
      Set depth level k=2
5.b)  For each (i,j) element in upper level k:
          count occupied nearest cells in level k-1: (i+1,j-1), (i+1,j+1), (i-1,j-1), (i-1,j+1)
          if count = 0 then remove cell (i,j) in level k of temporary array
      Switch array and temporary arrays
      Set depth level k=k+1, while k < depth loop to 5.b
6)    Write array
7)    Loop to step 4 for next time step
```

Chapter 7

Synthesis

In this chapter I will examine general phenomena that are encountered in MEMS fabrication, and show the significant impact these phenomena have on design.

7.1 Design Paths

The first step in systemizing MEMS design is to classify shapes into three broad classes. The first class is the limit shape class, the shape to which holes tend to evolve. Limit shapes are stable in that no planes appear or disappear; as time increases that retain their proportions. The second class is the linear shape class, which are "stretched" versions of the limit shapes. Linear shapes do change with time, but no new planes appear and none disappear. Linear shapes linearly converge to limit shapes and design inversion is always possible. This means that an input mask shape can always be found that will create a desired linear shape. These two types of shapes are then said to behave linearly. Linear behavior has two consequences:

a) The etching can be run backwards or forwards in time.

b) Given the shape at any time, the shape at any other time can be found.

The third class consists of general shapes. These shapes change non-linearly with time and planes appear and disappear. Types of non-linear behavior include:

a) The etching produces different results if run in different directions.

b) Knowing the shape at one time may not fully specify the system for all times.

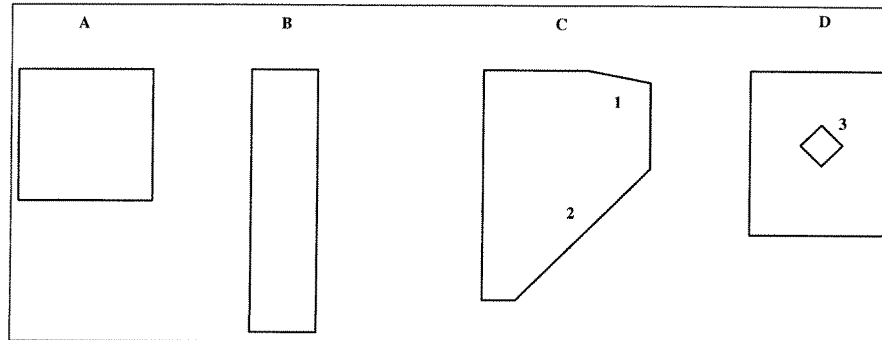

Figure 7-1: EDP etchant: (A) limit shape, (B) linear shape, general shapes (C) and (D).

Examples of such behavior will be presented later.

7.1.1 Linear zones

General shapes behave linearly until a plane disappears. Figure 7-1 shows some examples for and EDP etchant: A and B are limit and linear shapes, shape C is guaranteed to behave linearly until plane 1 or plane 2 disappears, and shape D is guaranteed to behave linearly until peg 3 disappears. Once a plane appears or disappears then the behavior changes. The time for which a shape behaves linearly is called the linear zone and may be very short. Linear and limit shapes are shapes whose linear zone is infinite. During the linear zone of a shape, inversion can always be performed. Inversion may be possible outside this zone, but there is no guarantee of this inversion.

7.2 Time Plots

Consider some initial shape modeled by an envelope of lines as shown in Figure 7-2. The initial shape can be described by sampling the shape at N θ values (N=8 for Figure 7-2) and finding the radius r_i for each sampled angle θ_i. The r_i's change with time; we can draw N two dimensional plots showing the radius of intersection as a function of time. Figure 7-3 shows one such plot. At time equals zero the radius is given by the initial value r_0. The radius then changes at some rate which depends on the plane present at the angle θ_i. The curve which describes the radius as a function of time is always continuous but may be

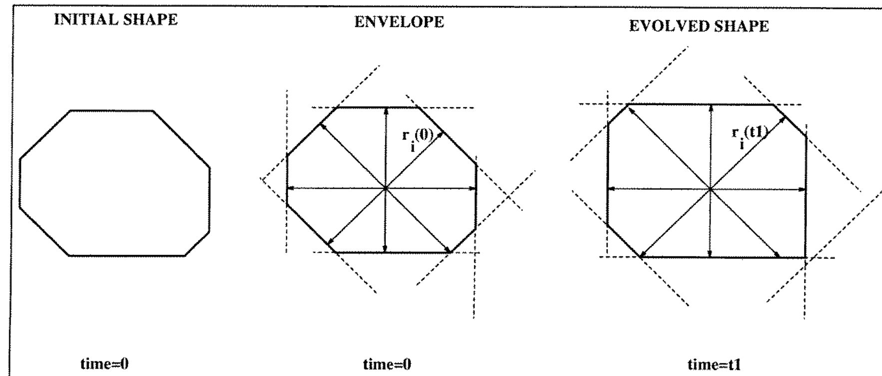

Figure 7-2: Sampling of a shape.

discontinuous in slope. The discontinuities in slope signal times at which the plane at θ_i changes due to the disappearance of one or more planes. Holes slope upward and pegs slope downward. Additionally, the radius is single valued in time since planes cannot reappear after they disappear.

What is the behavior of limit shapes in such plots? Limit shapes maintain their proportions, they simply become larger. No new planes emerge and no planes disappear. Therefore the time path in the plots is a constant slope line, and the limit shapes lie along a line termed the Limit Shape Line (LSL) (see Figure 7-3). At large times, the curve for a general shape parallels the limit shape line (see Figure 7-3) and the original dimensions become negligible compared to the etched dimensions. Thus any general shape eventually closely approximates the limit shape.

Because planes neither appear or disappear, the path of a linear shape is a straight line parallel to the Limit Shape Line (see Figure 7-4). The path of a linear shape is offset from the Limit Shape Line, but the offset become negligible for large times.

7.2.1 Design inversion

For linear shapes, changes in length occur linearly so that it is possible to interpolate between the present linear shape and the limit shape. More importantly, it is possible to extrapolate backward to the required initial mask shape (see Figure 7-4). A shape parameter, such as

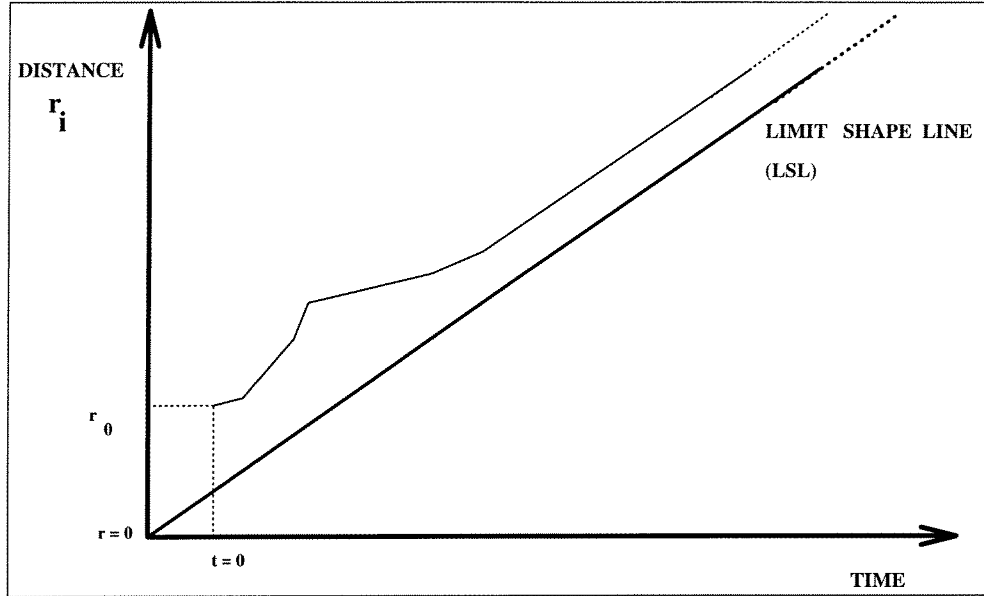

Figure 7-3: Radius versus time plots.

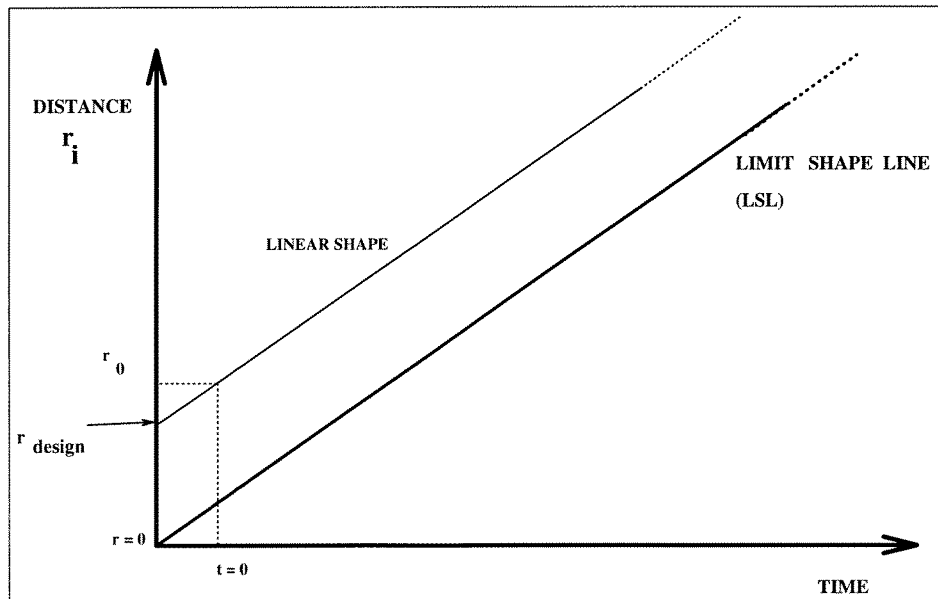

Figure 7-4: Extrapolation and interpolation of linear shapes.

r, at time t is given in terms its initial value at some time t_1 by

$$r(t) = r_1 + (t - t_1) * (r_\infty / t_\infty) \tag{7.1}$$

where r_∞/t_∞ is the slope of the limit shape line and r_∞ is the parameter r at large time t_∞. This design inversion is guaranteed to be possible with linear shapes.

Design inversion using time plots is done by extending the path of each radius backwards in time to determine the necessary input shape to obtain a desired output shape at some later time. For linear or limit shapes, the extension is simple since all paths are simply straight lines with known slopes. Moreover, the paths for linear and limit shapes are all independent of each other. For general shapes, this not necessarily true. As the path of a general shape are extended backwards, all N plots must be considered simultaneously since the changing length of some planes may cause the disappearance of some other planes. Once a plane disappears at some angle θ_i, the slope of the path for r_i changes which in turn effects the evolution of all N paths. While it may be possible to invert some general shapes, there is no guarantee that such an inversion is possible for any arbitrary shape, and the method for finding this inversion (if it exits) is certainly not trivial.

In fact for some shapes inversion is strictly impossible. For example, an isotropic etchant can never etch a square hole in one step. A square hole may be approximated and a square peg is possible, but the original problem is unsolvable. From Minkowski transformations the required initial shape is a self-intersecting square with cusps at its corners and is thus impossible to obtain since no real mask loops over onto itself. This topic will be explored at greater length below.

7.3 Path Plots

In order to better understand the different phenomena observed in MEMS we will look at the simultaneous change of two parameters as shown in Figure 7-5. In this case, the etching proceeds from one point on the plane to another. There is also a limit shape line in this diagram, but its slope depends on the slopes of the two limit shape lines associated with the distance versus time plots. In this plot holes have a positive radial component

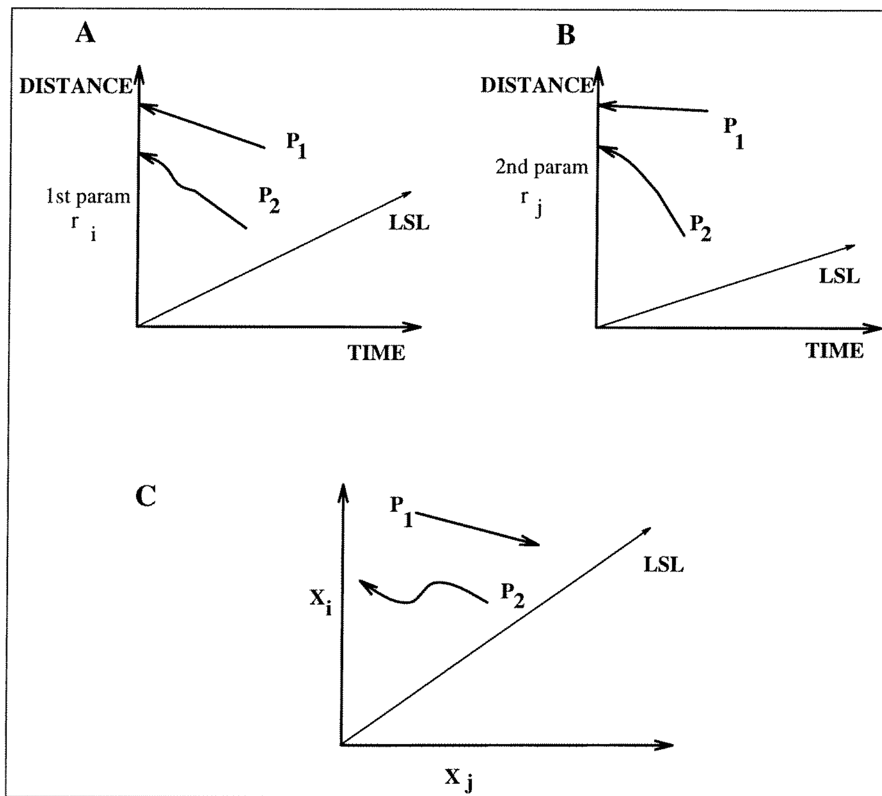

Figure 7-5: (A) and (B) distance parameters versus time; (C) distance parameter versus distance parameter.

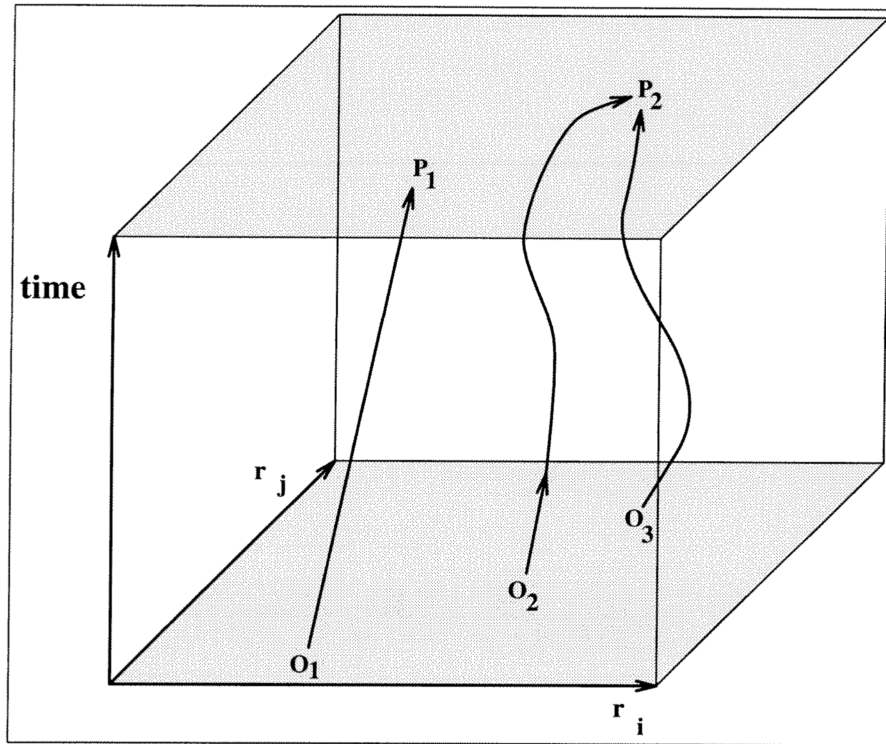

Figure 7-6: Two dimensional paths from zero time. Some paths are linear, some are not.

while pegs have a negative radial component. There is a time increase associated with the shape change. In reality, all N parameters need to be examined in order to find the path in N space, but only two at a time can be displayed in two dimensions. The third dimension will be used to denote time as shown in Figure 7-6.

In Figure 7-6, the initial shape in terms of two parameters X_i and X_j at time equals zero is represented by O, at a later time the shape is represented by P. In the linear shape case O_1 evolves linearly into P_1. The same holds for any shape within its linear zone, however a general shape O_2 evolves non linearly into its output P_2. While there is only one linear path to any particular point P_i, there may be multiple (or infinite) paths to a general point (e.g. $O_2 \rightarrow P_2$ and $O_3 \rightarrow P_2$). The reason why general shape transformations are unique in one direction, and non-unique in the other direction is because of disappearing lines in two dimensions and disappearing planes in three dimensions. Once a line or plane disappears, information is lost and cannot be recovered. The limit shape is an example of this: all holes

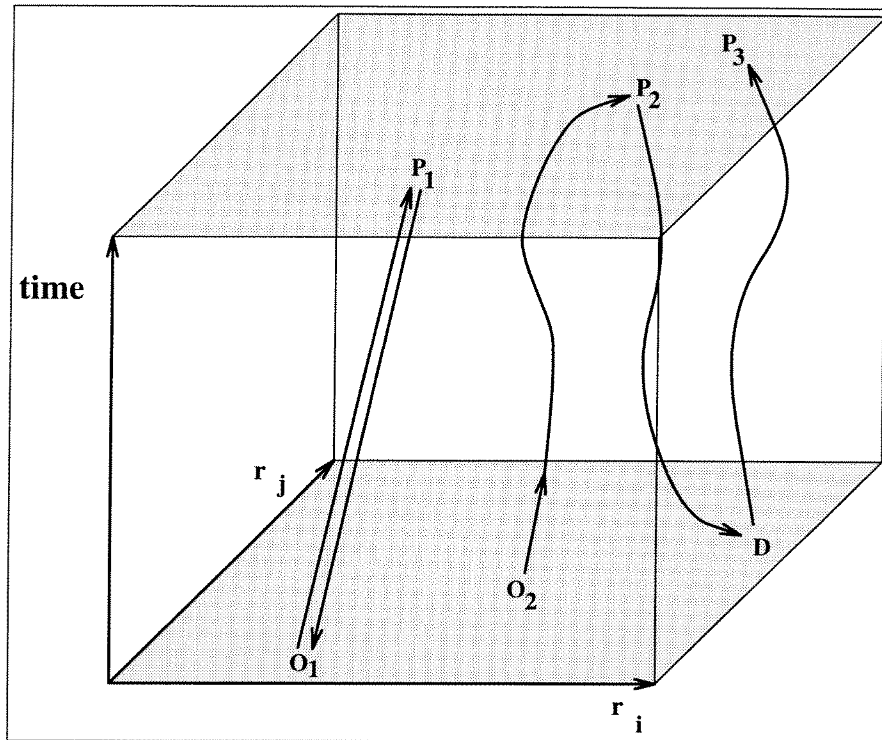

Figure 7-7: Paths forward and backward in time.

converge to the limit shape so it is impossible to determine a unique initial shape from the limit shape. The non-uniqueness of paths can (and does) complicate general design, while a given input will always produce the same output, many different inputs may give the same output.

7.4 Negative Time

One possible design method is to use an etch simulator with negative time. The desired output is used as input and the simulator is run backward in time. Running a simulation backwards in time will work for linear shapes and any shape in its linear zone, since such transformations are unique. As shown in Figure 7-7 the required input (O_1) for a desired output (P_1) can be found: $O_1 \rightarrow P_1$ and $P_1 \rightarrow O_1$. However, the case is different for a general shape. If P_2 is the desired output and O_2 is required input, the negative time simulation produces an input D which when simulated with positive time may, or may not,

produce some different output P_3. This can occur because the non-linear nature of the etch means that planes can appear and disappear; the simulator cannot recreate a plane once it has disappeared. Figure 7-8 shows a simple example of this behavior. A square torus (a square peg within a square hole) is etched in an EDP-like etchant until only a square remains, next the etching is run backwards in time to obtain a smaller square. Here the original shape and the derived shape differ since some lines have disappeared.

This same effect is observed in Minkowski transformations. Minkowski addition of two shapes is analogous to etching forward in time while Minkowski subtraction is analogous to etching backward in time. Consider a case where the desired shape is C. If A represents the required initial shape and B represents the etchant (or "brush" in the painting analogy), then $C = A \oplus B$ and negative time etching is $C \ominus B$. When B is added and subsequently subtracted from the input shape A this operation is termed "closing a shape" and does not necessarily return the original shape A:

$$(A \oplus B) \ominus B \neq A \tag{7.2}$$

Often the output shape can be drastically different from the input. In Figure 7-9 an input shape O_1 can produce P_1 rather than the desired output G_1. Design inversion means finding the input shape or shapes (D_{1a} and D_{1b}) that produce the desired output in the forward path. Some desired goals (G_2) may not be attainable and an approximate shape (A_2) should be used as a design goal.

This approach identifies the types of behavior associated with shape transformations. However it does not provide the necessary design inversion techniques. While it shows the types of paths possible, it does not specify how to find these paths. These factors will depend on the etchant used. Rather than being a prescription for design, this approach is perhaps best used as a diagnostic tool.

7.5 Possible and Impossible Shapes

In this section we will examine whether or not certain shapes can exist. This is not a question of whether or not a shape can be formed with an etchant, but rather is an examination of

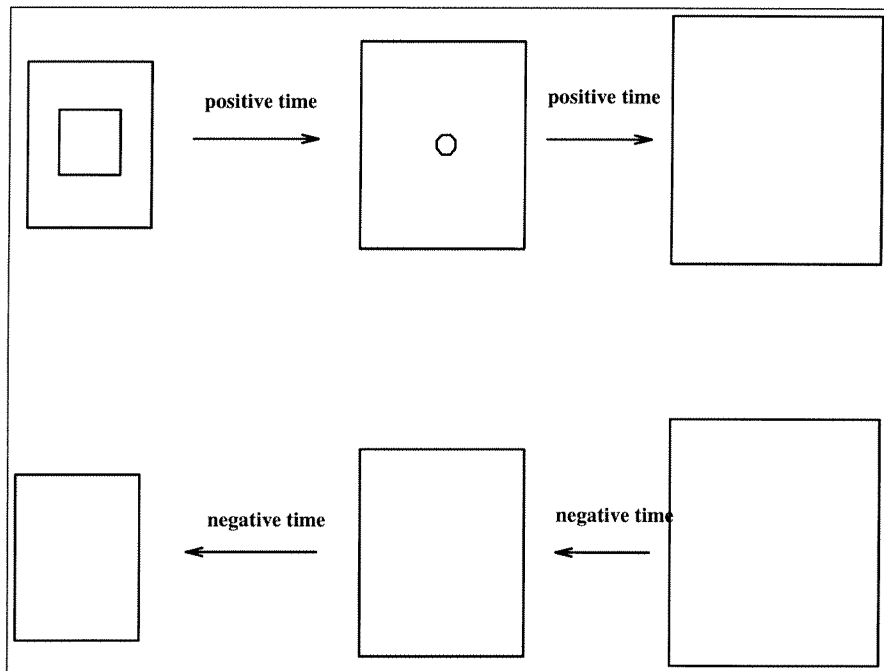

Figure 7-8: Running etch simulators backwards in time will not recreate the initial shape if lines disappear.

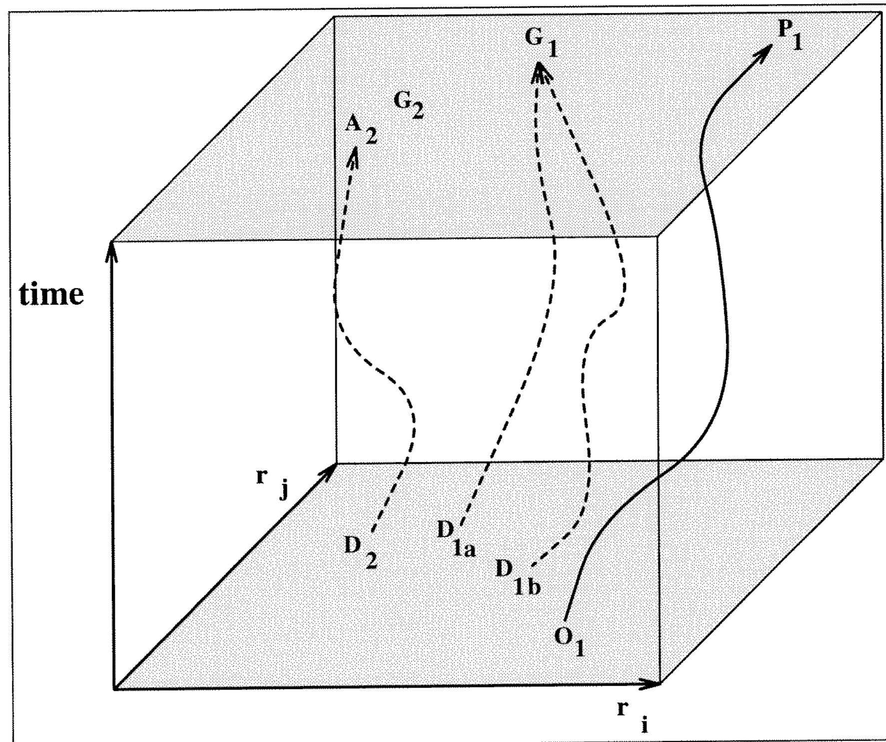

Figure 7-9: Design paths.

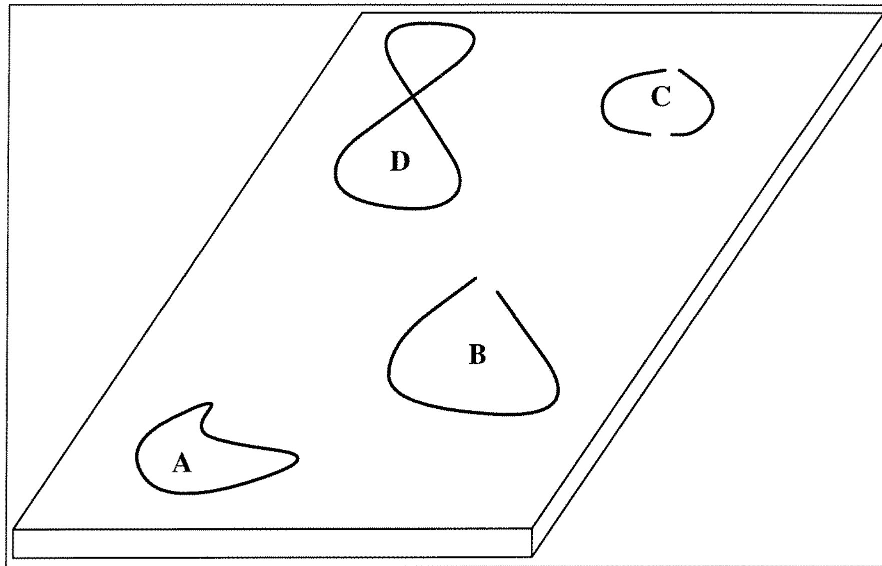

Figure 7-10: (A) possible hole shape; impossible hole shapes (B), (C), and (D).

the geometry of shapes. If a shape is to be made out of some real material it must obey certain rules.

Consider a number of holes in a block of material. Figure 7-10 shows the surface outlines of several holes some of which are possible (A), some of which are not (B, C, D). Hole B is impossible because the outline curve is not closed. Hole C is not connected which is just a double occurrence of hole B. Hole D is also not possible since it self intersects. We shall see that self intersections have a profound effect on both the simulation of etched shapes and the design inversion of such etching.

Figure 7-11 shows why self intersections cannot exist in real shapes. The surface outlines of a hole, a peg, and a self intersecting shape are shown, with a three dimensional figure below each. In the surface outlines, the shape is represented by two lines, the solid line is on the side of the shape which is still unetched, the dashed line is on the side which has been etched. If the process being modeled is not etching, then the solid line is where there is material and the dashed line where there is none. Thus a hole has a solid line surrounding a dashed one and the three dimensional view of the hole is shown below it. A peg has a dashed line surrounding a solid one and similarly the three dimensional view is directly

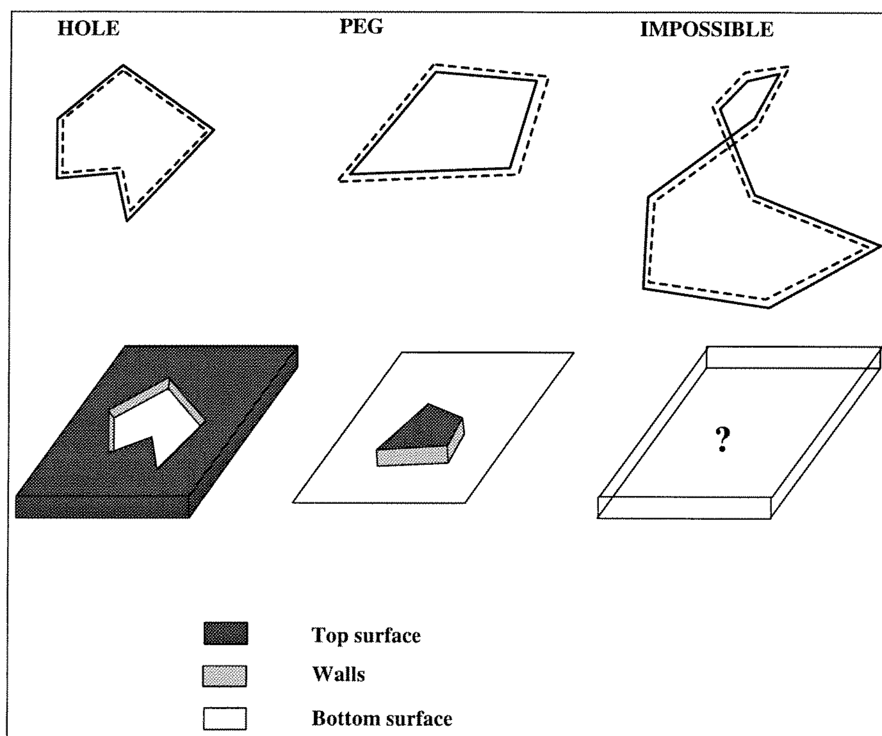

Figure 7-11: Holes, pegs and self intersecting shapes.

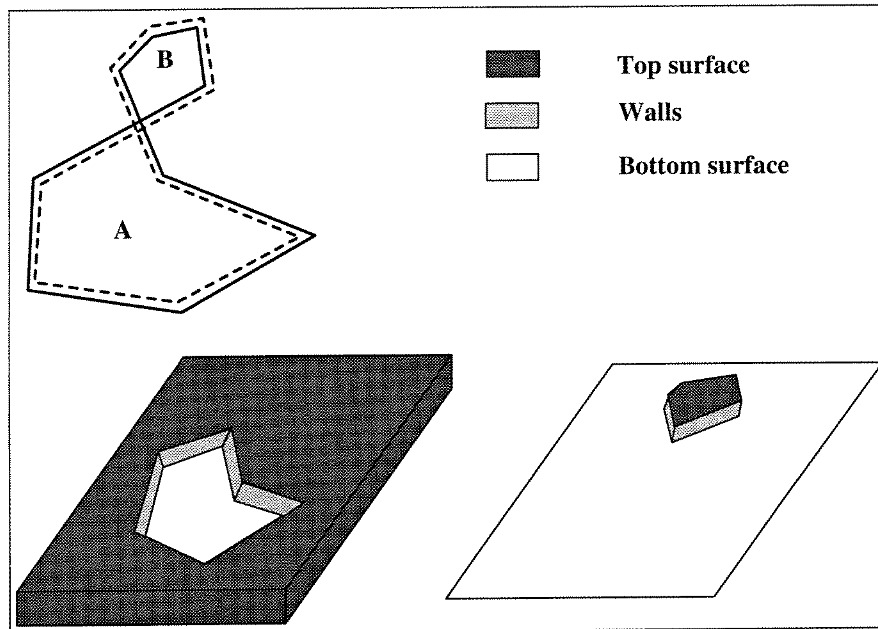

Figure 7-12: Contradictory three dimensional parts of self intersecting shape.

below. The self intersecting shape is impossible because different parts of the shape are hole-like and others are peg-like. As shown in Figure 7-12, part A is a hole while part B is a peg. But both these conditions can not be fulfilled simultaneously, the two conditions are mutually exclusive. In fact The two dimensional outline of a self intersecting shape is not "flat"; it is a sort of Mobius strip. Parts of the shape lie on the top surface, while others lie at the bottom surface making it impossible for both to exist at the same time. If we trace a circuit around a self intersecting shape the reference wafer plane changes from top to bottom and back to top; such shapes can be compared to M. C. Escher waterfalls where the water makes similar circuits.

If an etch simulation produces self intersecting shapes, then the non-physical portions should be removed. This is shown in Figure 7-13 where a rectangular peg is etched isotropically and the cusps on the simulated output shape are removed to get the final output shape.

Self intersecting shapes can occur in many different models and are not specific to any one simulation method. For example the offset surfaces encountered in NC milling are

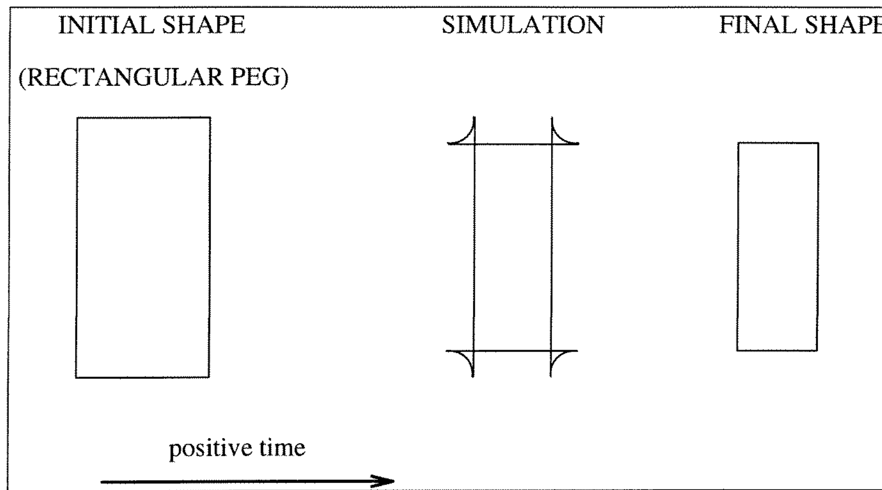

Figure 7-13: Isotropic etching of a rectangular peg and removal of cusps.

equivalent to isotropic etching. However since etching is often highly anisotropic, the self intersection problem is much more complicated and appears more often in etching. Much work has be done on the subject of offset surfaces yet many facets of the problem remain unresolved. The self intersection problem in etch simulation is even more challenging due to the added difficulty of anisotropy.

The theoretical existence of impossible shapes effects the design process greatly. We have seen that running a simulation backwards in time in order to do design inversion may fail if planes disappear. Unfortunately backwards simulation may also fail because of self intersecting shapes. If a desired output shape is etched backwards in time and a self intersecting shape occurs, then the only way to obtain the exact desired output shape is to begin with an impossible input shape: in other words some output shapes can never be etched with some etchants. For example Figure 7-14A shows a rectangular hole being etched backward in time with an isotropic etchant. If the desired output shape is a rectangular hole then the necessary input shape is impossible to obtain. Figure 7-14B shows a diamond shaped hole being etched with an EDP-like etchant and the resultant octagonal shape obtained. If a diamond shaped output is desired, then the backward simulation in part B of the figure once again produces impossible input shapes. This method can be used to determine whether or not a shape can be produced with a given etchant. If it is not

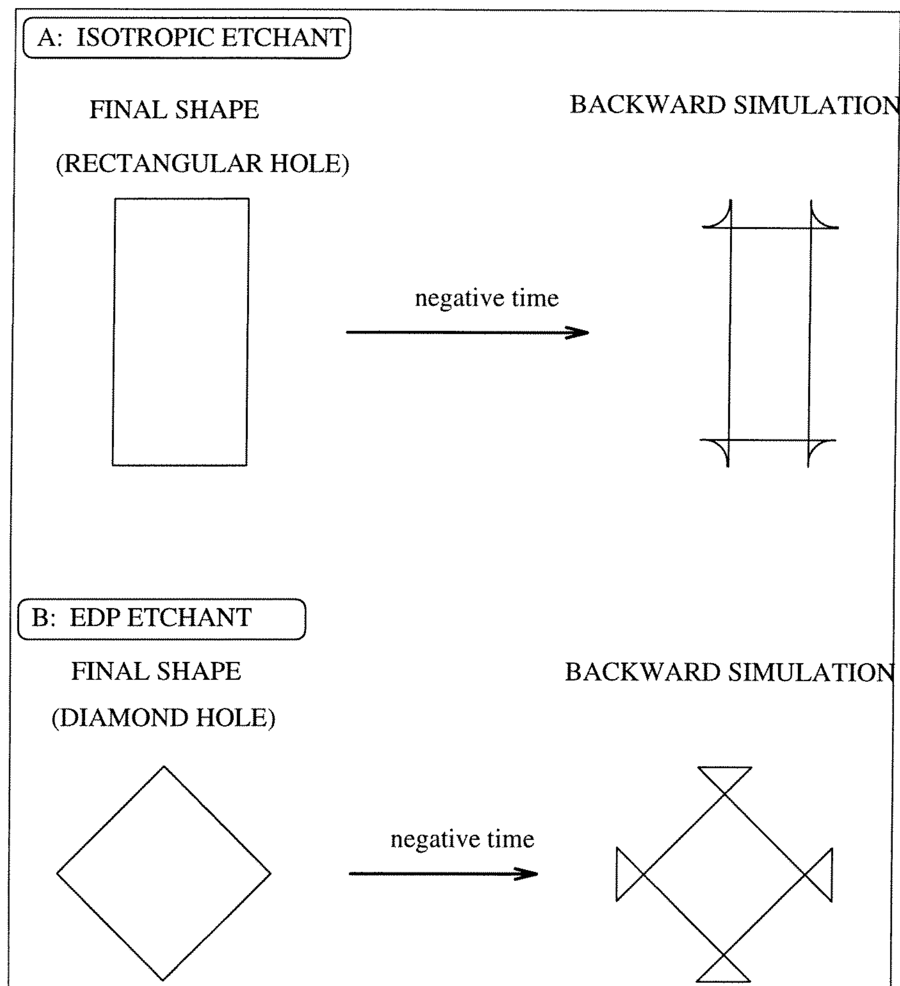

Figure 7-14: Backward simulations which yield impossible input shapes: (A) rectangular hole in isotropic etchant; (B) diamond hole in EDP-like etchant.

possible to obtain a certain shape, an approximation of that shape may still be obtained as was shown earlier for the diamond shaped hole in EDP-like etchants.

7.6 Model Comparisons

In this section we will compare different MEMS etch simulation modeling methods to determine their relative advantages and disadvantages. The methods I will compare are: Slowness method [27, 67], Wulff-Jaccodine method [36, 20, 16], Eshape method, and Cellular Automata method. The Eshape and Cellular Automata methods are described in

Chapters 5 and 6 respectively, while the other methods are described in Chapter 2.

7.6.1 How do the models differ?

In two respects, all the models discussed are similar: they give the same results (within the limiataions of each model) and they model the same processes. In fact the mathematics are the same for many models, for example the Eshape model and the Wulff-Jaccodine method are based on the same mathematics, although the implementation is completely diffeerent. The differences between all models lie in the trade-offs that are made, and in the aspects that are emphasized and those that are not.

What are the differences between existing models and the three models developed in this thesis, the Eshape model, the Shape Library method, and the Cellular Automata model? The Eshape model is most similar to the Wulff-Jaccodine method. The approachs are based on the same mathematics, but the Eshape method uses the mathematics as a starting point rather than an end point; this provides a method for design inversion. The Cellular Automata method departs from a formal mathematical treatment and instead uses a rule base system to model the interactions between atoms or cells in a shape; this provides more robustness. The Shape Library is perhaps the most different approach since it concentrates of the general behavior of etchants rather than providing specific shape modeling; this sacrifices detail for flexibility.

7.6.2 Itemized comparisions

Several criteria will be used and are described below. The results are summarized in Figures 7-15 and 7-16.

- Three Dimensionality

  Is the model strictly two dimensional or can it be extended to three dimensions?

  The Shape Library, Slowness, and Cellular Automata methods are all easily extended to three dimensions. The Eshape method theory can be extended to three dimensions and the approximate simulations maybe done for shallow depths. The Wulff-Jaccodine method is primarily but not exclusively two dimensional.

- Robustness and Through-cut

  Can the model deal with interactions between different parts of the shape?

  Robustness refers to interactions between neighboring planes or neighboring corners. Through-cut refers to interactions between two shapes or two initially distant but now adjacent parts of the same shape. Robustness is local while through-cut is global. The Cellular Automata model is robust in all cases and through-cut is handled automatically. The Eshape and Wulff-Jaccodine methods are not very robust and do not consider through-cut. The Slowness method performs nearest neighbor calculations and is relatively robust, although it also does not consider through-cut. The three previous methods can all be made to deal with through-cut, but additional processing must be done and the computational cost is very high. The Shape Library method deals only with limit shapes and robustness criteria are not applicable.

- Design

  Can the model be used to work backwards from the desired output to determine the required input?

  The Slowness, Wulff-Jaccodine, and Cellular Automata models offer few design capabilities. The Eshape model allows design inversion in some cases. The Shape Library method does allow design but the at the etchant and wafer cut level rather than at the input mask level.

- Speed

  Is the model relatively fast or slow?

  The Shape Library method is a one step process and is very fast. The Slowness, Wulff-Jaccodine, and Eshape methods are all relatively fast. However the Slowness method is iterative while the Eshape is one step. The Cellular Automata method is iterative and is relatively slow at larger scales and higher resolutions.

- Post-Processing

  Is some processing required after the simulation?

The Shape Library and Cellular Automata methods require no post-processing. The Eshape method requires some processing for self-intersecting corners while the Wulff-Jaccodine requires intensive post-processing to find intersections between planes. The Slowness method requires few post-processing operations since it performs nearest neighbor processing at each time step.

- Isotropic/Anisotropic Etchants

  Can both isotropic and anisotropic etchants be modeled?

  Models such as the Shape Library and the Eshape model can deal with arbitrary etchants. Models such as the Wulff-Jaccodine and Slowness methods work best on highly anisotropic etchants where a few planes dominate the etching. The Cellular Automata model approximates etchants using neighbor rules which may limit its accuracy in modeling some etchants. More refined rules may be formed using more neighbors, but the computational cost increases.

- Non-idealization

  Can non-ideal effects be included in the model?

  The Eshape and Wulff-Jaccodine models are strictly idealized. With some modification the Slowness method can incorporate time varying rates. The Shape Library method can model effects such as noise in etch rates and wafer misalignment. The Cellular Automata method easily models non-ideal effects such as time varying etch rates and location dependent effects such as diffusion. This is done by changing the local etch rules for each cell.

7.6.3 Disadvantages

The main disadvantages of each method are listed below:

- Cellular Automata: no formal design inversion capability, slower at larger scales and higher definitions, approximates etchants.

- Shape Library: changeable design parameters are etchant and wafer cut which are much less controllable than mask shape, limited number of output shapes.

	WULFF/ JACCODINE	SLOWNESS	ESHAPE	CELLULAR AUTOMATA	SHAPE LIBRARY
3D	✕	◎	○	◎	◎
ROBUSTNESS	✕	✕	✕	◎	⋇
TRU-CUT	⋇	✕	⋇	◎	⋇
DESIGN	⋇	✕	◎	✕	○
SPEED	○	○	○	⋇	◎
POST-PROCESS	⋇	○	✕	◎	◎
ISO/ANISO	◎	○	◎	⋇	◎
NON-IDEAL	⋇	✕	⋇	◎	○

WEAK ⋇ ✕ ○ ◎ **STRONG**

Figure 7-15: Graphical comparison of different methods.

	WULFF/ JACCODINE	SLOWNESS	ESHAPE	CELLULAR AUTOMATA	SHAPE LIBRARY
3D	mostly 2D	yes	shallow 3D	yes	yes
ROBUSTNESS	no	n. n. only	no	yes	N/A
TRU-CUT	no	no	no	automatic	N/A
DESIGN	N/A	no	yes	no	no
SPEED	graphical	iterative	one step	slower	one step
POST-PROCESS	many	few	intersections	none	none
ISO/ANISO	yes	best on aniso	yes	approx.	yes
NON-IDEAL	no	can be done	no	yes	can be done

Figure 7-16: Comparison of different methods.

- Slowness: no formal design inversion capability, less design capabilities than Eshape, not robust for through-cut, best on anisotropic etchants.
- Eshape: unrobust (less robust than Slowness).
- Wulff-Jaccodine: no formal design inversion capability, unrobust (less robust than Eshape or Slowness), best on anisotropic etchants.

7.6.4 Advantages

The main advantages are listed below:

- Cellular Automata: robust (including through-cut), can be non-linear
- Shape Library: models rate and wafer cut effects
- Slowness: good simulator
- Eshape: fair simulator, good design capabilities
- Wulff-Jaccodine: easy to implement, graphical

7.7 Design Approaches

Which is the best design tool?

No best design tool exists since each tool has its own advantages and disadvantages. The best choice will depend on the specific application. While design inversion is the ultimate goal, all the models discussed can perform simulations. In many cases what is called design is actually the iterative use of simulators to informally converge on some suitable input for a desired output. All the models discussed can be used in this fashion and a user can develop considerable skill in this iterative process.

If the application calls for relatively straight forward simulations then the Slowness, Wulff-Jaccodine or Eshape would be good choices. If a more design oriented approach is desired then the Eshape is a good choice. If the application has flexibility in etchant or wafer then the Shape Library is a good choice. Very complicated structures with many

interactions are well suited to Cellular Automata methods. Finally different parts of a structure may be analyzed using a combination of models.

Chapter 8

Applications

8.1 Compensation Simulation and Optimization

8.1.1 Introduction

This chapter presents examples of simulation and optimization of wet etching corner compensation as utilized in bulk micromachining.

As previously discussed, when silicon is etched with anisotropic etchants, the corners change shape as a function of time. If the output shape at a certain time is not the desired final shape, the initial mask defining the input shape must be modified so as to produce a more desirable output shape. One way to counteract the distortion is to cover or extend the corners in question with compensation structures which are sacrificial in nature [2, 5, 49, 56, 61, 88].

Until the structures themselves are etched away the original corner is temporarily protected. In effect the structures delay the time at which etching of the corners begins; they "buy time". In most cases, though this chapter will consider other cases, the corners in question are 90 degree corners such as would be found on an originally square peg. For such a shape, there are a variety of structures which will provide some protection. This chapter will address the following question: given a list of possible structures, what is the best optimization strategy in order to obtain maximum delay time and high reproducibility while minimizing the required structure size?

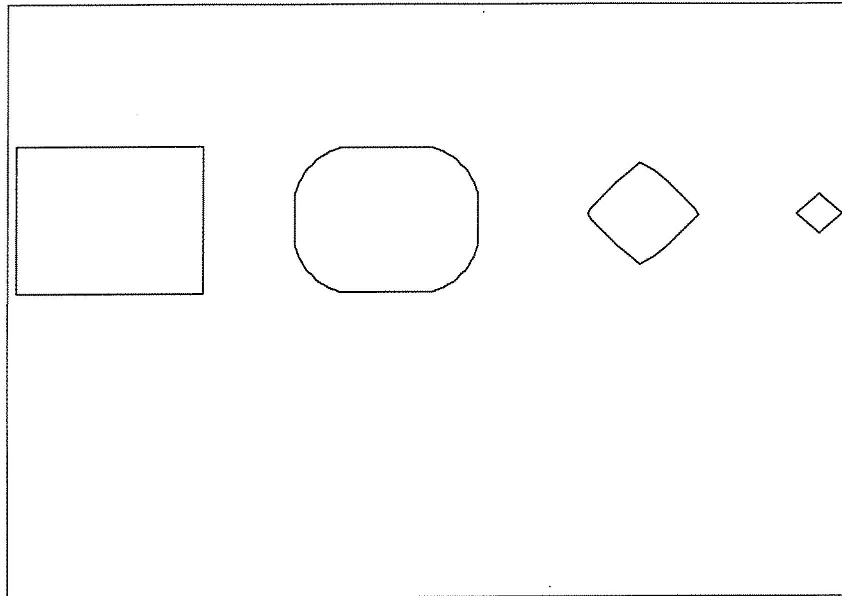

Figure 8-1: Successive degradation of initially square peg.

8.1.2 Experiments

Multiple experiments were carried out on (100) silicon wafers with a 8000 $A°$ thick oxide masking layer. The experiments were done with both EDP and KOH at 95°C and 60°C respectively.

One of the experiments was the preservation of a rectangular peg, Figure 8-2 shows the initial mask used. For long etch durations, the uncompensated peg becomes rounded and for very long etches the top surface is pinched off as shown in Figure 8-1.

The purpose of the compensation was to provide as large a final top surface area as possible with a limited compensation area. The compensation structure was limited to lie within the rectangle bounded by the four tiny squares in the top right hand corner of Figure 8-2; the compensation size could only be of the same order as the original rectangle. While most of the compensation structures are pegs, holes were also used in to make an ring-like final shape that has a large top perimeter.

A 5 x 5 array of compensation structures was repeated at full, three quarter, and half scale and etched for 4.5 and 6 hours in EDP, producing etching depths of about 200 and 350 microns respectively. By the time scaling rule (discussed in Chapter 5), this produces

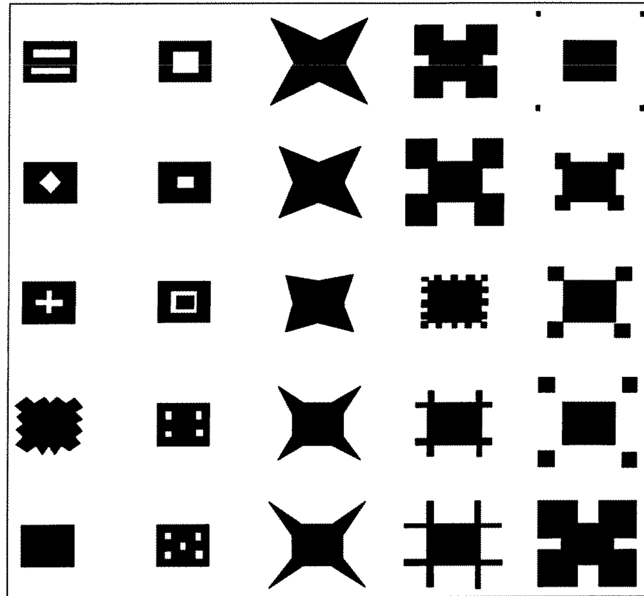

Figure 8-2: Initial mask of array of compensation structures including uncompensated rectangles (lower left and upper right).

snapshots of the time evolution at 4.5, 6, and 9 effective hours for the 4.5 hour etch and 6, 8, and 12 effective hours for the 6 hour etch. Comparison of the full scale 6 hour etch and the three-quarters scale 4.5 hour etch confirms the time scaling rule.

Figure 8-3 shows the simulated output shapes at various times for various compensation structures. Each unit of time corresponds to approximately one hour etch in EDP.

Figure 8-4 shows the output shapes at various times. The simulations and experiment show good agreement.

8.1.3 Optimization and Design Guidelines

The following design guidelines were established based on the preceding simulations and experiments.

8.1.4 Quality versus quantity compensation

For a given limited area it was found that the maximum compensation was provided by a rectangular structure (shown in Figure 8-3D). However, the most reliable and uniform

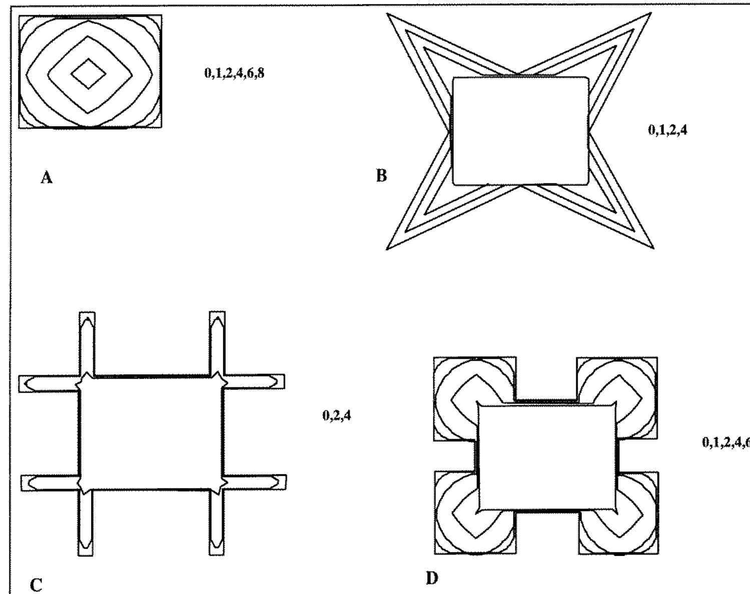

Figure 8-3: Evolved shapes at different times. (A) uncompensated rectangle; (B) fin compensation; (C) bar compensation; (D) rectangular compensation.

compensation was provided by fin structures as shown in the center row of Figure 8-4. The reason for this is apparent from the simulations. The squares distort and change shape as time increases. In contrast, the fin structures simply get smaller, they maintain their proportions.

8.1.5 Observations

Unfortunately, compensation is governed by the fastest planes, so reproducibility is impaired because the fastest etch rates are especially sensitive to variations in etching time and etching behavior.

It was found that for fin structures, the maximum etch duration and compensation quality was largely independent of fin angle. This is due to the fact that the fins are quickl dominated by the fastest planes and are identical thereafter.

It was found that for sharpened bars (shown in Figure 8-3C) , the lateral speec dissolution was linear in time and independent of bar width. However, square bars of larger width have a time offset compared to thinner or sharpened bars. This time offset

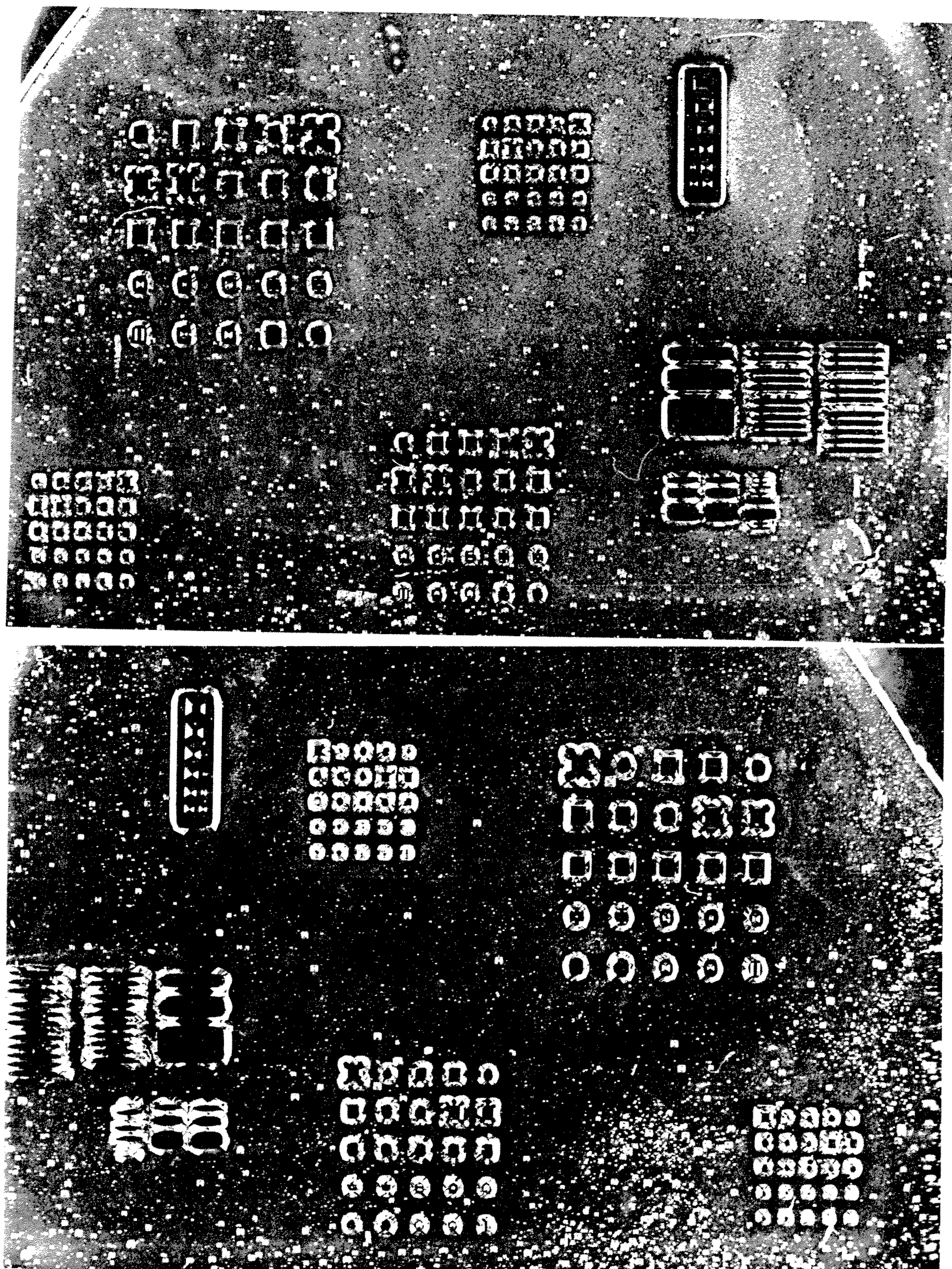

Figure 8-4: Output shapes: (A) 4 1/2 hours (B) 6 hours; the array is about 1 cm by 1 cm.

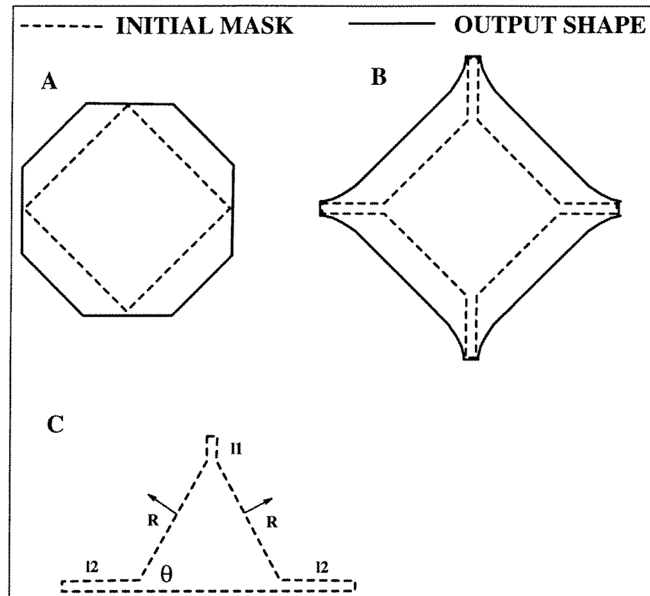

Figure 8-5: (A) diamond mask evolves to octagon. (B) modified diamond evolves to approximate diamond. (C) compensation for isosceles triangle.

corresponds to the time necessary to sharpen the ends to (311) planes which are the fastest and thus dominant planes for pegs.

It was also found that two perpendicular bars produce more uniform and reliable corners than one bar. For bar compensation it is possible to orient the bars either vertically or horizontally, which tends to produce structures that resemble castles.

8.1.6 Hole Compensation

In addition to peg compensation, a test pattern to examine the compensation of polygonal holes was etched. In EDP and KOH, diamond shaped holes distort to octagonal shapes and finally to squares composed of (111) planes. It is impossible to etch a perfect diamond shaped hole, but the shape can be approximated as shown in Figure 8-5. Figure 8-6 shows the experimental output shape. Here the diamond has thin extensions which lead to the desired output shape. The extensions should be $1.4 * \frac{R_{110}}{R_{100}} * depth$. The difference between the output and a perfect diamond will be about $.7 * depth$.

This also works for isosceles triangles but the side and top extensions are of different length:

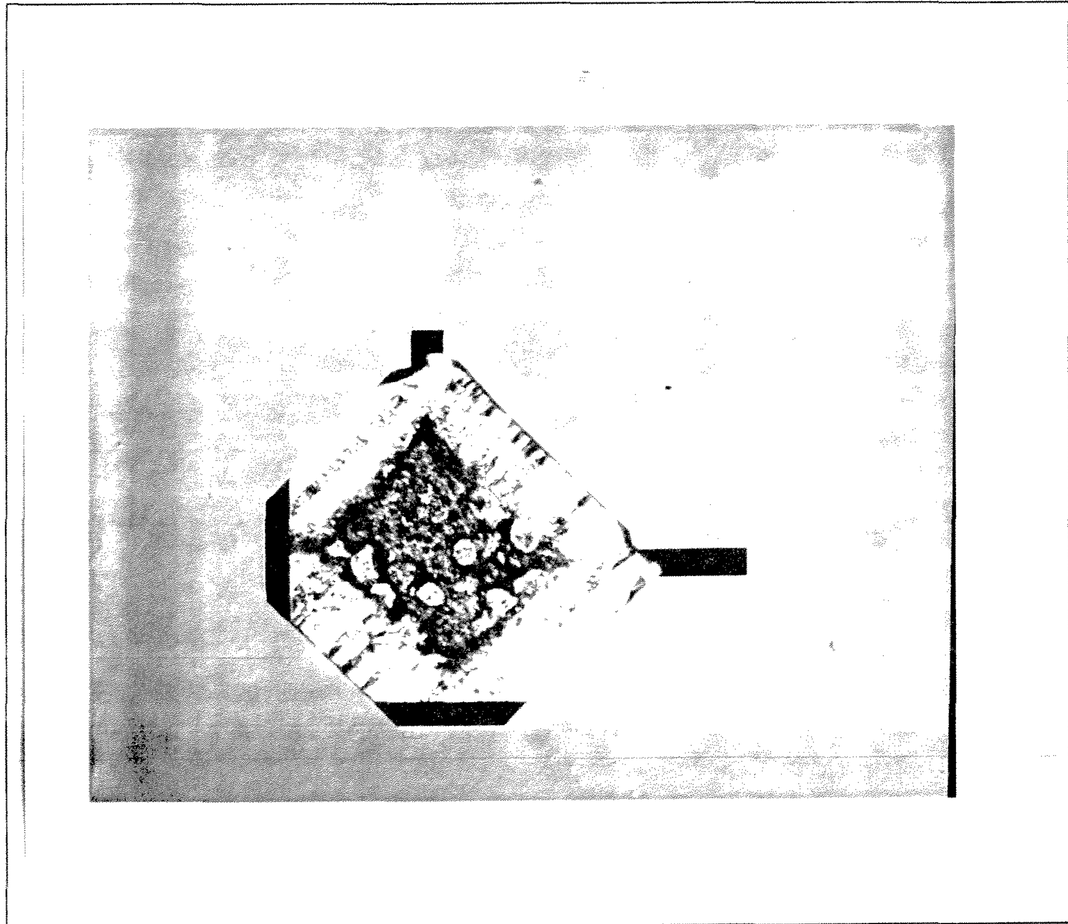

Figure 8-6: Experimental output shape for diamond hole compensation.

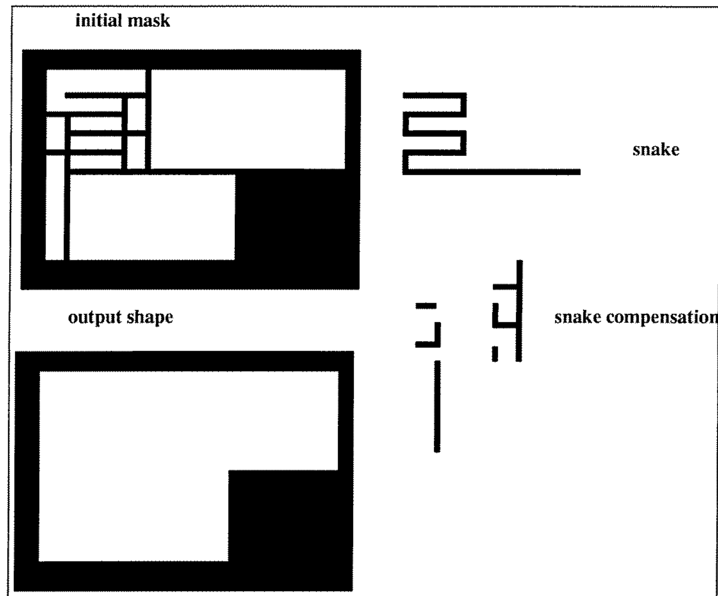

Figure 8-7: Initial mask for snake-like compensation.

$l1 = \frac{1}{\sin\theta}\frac{R_{110}}{R_{100}} * depth$ and $l2 = \frac{1}{\cos\theta}\frac{R_{110}}{R_{100}} * depth$
where θ is the angle at either base (see Figure 8-5C). Using this method it may be possible to predistort a many sided polygon in order to produce an approximate circle as output.

8.1.7 Folded Compensation

The previous structures are suitable for short compensation times. If a very long etch time is required, then a correspondingly large compensating structure is required. However, the available space may not be sufficient to allow the necessary compensation. The solution lies in folding the compensation so as to require less space. However, in order to fold compensation structures, the structures themselves have to be compensated. A bar compensation may be folded over onto itself to form the snake-like pattern shown in Figure 8-7 allowing very long compensation times. The guidelines to folding compensation are:
(i)The compensation must constist of horizontal and vertical bars.
(ii)The width of the segments should be large enough to ensure that they survive the (111) etching.
(iii)Starting at the exposed end of the compensation, whenever a fold is made, the original

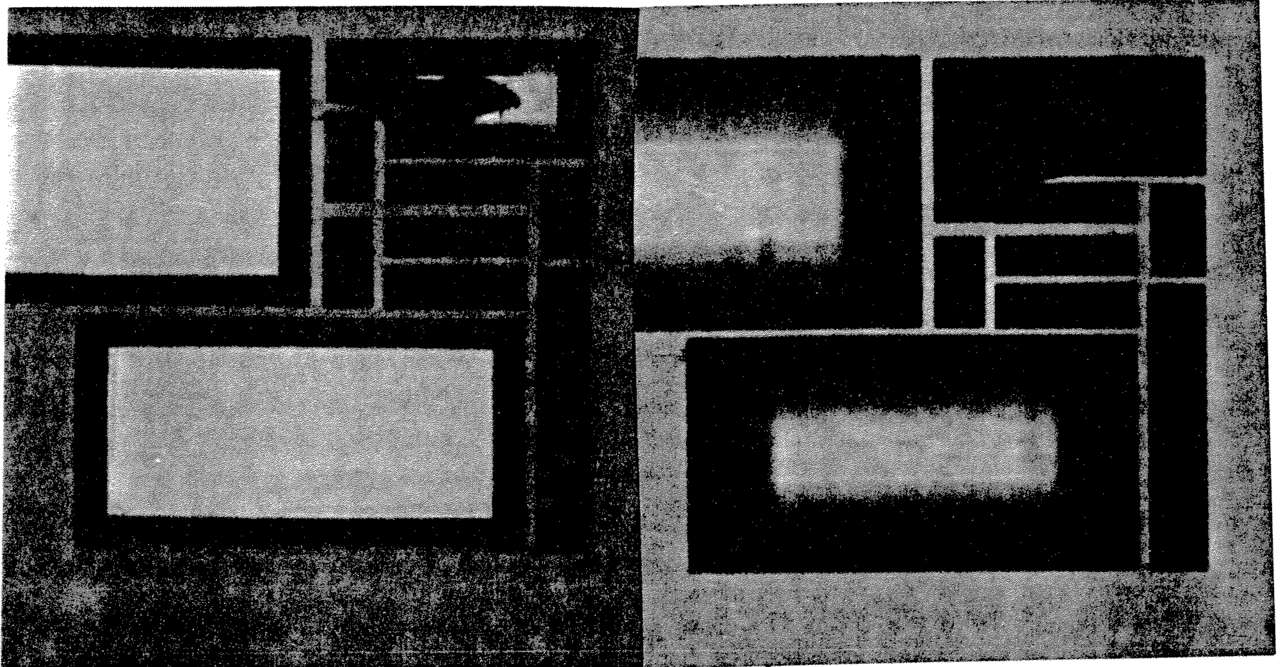

Figure 8-8: Two samples of snake-like compensation after etching $\sim$ 7 hrs (left) and $\sim$ 14 hrs (right) in EDP.

path must be continue until the fold is anchored either to a fixed wall, or another compensation structure.

In essence the etchant must travel the entire length of the snake whose corners are protected by short compensation members.

Figure 8-8 shows the structure after etching in EDP. The hole width was about 500 microns.

A very long linear path can be compressed into a very small space; as a first approximation given a line width w the maximum length is $area/width$. Note that the two long final compensation members are the same length so that no compensation structures remain at the end of the etch. This concept can be further extended to compensate a rectangular peg tightly enclosed by a rectangular hole. The close quarters preclude ordinary compensation, but as shown in Figure 8-9 the compensation can be folded so that the limiting dimension

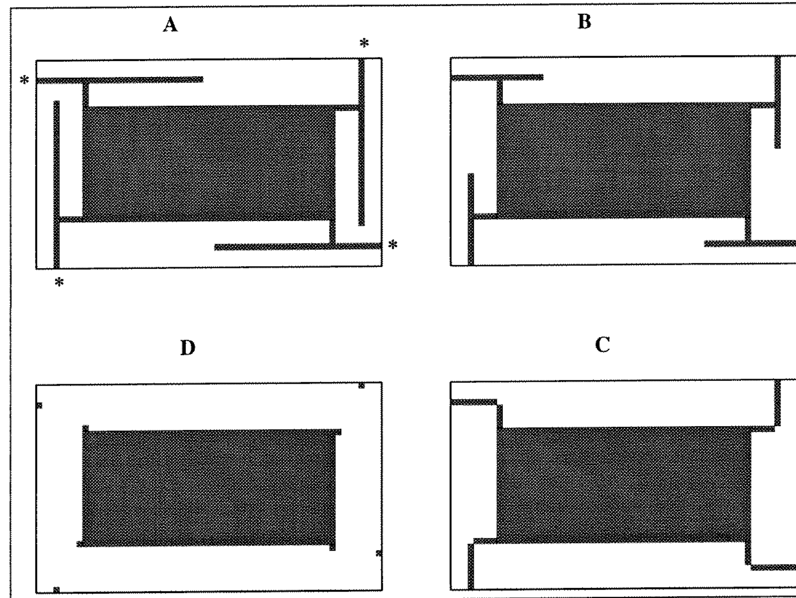

Figure 8-9: Progressive etching of a a folded compensation structure. Time increases from A to D.

is the length of the peg and not the gap between hole and peg. The *'s in A are the anchor points for the folding and the rounding off of compensation bars has not been shown. If one fold is not sufficient, a flattened version of the snake compensation can be constructed.

Figure 8-10 shows an improvement on the last two methods where nearly 100% of the available area is used. It effectively doubles the maximum path length by using staggered holes such that the etching path jacknifes back and forth.

Area versus linear constraints

If the compensation structure is to be in a confined space, there are two types of constraints: area and linear. Area constraints mean that the compensation must fit in a small delimited area. In such a case compensations squares and fins are appropriate. Linear constraints means that the compensation structure may be very long in one dimension and bar and snake structures are best suited for this purpose.

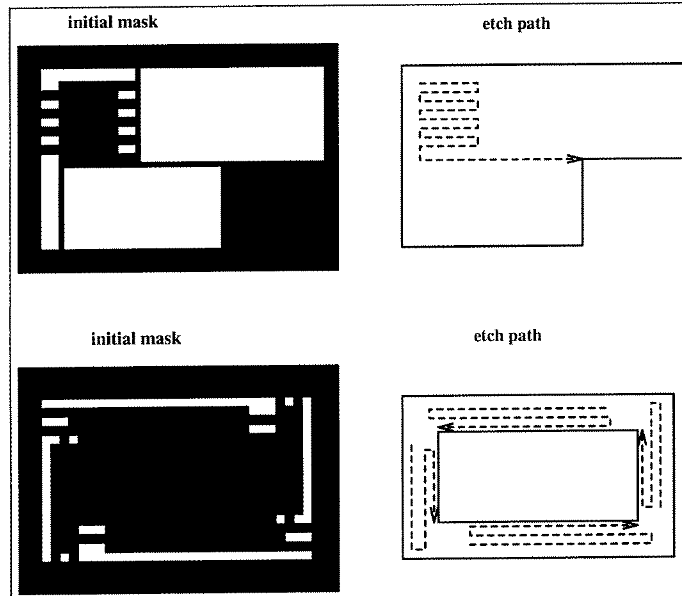

Figure 8-10: Compressed version of folded compensation. Note staggered holes.

8.1.8 Limitations

The previous experiments and simulations are dependent on using the proper etch behavior. Among the factors found to change the compensation behavior are the following:

(1) Aging of etchant: it was found that when EDP etchant is left to age, the etchant behavior is faster with different ratios for the major planes.

(2) The use of an epitaxial wafer with a buried boron layer tends to increase the lateral etch rate with respect to the vertical etch rate. Specifically, for bulk wafers the lateral motion of a bar compensation structure in EDP was found to be approximately equal to the vertical depth of etching. However, for an epitaxial wafer with a boron layer buried 20 microns beneath the surface, the lateral etch rate was increased by a factor of three relative to the vertical rate (measured on the non-boron side).

(3) The structures considered thus far are relatively large, for cases where the typical dimensions are microns, the results are not necessarily valid due to such non-linear effects as diffusion.

8.1.9 Three Dimensions

Thus far the simulations have been two dimensional. We can use the two dimensional outline as a function of time to simulate the three dimensional evolution of the edges which make up the shape. We make two assumptions: (1) the etching is anisotropic, thus the cross section of any edge perpendicular to the (100) plane is a straight line inclined at some angle; (2) the depth is shallow, such that three dimensional corners do not intersect. The shape is given by the two dimensional outline extended into the (100) plane at the appropriate angles. In order to do this, the inclination of planes (with respect to the z axis) versus orientation within the (100) plane must be obtained.

EDP and KOH have similar etch rate diagrams in the (100) plane but they differ out of the (100) plane. Both produce 54.7 degree z-inclined planes for lines inclined at 0 or 90 degrees in the (100) plane. However, for planes inclined 45 degrees in the (100) plane, EDP produces a z-incline of 45 degrees while KOH can produce vertical walls. Using this data and intermediate values, we can add to the two dimensional outline and produce three dimensional images. The three dimensional representation allows us to view the shape from any direction we choose (see Figure 8-11).

8.1.10 Summary

The use of compensation structures to preserve corners was investigated and simulated. The simulations were found to agree well with experiment. From the simulations and experiments, design guidelines were established that allow optimum compensation for various criteria and constraints. It was found that the best compensation structure is application dependent with rectangular structures providing long time compensation while fin shaped structures provide more reproducibility. Polygonal holes were also successfully compensated to produce desired output shapes. The concept of folded compensation was introduced and experimentally verified. These structures allow very large compensation times. The design tools and guidelines presented provide powerful mechanisms to better design final etch shapes used in bulk micromachining.

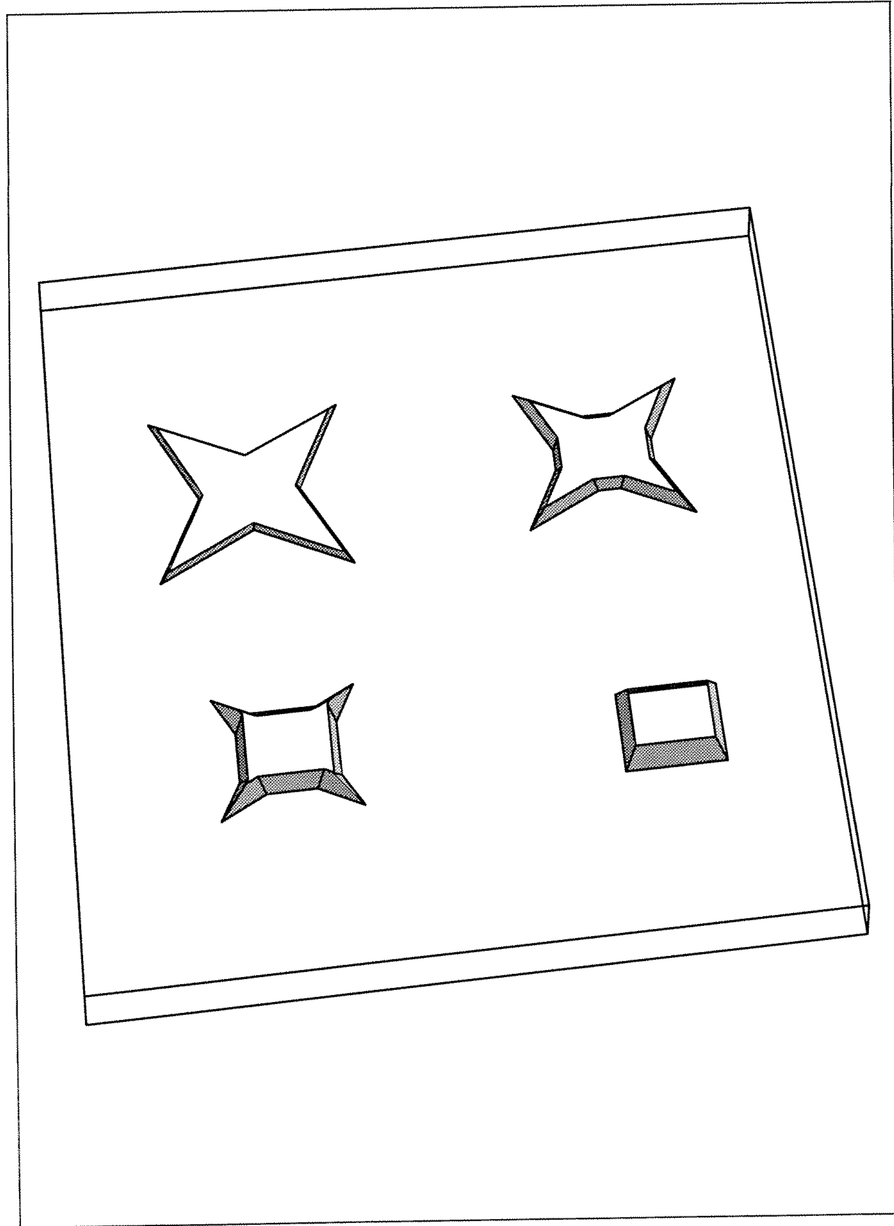

Figure 8-11: Extension of simulation to third dimension. Simulation proceeds from top left to bottom right.

8.2 Compensation Fuses

8.2.1 Introduction

This section presents a novel process with one lithography step and two etchants to increase the reliability and capability in all aspects of anisotropic etching. In particular, improved compensation and delay structures are presented.

When silicon is etched with anisotropic etchants, exposed corners change shape as a function of time. Some planes etch much more slowly than others, for example, the etch rate ratios for (100) planes to (111) planes are of approximately 400:1 and 35:1 for KOH and EDP respectively. Because of this, holes of any shape become pyramidal pits bounded by four (111) planes, and convex corners get rounded off by the faster planes.

During simulations of this etching it is important to bear in mind that there are two types of corners (in two dimensions): convex and concave. The inside of a corner is taken to mean the region defined by an angle smaller than 180 degrees. For a convex corner, the inside is unetched, while the inside of a concave corner is etched. Thus a square peg has four convex corners and a triangular hole has three concave corners. While etching convex corners fast planes dominate; for concave corners, slow planes dominate.

8.2.2 Previous Compensation Techniques

One way to counteract the rounding of convex corners is to cover the corners in question with compensation structures which are sacrificial in nature [2, 5, 49, 56, 61, 88]. This is shown in Figure 8-12. The desired output shape is an "L" shaped hole with one convex corner and four concave corners[1]. Until the structures themselves are etched away the original corner is temporarily protected. In effect the structures delay the time at which etching of the corners begins; they "buy time". However, for large compensation times, a large amount of space is required (there are compression techniques available). As previously mentioned, compensation is governed by the fastest planes, so reproducibility is impaired because the fastest etch rates are especially sensitive to variations in etching time and etching behavior.

One way to solve both of these problems is to anchor the convex corners to a fixed wall

[1] Unless otherwise stated, this will be the desired output shape throughout this chapter.

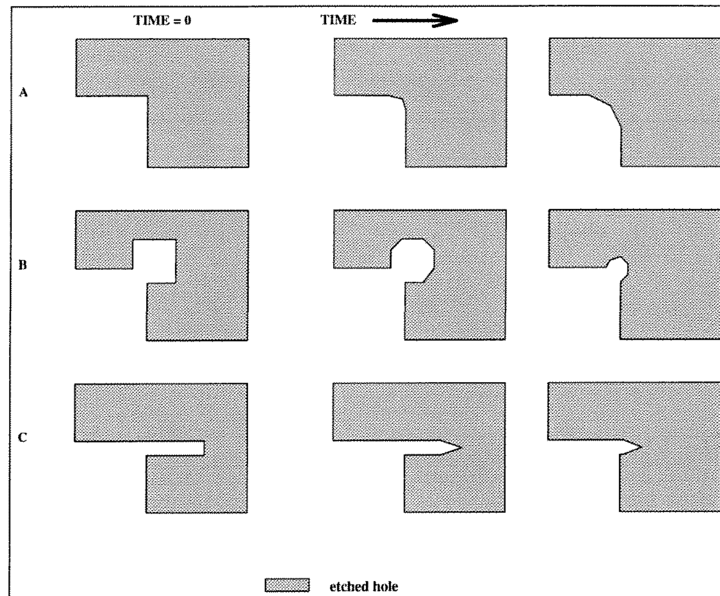

Figure 8-12: Schematic representation of compensation techniques. (A) uncompensated; (B) square compensation; (C) bar compensation.

with a thin web (as shown in Figure 8-13A). This web is not appreciably etched and so provides near perfect compensation. Unfortunately, this also means that the web is always present. What is needed is some way to remove this web after it has served its purpose.

Another solution is to make the webs of a particular width such that the slow but finite (e.g. 111) etch rate will eventually break the web (see Figure 8-13B). This approach has been used such that the webs formed a grid in order to delay the depth progression of that area [43]. This allows (i) front to back alignment, and (ii) multiple depths from one etch. Unfortunately, because the web breaking time depends on the web width, and because the (111) planes are very slow, reproducibility is difficult. If two webs vary by x microns in width and the (100)/(111) selectivity is s then the depth difference produced will be on the order of $x * s$. In the time it takes for the (111) planes to etch through an extra micron, the depth has increased by about s microns. In practice, the etchant's (100)/(111) selectivity is usually chosen to be low (4 to 5). This modification reduces the sensitivity of the web breaking times. The reproducibility and smoothness are improved but are still not optimal. Thus the desirable slow etching time of (111) planes involves trade offs with

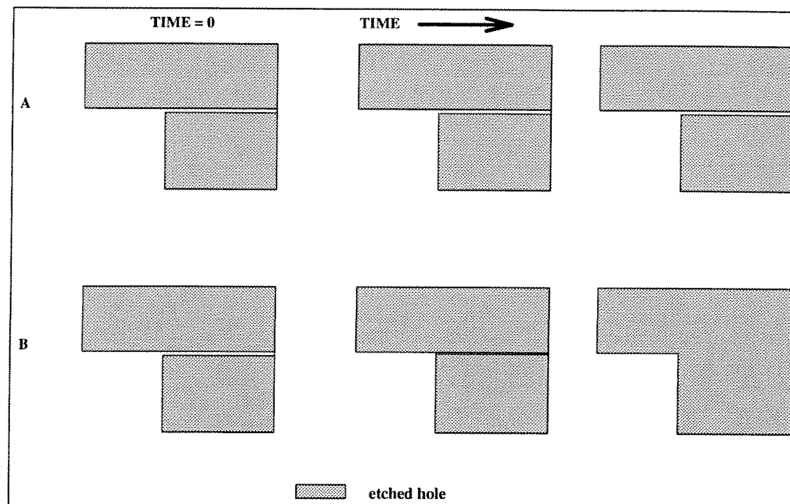

Figure 8-13: Web compensation.(A) webs are permanent (B) (111) planes slowly etch through webs.

increased magnification of lithography errors: two seemingly mutually exclusive goals.

8.2.3 Compensation Tuning

What is needed is a method to take advantage of the slow planes' reliability without incurring their disadvantages. The key lies in realizing that only a short period of the etch is susceptible to error magnification. Before or after this time, the selectivity produces no undesirable effects. Thus the two seemingly mutually exclusive goals are not, because they are not simultaneously required.

The method developed incorporates two elements:

1) Anisotropic etching followed by an approximately isotropic etch to pass the critical point in the etch where reliability and error magnification are both important, and then resumption of the anisotropic etch. For this reason the method is called compensation tuning, as the etching behavior is tailored to pass the critical point.

2) Fuses on the webs are used in order that the webs break at predetermined, reproducible points.

As shown in Figure 8-14 an anisotropic etch (with high (100)/(111)) selectivity is used first. The etch must stop before any of the webs are broken. Next, an isotropic (e.g. HNA

formula) is used to break the fuses. Then the etch is completed with a short anisotropic etch. Note that the isotropic etch needs only be approximately isotropic. Alternatives to HNA include : dry etching (Plasma/RIE) and very low selectivity KOH or EDP (accomplished by varying chemistry/dilution/temperature).

8.2.4 Fuses

The fuses are shown in Figure 8-15A. Note that the configuration shown in Figure 8-15B will not work since it exposes convex corners. The first fuse is stable with respect to anisotropic etchants, but can be broken by approximately isotropic etchants. By varying the width (w) of the fuse sides and the length (l) and height (h) of the fuse from the corner, a great deal of control of behavior is possible: w determines the duration of the isotropic etch while l and h determine the duration of the second anisotropic etch.

8.2.5 Masking

The most important consideration is that the masking layers be able to withstand both etchants. In this case both EDP and HNA were used in conjunction with silicon dioxide as a mask. While HNA does attack SiO_2, the fuse breaking time is short and hence the mask is not seriously eroded. Unfortunately, the particular formulation of HNA that was used (2% hydrochloric acid, 95% nitric acid, 3% acetic acid) did not have as high a Si/SiO_2 selectivity as was hoped for ($\sim$ 100) and the mask was eroded. Other masks such as nitride and metals may be used with an appropriate etchant pair. In our case a chrome-gold mask(300-1000 Ångstroms) can withstand both EDP and HNA (5%, 70%, 25%) etching. Even with this change, the etchant combination is still not optimum and experimental results were of poor quality.

It is possible to utilize the fuse concept with a multiple lithography, and multiple etch steps (with a single etchant). However this method is not immune to alignment errors.

8.2.6 Summary

This chapter presented a novel process with one lithography step and two etchants to increase the reliability and capability in all aspects of anisotropic etching. In particular,

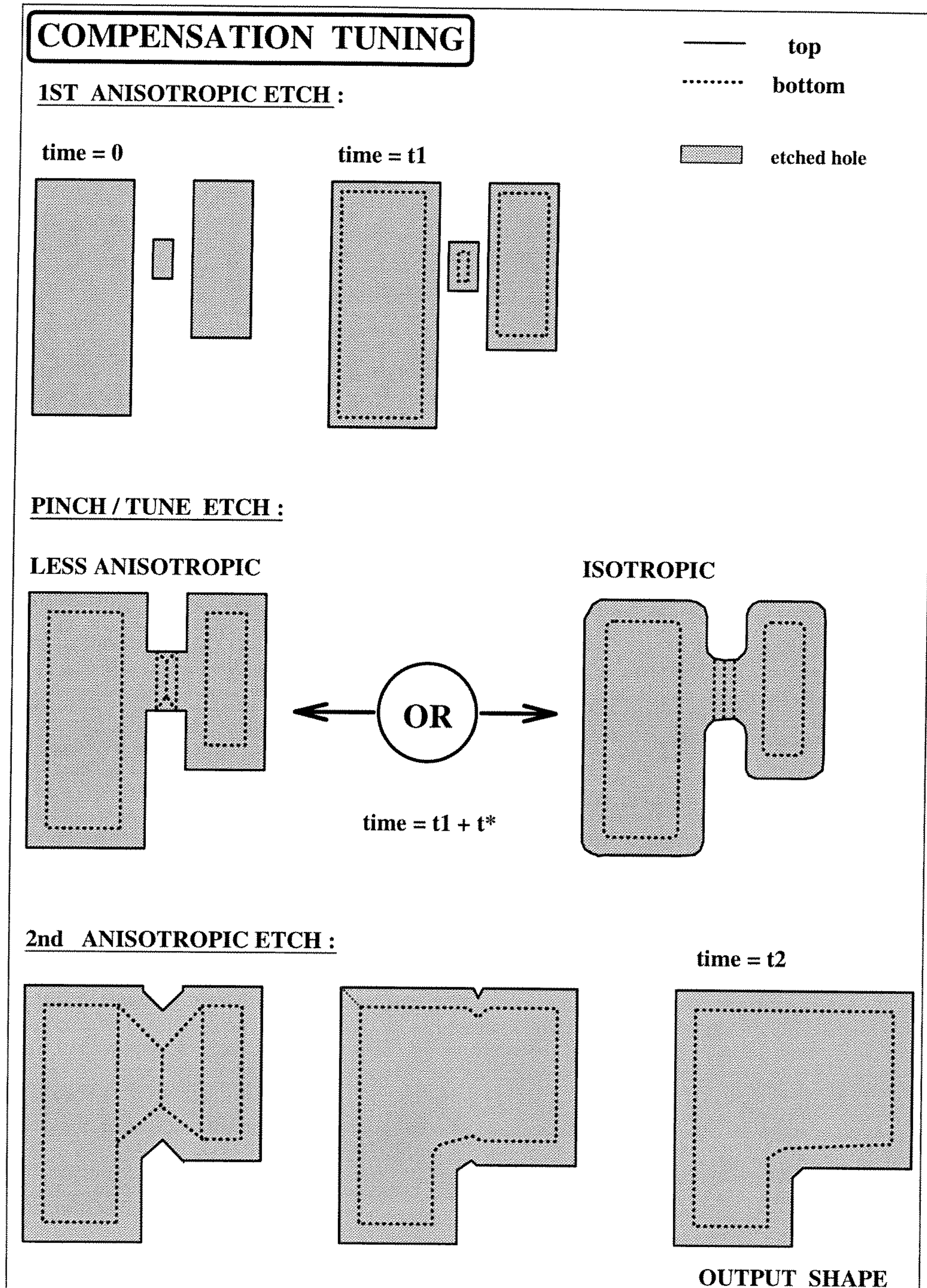

Figure 8-14: Compensation tuning. An anisotropic etch is followed by an ~ isotropic etch and a second anisotropic etch.

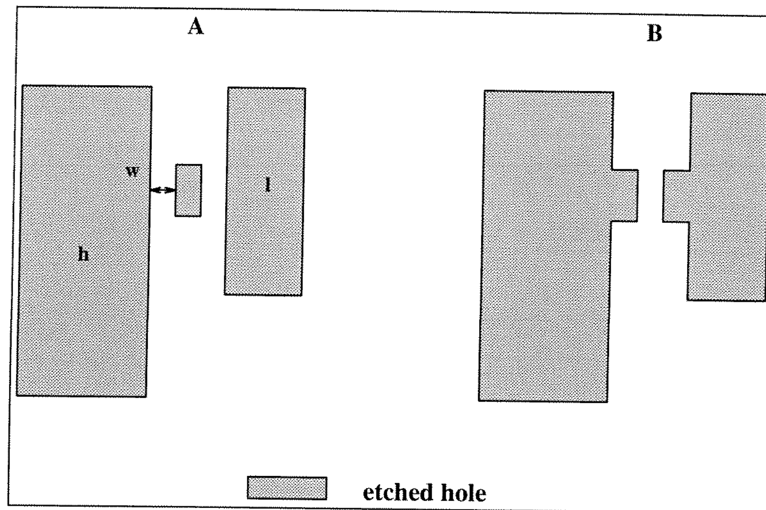

Figure 8-15: Compensation fuses (A) Stable fuse with some variable parameters. (B) Unstable fuse exposes convex corners.

improved compensation and delay structures were presented. The concepts of compensation tuning and compensation fuses were introduced. This process allows precise control of the final shape over very long etch times and allows designers to more easily specify a desired output shape. More work needs to be done on finding suitable etchant combinations.

8.3 Application Examples

8.3.1 Introduction

In this section I present some preliminary design studies on four micro-machined components. Each component is part of a more complex micro-machined structure. Most of these structures are being constructed by other groups who requested design advice for portions of their structures. The structures are relatively large and the simulations involved will be relatively simple but the use of some of the previously discussed methods in real world applications will be demonstrated. The wide range of examples chosen shows the generality of the methods. In all cases the design will deal with the shape transformations which occur during etching. The examples are as follows: spiral springs, a slotted fan blade, valves, and a circular structure.

8.3.2 Spiral Springs

A large (1 cm by 1 cm) spiral spring[2]

is to be constructed using wet etching techniques. The spiral spring is to be compliant perpendicular to the plane. Previous designs had used dry etching techniques which were not as reliable and had difficulty attaining large depths. Because of the anisotropic nature of wet etching, a square rather than round spiral is used. If no compensation is used the exposed corners are etched away and the center of the spring is separated as shown schematically in Figure 8-16A.

By applying square compensation structures the exposed corners are temporarily protected as shown in Figure 8-16C and Figure 8-17A.

Figure 8-18 shows the final etched shapes. A more compliant spring may be made by including more turns in the spiral. The compliance can also be increased by performing a backside etch which will reduce the thickness of the spring. This can also allow for a smaller spacing between spiral arms (remember that the sidewall profile is at 54.7 degrees).

8.3.3 Slotted Fan

A slotted fan blade assembly[3] was designed to force air to move along the axis of rotation of the fan . The fan consists of angled slots in a circular wafer with an axial hole as shown in Figure 8-19.

Rotation is to be provided by non-micro machined components. The fan should have as many slots as possible. The design is complicated by the fact that the sidewall angle ϕ varies greatly with orientation θ. In order to make each slot, two "V" grooves were etched, one on the front and a backside groove is etched at a slight offset angle. The required mask parameters for constant width slots are shown in Figure 8-20. The sidewall variation with orientation should be obtained from experiments on a test wafer.

Figure 8-21 and Figure 8-22 show the simulated two and three dimensional output shapes for one quarter of a circle with a one-sided etch only.

By stacking many fans together with each subsequent fan rotated by one fan slot, the

[2]This spiral spring design was requested by Dr. Lin Muller of JPL for possible use in a deformable mirror.
[3]This fan blade design was requested by James Lamb of JPL for possible use in a pump.

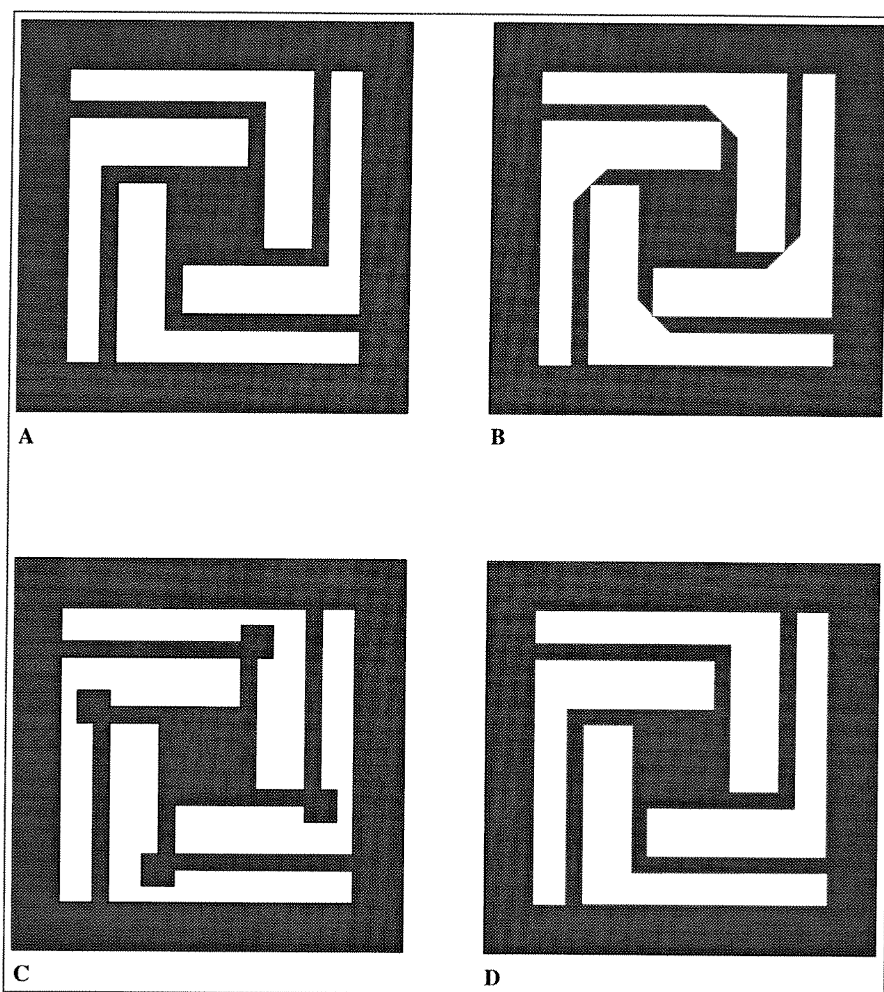

Figure 8-16: Uncompensated spiral spring mask/design (A), and expected output (B). Compensated spiral spring mask/design (C) and simulated output (D).

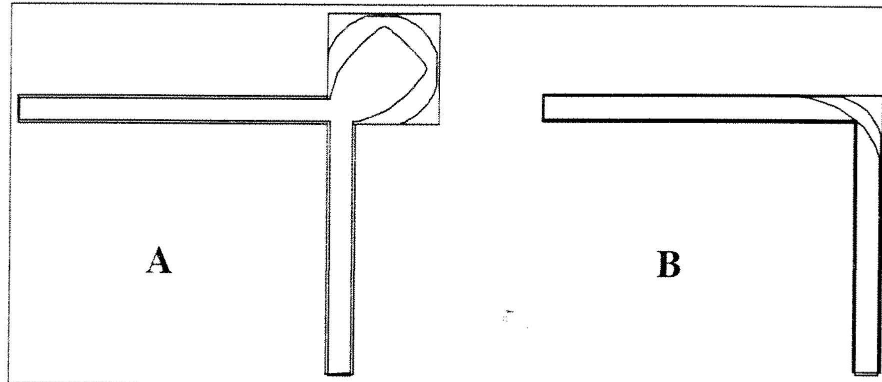

Figure 8-17: Compensated spiral spring (A) and uncompensated spiral spring (B) two dimensional simulations. Contours represent two dimensional shape at different times.

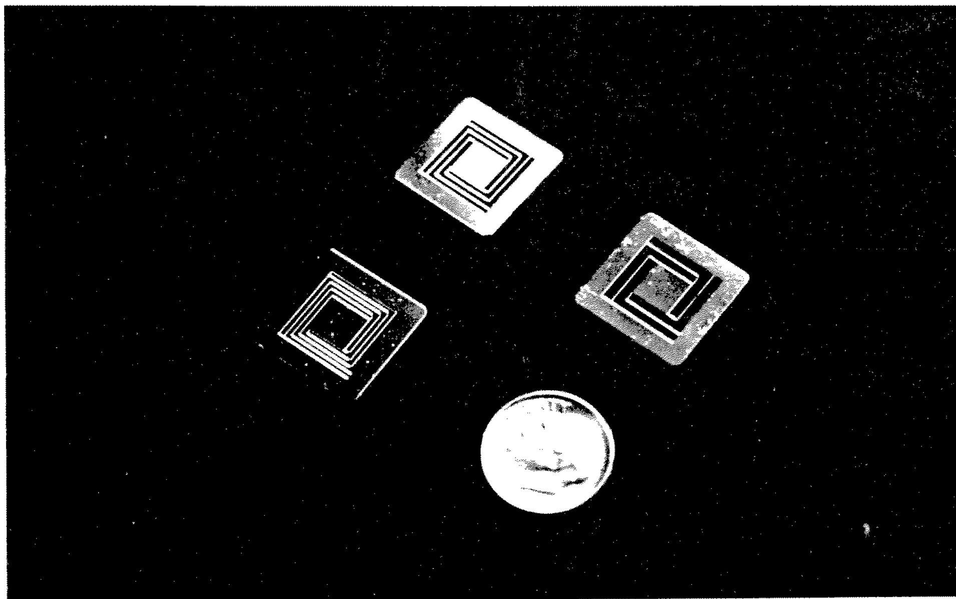

Figure 8-18: Etched spiral spring.

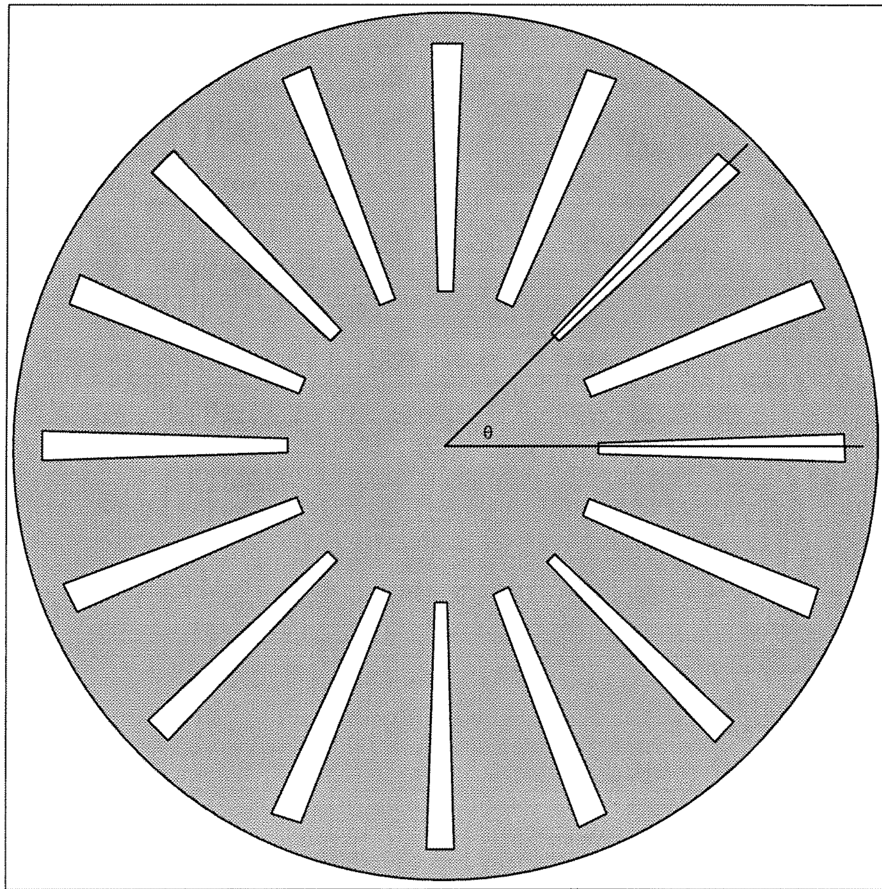

Figure 8-19: Overhead view of slotted fan design.

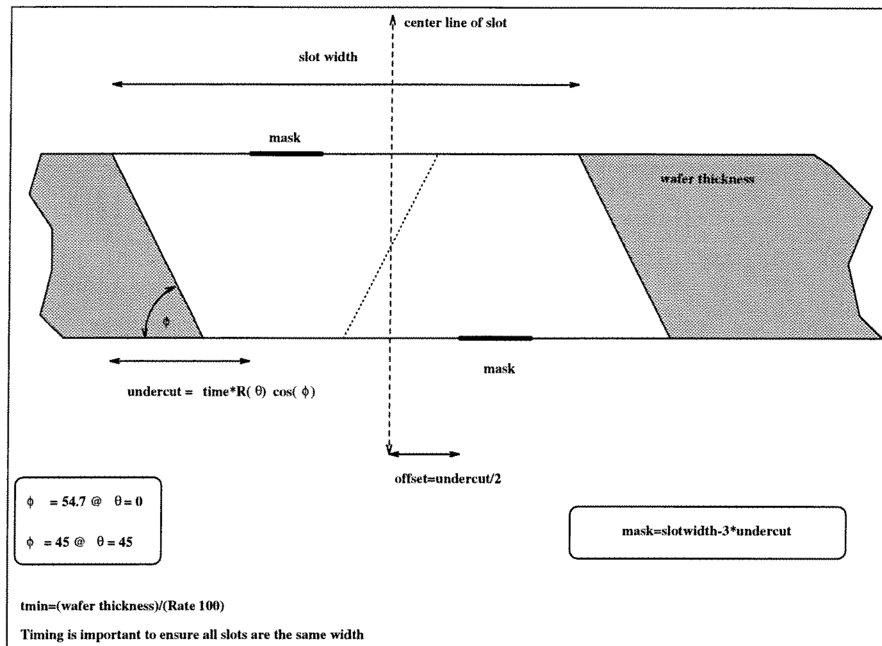

Figure 8-20: Cross-sectional view of slotted fan design.

effects of orientation dependent sidewall profile can be reduced. If this is done the slots can be made to have the same average side wall profiles.

8.3.4 Valves

Many micro machined valves[4] have been designed, most of which can accurately control minute quantities of liquids. For some applications, an intermediate sized valve would be useful. To that end a valve system that is of the order of 1 cm by 1 cm with typical dimensions on the order of 1 mm was designed. This is much larger than most micro machined valves, while being smaller than most conventional valves. The design centered on the geometry of the valve, and issues such as friction and actuation are not considered. The preliminary design consists of two cut sections of silicon one of which is turned upside down and placed on the other. By moving the two sections relatively to each other, the flow of a fluid may be controlled. Figure 8-23 and Figure 8-24 show the geometries being considered. Figure 8-25 and Figure 8-26 show the simulated three dimensional output shapes

[4]This valve design was requested by Prof. Joel Burdick of CIT for possible use in a micro-machine valve.

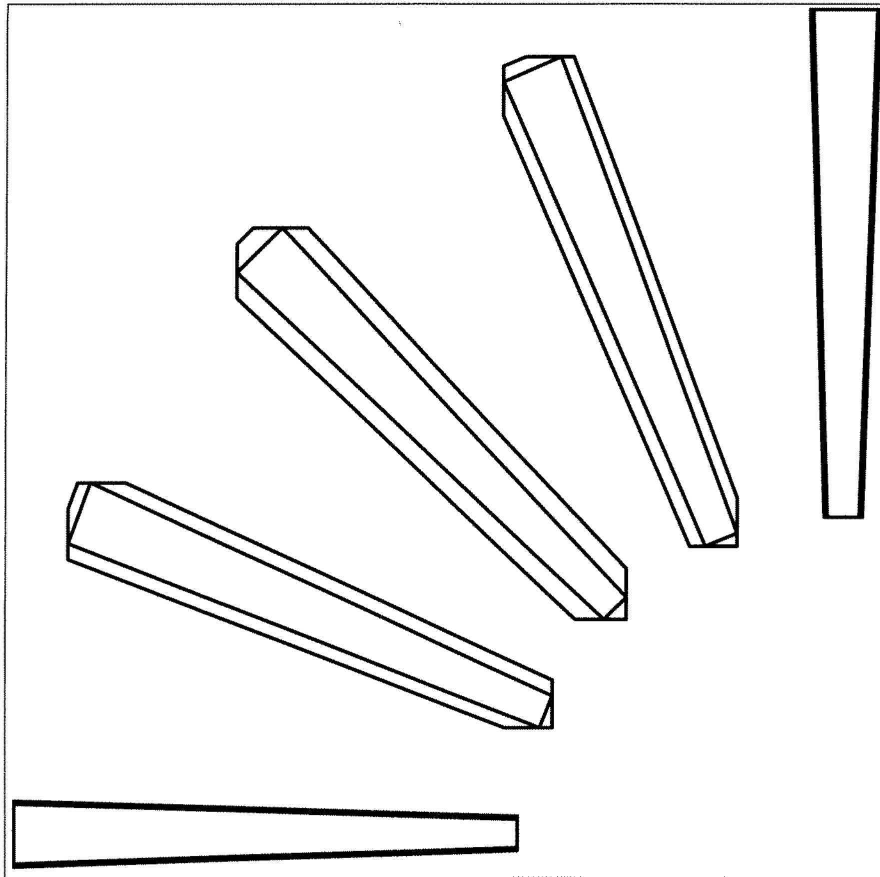

Figure 8-21: Two dimensional simulation of slotted fan design (one quarter circle). Origir mask and two dimensional output contours are shown.

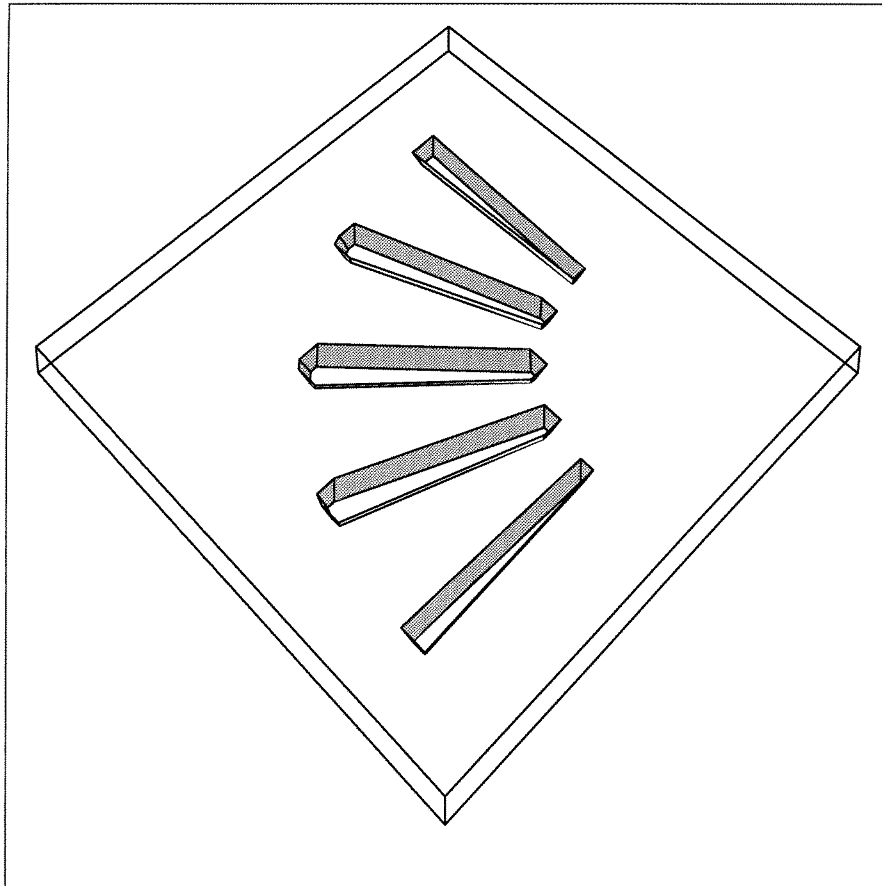

Figure 8-22: Three dimensional simulation of etched slotted fan (one quarter circle, one sided etch only).

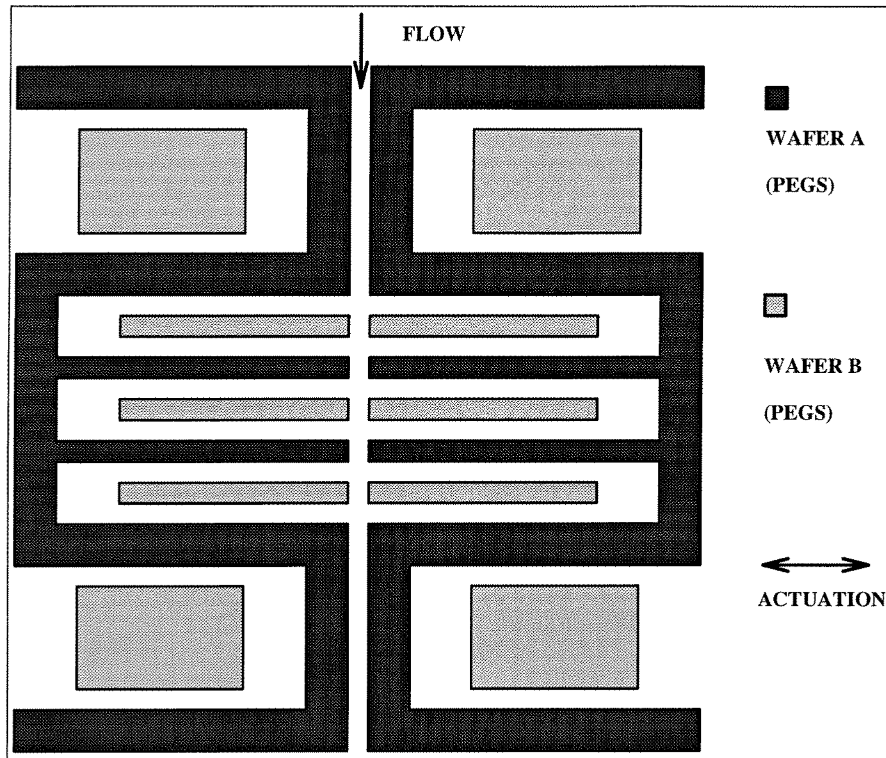

Figure 8-23: Preliminary valve design mask, actuation perpendicular to flow. Interlocking raised pegs control flow.

for both silicon pieces. The actuation may be along the flow or parallel to it. In each case a number of interlocking vanes block or allow the flow depending on their position. The number of vanes may be varied. A larger number of vanes would tend to impede the flow but may be necessary to reduce leakage since the relative tolerances are worse at smaller scales.

8.3.5 Circular Structures

One of the most common design goals is to produce circular structures with anisotropic etchants[5] . Circular structures are desirable since the mechanical properties are generally advantageous. For example, stresses can be reduced compared to other structures, and fluid

[5]This circular structure design was requested by Dr. John Gilbert of MIT for possible use in a micro-machined valve.

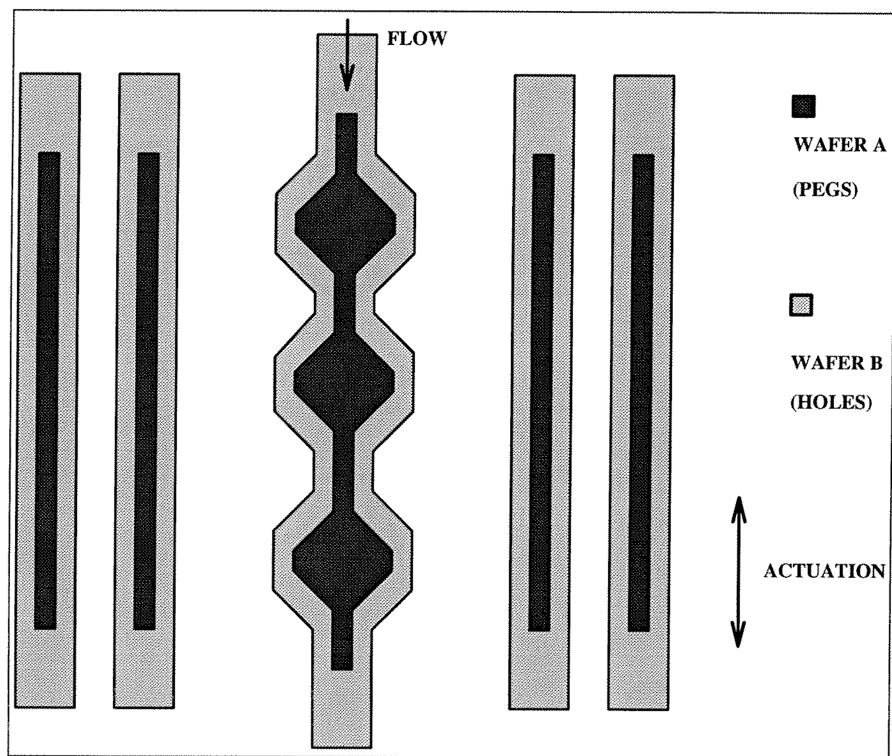

Figure 8-24: Preliminary valve design mask, actuation along flow, pegs within holes control flow.

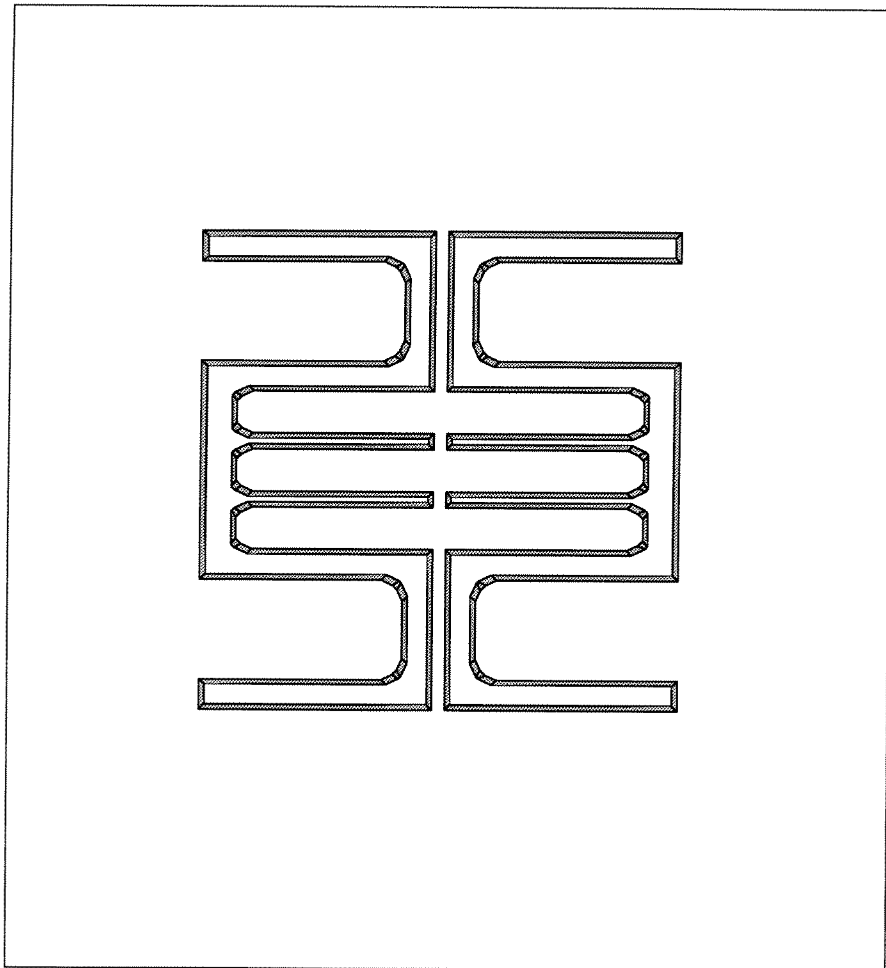

Figure 8-25: Simulated three dimensional output shapes for part a of first valve.

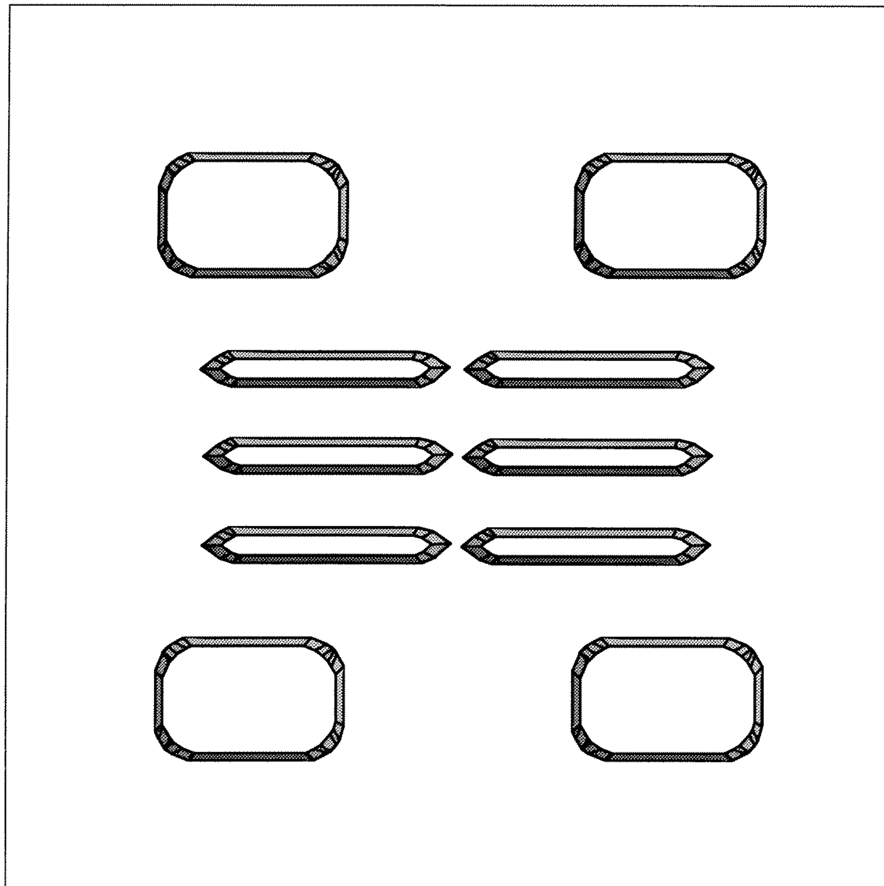

Figure 8-26: Simulated three dimensional output shapes for part b of first valve.

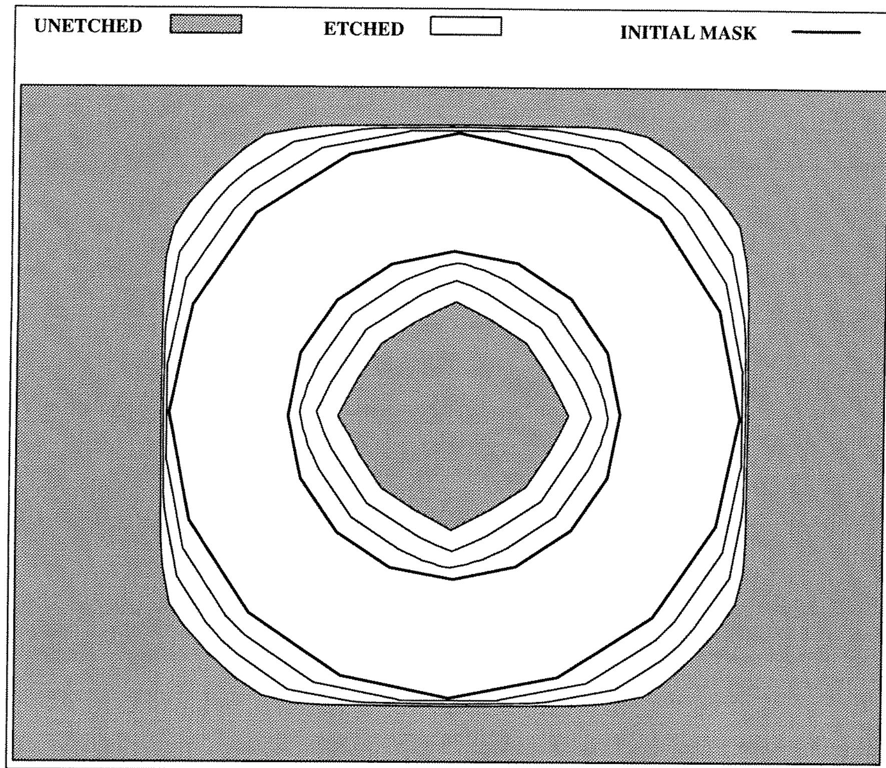

Figure 8-27: Two dimensional simulations for annular mask.

flow around circular structures is smoother than around faceted structures. Unfortunately a true circle can never be etched with an anisotropic etchant, just as an isotropic etchant can never produce a perfect square hole. However, circles can be approximated, and simulations may be used to quantify the difference between a perfect circle an the approximated circles. As the time and depth of etch increases, the error in approximation also increases. In order to model the changes in both holes and pegs, a donut shaped annular mask is used. Many sided polygons are used to model the circles. Figure 8-27 shows some simulated two dimensional outputs for this initial mask. Three dimensional simulations are shown in Figure 8-28

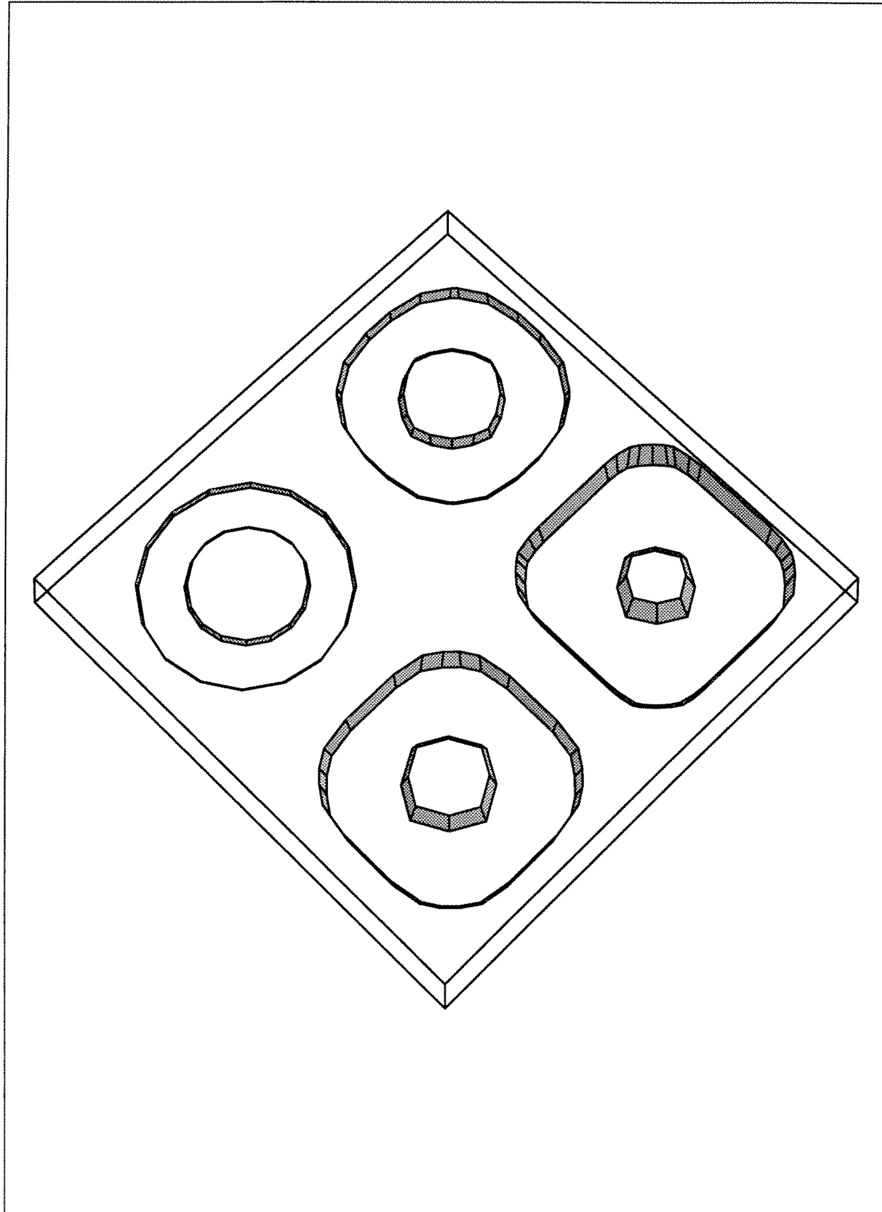

Figure 8-28: Three dimensional simulations for annular mask. In this oblique view, the mask is etched for longer times and increasing depths in the following order: west, north, south, and east.

Chapter 9

Conclusion

9.1 Summary

This work begins with the crystal structure of silicon and ends with etched shapes. The underlying crystal structure causes different rates of etching for different directions; this behavior has been modeled to obtain rate models. The information in these rate models has then been used in a number of shape modelers. High level models like the Eshape model provide not only simulation but a framework for design inversion. Other models such as the Cellular Automata model take a different approach and provide flexible and robust simulators. The tools were used to develop real world MEMS applications such as compensation structures.

A very broad base of knowledge has been developed as part of this research concerning the etching processes commonly used in MEMS fabrication. The fundamental problem is how to model the shape transformations that occur in MEMS fabrication. The ultimate goal is to determine the required input for a desired output. While much work remains to be done, significant progress has been achieved. The work presented here provides a significant first step in developing formal MEMS design methods.

While the methods presented here can ultimately be extended, at present they have the following limitations: (i) the thesis deals specifically with the transition between initial mask and final shape, rather than the full path from initial mask to final function (ii) the thesis concentrates on one fabrication method, wet bulk etching (iii) the analysis of the etching of silicon has been empirical rather than theoretical. Nevertheless, the methods developed in

this thesis are sufficiently general to be applicable to many shape transformation processes.

9.2 Future Work

9.2.1 Information Standards

The problem examined is only the first part of MEMS design. Once the output shape is obtained an analysis of the performance of the structure needs to be made. This may include the characterization of mechanical properties such as stress and resonant frequencies using FEM tools. For this reason a standard communication format for the transfer of information between different levels of MEMS design is needed. In the same way that the interchange of information between different modelers in this thesis produced a better design system, information interchange between this system and others would be beneficial. The exact layout of such a format is not clear as different parts of the design community may have different requirements, but the entire community would benefit from the establishment of such a standard.

9.2.2 Robust/tolerant shapes

We have seen that the output shape is susceptible to variation due to changing conditions. In particular changing etching environments, noise in the etch rate, crystal defects, misalignment in the wafer, and lithography errors in the mask can cause undesirable changes in the final shape. For these reasons valuable work could be done in first quantifying the amount of output error expected from a change in initial conditions and secondly in developing a method for making MEMS fabrication more robust to these changes. While this thesis has addressed the first question, the second remains largely unanswered.

9.2.3 Etch rate data (Standard test patterns)

Relatively little published etch rate data is available, and what little there is tends to concentrate on a few major planes. The rate modeler presented previously partially addresses this problem but more data needs to be collected. The simulations and design solutions obtained can only be as good as the etch rate data provided. Standardized test patterns

that users from different groups could include with their etches would be of great use. Such patterns should be relatively compact and should extract as much information about the etchant as possible.

9.2.4 Improved models

The following is a list (grouped by each of the etch simulation methods) of some of the issues that should be the subject of future work.

- Rates Model

  More experimental etch rate data points need to be collected and compared with rate model results.

  Because the choice of principal basis planes is very important, a more formal method for determining the best planes to choose in order to model a particular etchant needs to be developed. In general the fastest and slowest planes are good choices, anisotropic etchants need fewer planes than isotropic etchants, and at least one plane is required for every minimum or maximum in the etch rate diagram.

- Shapes Model

  The effects of noise in etch rate and of wafer misalignment have been studied in an empirical manner. A more formal approach yielding quantitative results would be an improvement.

  In the case of the of the Shape Library method, users have relatively little control over the etchant behavior and that wafer cuts are usually available in a few limited cuts. The ability to tailor etchants would greatly increase the model's usefulness.

  The Shape Library should be extended to peg shapes as well as hole shapes.

- Eshape Model

  The calculation of intersections between corners could be made more efficient. This would make the model more robust.

  More work needs to be done on through-cut where new Esections are introduced.

The shallow three dimensional extension should be made more robust so that deeper etches are possible. Also the true three dimensional model should be explored further.

The design capabilities of the model should be expanded.

- Cellular Automata Model

  Algorithms for increasing the speed of the Cellular Automata by only considering the changing surface area and not the entire volume are very important.

  Etching rules for neighbor cells for different etchants and for different wafer orientations need to be developed.

  Non-linear effects such as diffusion, mask erosion, and changing etch rate behavior can be incorporated into the model via different neighbor rules. In the same manner that we have an array to represent the silicon, the empty cells can be used to form an etchant array to investigate the interaction of silicon and etchant and model such effects as loading and saturation.

  An output filter which reduces the quantity of data to more manageable levels would be useful in speeding up the display.

  Other fabrication techniques such as RIE and plasma etching can also be simulated with the proper algorithms and this avenue holds particular promise.

  A hardware parallel processing implementation would many times faster.

- Compensation

  Compensation techniques tend to depend on the fastest planes which make compensation methods very sensitive to changing rates and the timing of the etch. Better, more robust, compensation techniques need to be developed that produce reliable, predictable results despite changing initial conditions.

9.3 Wish List

The following is a list of some items which would greatly increase the capabilities of MEMS designers.

- Tailorable etchants

  Ultimately there are some shapes that are simply not obtainable with some etchants. The availability of more varied etchants would open up the possibility of a much wider range of output shapes. The methods developed in this thesis are not etchant specific and could easily be applied to any new etchant. An ideal etchant is one whose properties could be tailored to suit the needs of the application, unfortunately such an etchant is not likely to be found in the near term.

- Asymmetrical etchants (vertical walls)

  An asymmetric etchant is different from an anisotropic etchant and this difference is often overlooked. An anisotropic etchant has rates that depend on direction but that can be divided into families of planes. An asymmetric etchant is an etchant where planes that would normally belong to the same family and that would normally have the same rate, do not. In a sense there would exist preferred directions to the etching. For example the x, y, and z directions (100, 010, and 001) in a (100) wafer) would normally be equal for most etchants but the z direction may be different for some etchants. The methods developed in this thesis work equally well for asymmetric etchants.

  This subject is of tremendous practical importance because of its application to the production of vertical walls. Vertical walls are highly desirable in many structures

and much work has been done to try and obtain them. Usually this means that using more and more anisotropic etchants. What is really desired, however, is an etchant with high asymmetry between z and the planar dimensions x and y; the goal is to decouple the vertical etching from the planar etching. The difference between the two approaches is that an asymmetric etchant can still be relatively isotropic in the plane while highly anisotropic etchants tend to be dominated by a few planes which limits the output shapes and lowers the resolution in the planar directions. For example vertical walls can be produced on a (110) wafer with KOH, but only long channels may be formed. Conversely, methods such as LIGA are highly asymmetric (due to the imposed axis of energy flow) while at the same time allowing flexibility and good resolution in the planar directions. An asymmetric etchant which would not require the expensive equipment of LIGA fabrication techniques and which would be more versatile than present anisotropic etchants would be very valuable.

- Overhang

The silicon etchants studied in this thesis do not produce overhang, that is to say that when an etched shape is viewed from the side, the walls slope inward towards the open section of the mask. An etchant with overhang would cut into the mask such that the shape would be larger at the bottom than at the top. This would allow structures to be separated from the substrate. Currently this is usually done by means of a back side etch. The development of a silicon etchant with overhang would be of great commercial value. Other crystals such as gallium arsenide do have etchants which produce overhang but there is strong reason to believe that an etchant must be asymmetrical to produce overhang and this asymmetry may be difficult to produce in silicon.

Appendix A

A.1 Implementation

A computer menu program has been written to coordinate the information flow between various design tools. Figure A-1 shows the links between the different tools. The initial mask geometry is input into one of two simulators, the Eshape modeler or the Cellular Automata modeler. These modelers use rate information and the input mask to calculate the final shape. The rate information is obtained from experiments such as spoke patterns and may be fit to some function or may be modeled using the techniques developed earlier. This rate information may also be used with the shape Library method. In the case of linear shapes, it is always possible to completely invert the process to obtain the required input shape. With the Eshape modeler it is sometimes possible to invert the process for general shapes, but the same does not hold for the cellular automata modeler. In addition approximate shapes may be simulated if the exact final shape is unattainable.

The actual implementation of this program is done via the commercial package Mathematica. The Mathematica program is a hierarchical menu program, which calls other menus which in turn call either C or Mathematica programs. C is used for tools that are computationally intensive such as the cellular automata modeler and the rate modeler while Mathematica is used for less intensive modelers such as the Eshape. Mathematica is used for graphical output; faster graphics have been obtained using more specialized programs such as PHIGS, but Mathematica was used more often since it is much more widely available. The initial masks are input using the graphics program xfig. The Eshape modeler accepts polygonal input while the cellular automata modeler accepts combinations of rectangular

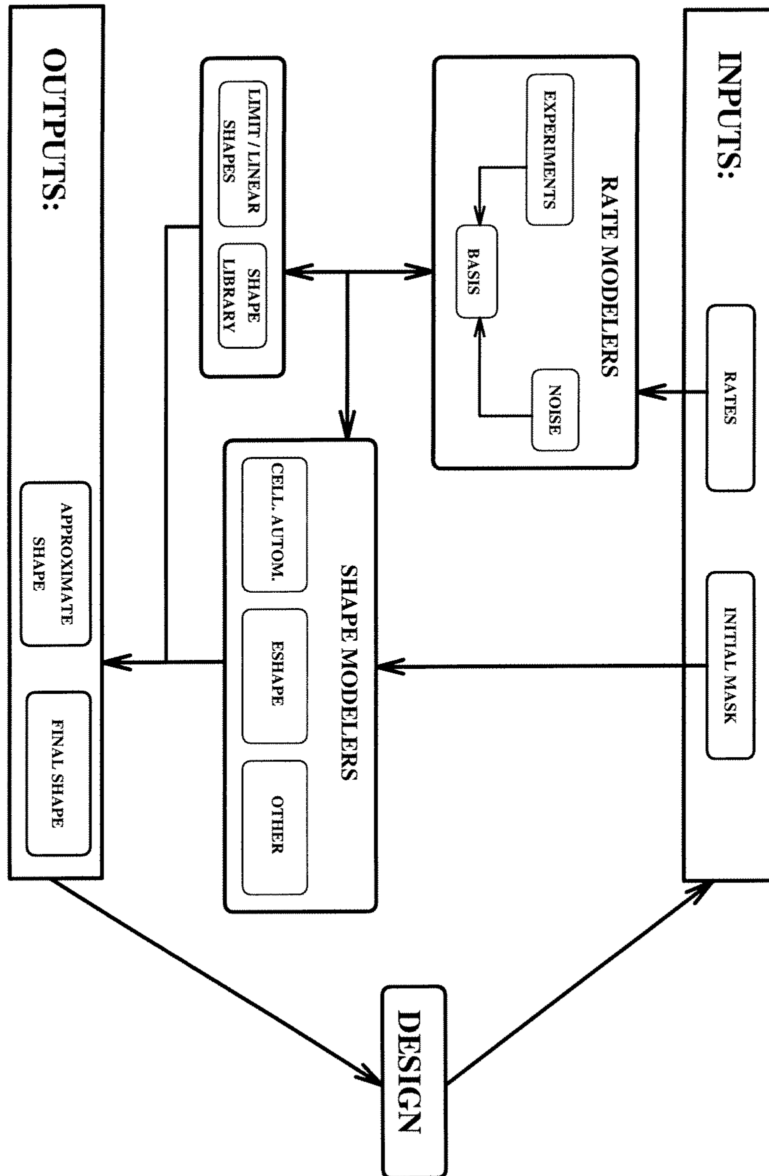

Figure A-1: Links between different design tools.

```
*******************************************************
*                     MEMS DESIGN                     *
*******************************************************
*                                                     *
*  H)  HELP                                           *
*  R)  rate modeling                                  *
*  E)  Eshape modeling                                *
*  C)  cellular automata modeling                     *
*  P)  crystal planes                                 *
*  M)  Minkowski transforms                           *
*  Q)  QUIT                                           *
*                                                     *
*******************************************************

H, R, E, C, P, M, or Q :
```

Figure A-2: Main menu screen.

holes and pegs which are then converted to an array of cells.

Figure A-2 shows the initial menu screen. The design tool options include a help submenu, rate modeling, Eshape modeling, and cellular automata modeling. In addition two teaching tools, a simple Minkowski transformer and a crystal planes viewer are included.

Figure A-3 shows the Eshape submenu screen. Options include help, generating Eshapes, two and three dimensional modeling, and returning to the main menu.

A.2 Link between Eshape and Minkowski operations

The Eshape method and Minkowski transformations share the same mathematics. Consider the case of an anisotropic etchant where the Eshape is convex and has no self intersections. An elliptical etch rate diagram is one such example; the Eshape is an oval. The etching process is equivalent to painting the initial mask with a brush in the shape of the Eshape and scaled by time. Thus the Minkowski operation which models the etching is

$$output = mask \oplus (eshape * time) \tag{A.1}$$

```
*******************************************************
*                     ESHAPE                          *
*******************************************************
*                                                     *
*  H)  HELP                                           *
*  E)  Eshape                                         *
*  2)  2D Eshape modeling                             *
*  T)  change output timesteps                        *
*  C)  intersection cleanup                           *
*  P)  3D profile                                     *
*  3)  3D extension                                   *
*  M)  RETURN TO MAIN                                 *
*                                                     *
*******************************************************

H, E, 2, T, C, P, 3, or M :
```

Figure A-3: Eshape submenu screen.

Time scaling laws follow directly from the linear nature of Equation A.1 since

$$k * (mask \oplus (eshape * time)) = (k * mask) \oplus (eshape * (k * time) \tag{A.2}$$

In the case of a convex mask, the Minkowski transform arranges the vectors of the mask and of the brush in a slope sorted list. The same is done in the Eshape method by tangent matching: the parts of the Eshape whose slopes lie between the slopes of the two of the mask vectors are inserted into a new output vector list. If the mask is not convex, then additional sorting steps are needed for the Minkowski transform; the same holds true for the Eshape where corner selection rules are used.

However the Eshape method differs from Minkowski transforms in that the etch rates are highly non-convex and that the Eshape often has self-intersections. The corner rules of the Eshape ensure that the proper sorting is performed.

A.3 Trapezoidal correction for beams

Most of the shapes made by wet bulk etching are trapezoidal in cross section. If the mechanical analysis is done assuming a square cross section, the results will be inaccurate. For example the resonant frequency of a beam is given by

$$\omega = (\beta l)^2 * \sqrt{\frac{EI}{lA}} * \frac{1}{l^2} \tag{A.3}$$

where E is the Young's Modulus, l is the length, A is the area, I is the area moment, and βl is a number dependent on the end conditions only.

For a square with side h, I/A is given by

$$I/A = h^2/12 \tag{A.4}$$

For a trapezoid with height h and lengths a and b, I/A is given by

$$I/A = \frac{a^2 + 4ab + b^2}{(a+b)^2} h^2/18 \tag{A.5}$$

In terms of the side wall angle θ

$$I/A = (1 + \frac{1}{2}\frac{c(c + 2\tan(\theta)}{(c + \tan(\theta))^2})h^2/18 \tag{A.6}$$

where c is the normalized top width a/h.

Figure A-4 shows the relative error in I/A of a trapezoid compared to a square. The figure shows results for two θ values: 45 and 35.3 degrees. The error is large for triangular beams and is small for thin beams. The error is probably negligible for width to height ratios greater than four.

A.4 Comparison of EDP, KOH, and TMAH etches

A comparison of output shapes for EDP, KOH, and TMAH was made. The EDP and KOH samples were etched by the author while the TMAH samples were etched by a member of professor Y. C. Tai's laboratory at Caltech. All three have similar etch rate diagrams and

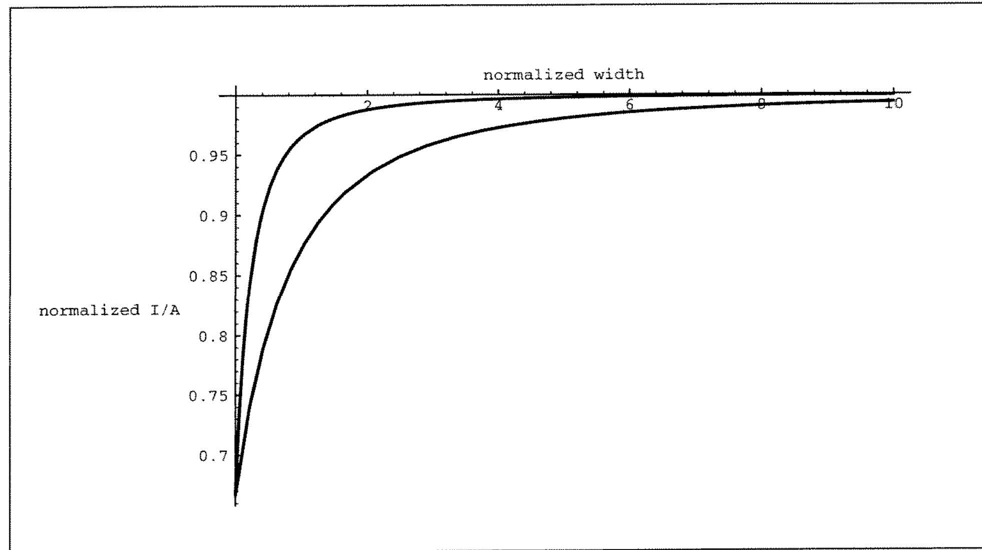

Figure A-4: Trapezoidal I/A as a fraction of square I/A versus normalized width. Top curve is θ =35.3 degrees, bottom curve is θ =45 degrees.

all have square pyramidal pits as limit shapes as shown in Figure A-5. KOH differs from the other two in that the 45 degree walls are the (010) plane rather than the (110) plane and are thus vertical. Compensation works well for EDP and KOH but is less successful with TMAH because of higher variability in rates for TMAH.

A.5 Table of abbreviations

Table A.1 shows some of the more commonly used abbreviations in MEMS (Micro Electro Mechanical Systems).

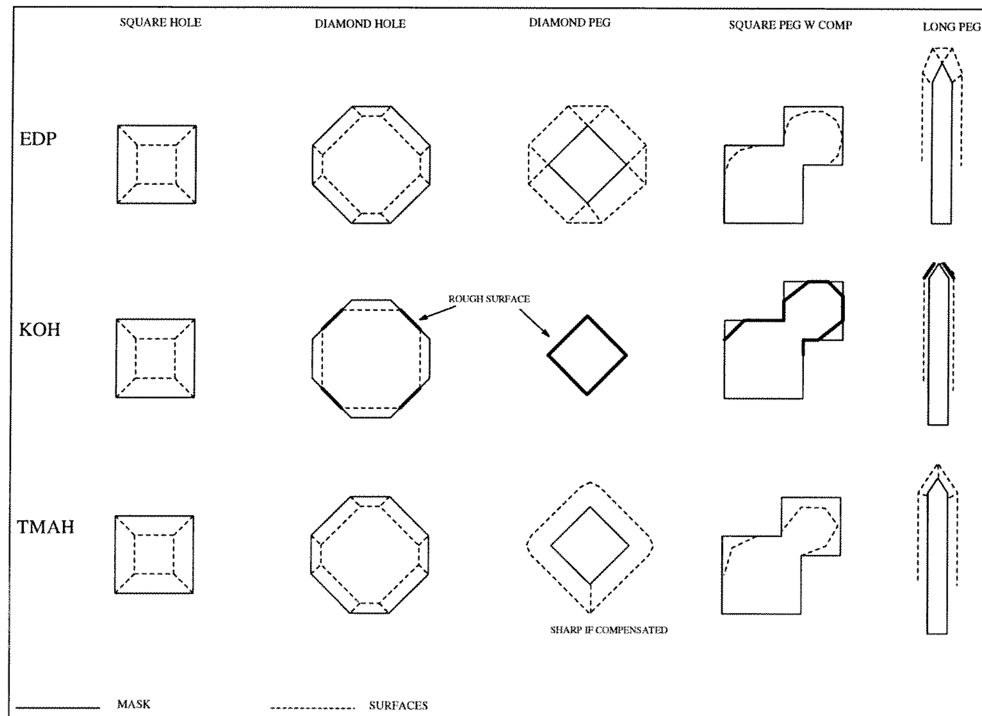

Figure A-5: Comparison of EDP, KOH, and TMAH etches.

abbreviation	meaning
AFM	atomic force microscope
ASEP	anisotropic silicon etching program
BOE	buffered oxide etch
CAA	computer aided analysis
CAD	computer aided design
CVD	chemical vapor deposition
DI	deionized water
EDP	ethyline diamine pyrocathecol
FEM	finite element modeling
PSG	phosphosilicate glass
HNA	hydrochloric nitric acetic
KOH	potassium hydroxide
LIGA	lithographie galvanoformung
MBE	molecular beam epitaxy
MEMS	micro electro mechanical systems
PR	photoresist
RIE	reactive ion etching
SEM	scanning electron microscope
STM	scanning tunneling microscope
TEM	transmission electron microscope
TMAH	tetramethyl ammonium hydroxide
UV	ultraviolet
VLSI	very large scale integration

Table A.1: Common abbreviations.

References

[1] H. Abe, Y. Sonobe, and T. Enomoto. Etching characteristics of silicon and its compounds by gas plasma. *Jpn. J. Appl. Phy.*, 12:154–155, 1973.

[2] M.M. Abu-Zeid. Corner undercutting in anisotropically etched isolation contours. *J. Electrochem. Soc.*, 131:2138–2142, 1984.

[3] M. Alavi. Fabrication of microchannels by laser machining and anisotropic etching of silicon. *Sensors and Actuators*, 32:299–302, 1992.

[4] M. Alavi. Monolithic microbridges in silicon using laser machining and anisotropic etching. *Sensors and Actuators*, A37-38:661–665, 1993.

[5] M. Bao, C. Burrer, J. Esteve, J. Bausells, and S. Marco. Etching front control of (110) strips for corner compensation. *Sensors and Actuators*, A37-38:727–732, 1993.

[6] J. Bardeen and W. H. Brattain. The transistor, a semi-conductor triode. *Phys. Rev*, 74:130–231, 1948.

[7] E. Bassous. Fabrication of novel three dimensional microstructures by the anisotropic etching of (100) and (110) silicon. *IEEE Transactions on Electron Devices*, ED-25(10):1178–1185, October 1978.

[8] E. Bassous, H. H. Taub, and L. Kuhn. Ink jet printing nozzle arrays etched in silicon. *Appl. Phys. Letters*, 31:135–137, 1977.

[9] K.E. Bean. Anisotropic etching of silicon. *IEEE Transactions on Electron Devices*, ED-25(10):1185–1193, October 1978.

[10] T. Bloomstein and D. Ehrlich. Laser-chemical three-dimensional writing of multimaterial structures for microelectromechanics. In *MEMS '91*, pages 162–167, Institute of Electrical Engineers, 1991.

[11] T. Bloomstein and D. Ehrlich. Stereo laser machining of silicon. *Appl. Phys. Lett.*, 61(6):708 –710, August 1992.

[12] A. Bohg. Ethylene diamine-pyrocathecol-water mixture shows etching anomaly in boron-doped silicon. *J. Electrochem. Soc.: Solid State Science and Technology*, pages 401–402, 1971.

[13] M. Boman. Helical microstructures grown by laser assisted chemical vapour deposition. In *MEMS '92*, pages 162–167, Institute of Electrical Engineers, 1992.

[14] J. M. Borky and K. D. Wise. Integrated signal conditioning for silicon pressure sensors. *IEEE Trans. on Elect. Devices*, 26:1906–1910, 1979.

[15] R. A. Buser, S. B. Crary, and O. S. Juma. Integration of the anisotropic-silicon-etching program ASEP within the CAEMEMS CAD/CAE framework. In *MEMS 92*, pages 133–138, Institute of Electrical Engineers, 1992.

[16] R. A. Buser and N. F. de Rooij. ASEP: A CAD program for silicon anisotropic etching. *Sensors and Actuators*, 28:71–78, 1991.

[17] N. Cade, R. Lee, and C. Patel. Wet etching of cusp structures for field emission devices. *IEEE Transactions of electron devices*, 36-11:2709–2714, 1989.

[18] H. Camon and A. Gue. Modelling of an anisotropic etching in silicon-based sensor applications. *Sensors and Actuators*, 33:103–105, 1992.

[19] D.R. Ciarlo. A latching accelerometer fabricated by the anisotropic etching of (110) oriented silicon wafers. *J. Micromech. Microeng.*, 2:10–13, 1992.

[20] G. DeLapierre. Anisotropic crystal etching: A simulation program. *Sensors and Actuators*, 31:267–274, 1992.

[21] D. Dietrich and J. Fruhauf. Computer simulations of the development of dish-shaped deepenings by orientation-dependent etching of (100) silicon. *Sensors and Actuators*, 39:261–262, 1993.

[22] D. J. Ehrlich, R. M. Osgood Jr., and T. F. Deutsch. Laser chemical technique for rapid direct writing of surface relief in silicon. *Appl. Phys. Lett.*, 38:1018–1020, 1981.

[23] M. M. Farooqui and A. G. R. Evans. Polysilicon microstructures. In *MEMS '91*, pages 187–191, Institute of Electrical Engineers, 1991.

[24] R. Farouki and C. Neff. Analytic properties of plane offset curves. *Computer aided geometric design*, 7:83–99, 1990.

[25] R. M. Finne and D. L. Klein. A water-amine-complexing agent system for etching silicon. *J. Electrochem. Soc.: Solid State Science and Technology*, pages 965–970, September 1967.

[26] D. L. Flamm, V. M. Donnelly, and D. E. Ibbotson. Basic chemistry and mechanisms of plasma etching. *J. Vac. Sci. Technol.*, B1(1):23–30, jan/mar 1990.

[27] F. C. Frank and M. B. Ives. Orientation-dependent dissolution of Germanium. *J. Appl. Phys.*, 31(11):1996–1999, November 1960.

[28] P. K. Ghosh. A mathematical model for shape description using Minkowski operators. *Computer Vision, Graphics and Image Processing*, 44(1):239–269, 1988.

[29] P. K. Ghosh. A solution to polygon containment, spatial planning, and other related problems using Minkowski operators. *Computer Vision, Graphics and Image Processing*, 49(1):1–35, 1990.

[30] P. K. Ghosh. An algebra of polygons through the notion of negative shapes. *Computer Vision, Graphics and Image Processing*, 54(1):119–144, 1991.

[31] H. Guckel, K. J. Skrobis, T. R. Christenson, J. Klein, S. Ahn, Choi, and E. G. Lovel. Fabrication of assembled micromechanical components via deep x-ray lithography. In *MEMS '91*, pages 74–79, Institute of Electrical Engineers, 1991.

[32] H. Guckel, K. J. Skrobis, T. R. Christenson, J. Klein, S. Han, B. Choi, E. G. Lovel, and T. W. Chapman. Fabrication and testing of the planar magnetic microrotor. *J. of Micromechanics and Microengineering*, 1:135–138, 1991.

[33] M. Harmening, W. Bacher, P. Bley, A. El-Kholi, H. Kalb, B. Kowanz, W. Menz, A. Michel, and J. Mohr. Molding of three dimensional microstructures by the LIGA process. In *MEMS '92*, pages 202–207, Institute of Electrical Engineers, 1991.

[34] E. Herr and H. Balles. KOH etching of high index crystal planes in silicon. *Sensors and Actuators*, 31:283–287, 1992.

[35] J. Hoschek. Offset curves in the plane. *Computer-aided Design*, 17(2):77–82, 1984.

[36] R.J. Jaccodine. Use of modified free energy theorems to predict equilibrium growing and etching shapes. *J. Appl. Phys.*, 33(8):2643–2647, August 1962.

[37] C. Ju and P.J. Hesketh. Measurements of the anisotropic etching of a single-crystal silicon sphere in aqueous cesium hydroxide. *Sensors and Actuators*, A33:191–196, 1992.

[38] F. J. Kamphoefner. Ink jet printing. *IEEE Trans. on Elect. Devices*, 19:584–593, 1972.

[39] D.L. Kendall. On etching very narrow grooves in silicon. *Appl. Phys. Letters*, 26:195–198, 1975.

[40] D.L. Kendall. Vertical etching of silicon at very high aspect ratios. *Ann. Rev. Mater. Sci.*, 9:373–403, 1979.

[41] D.L. Kendall. A new theory for the anisotropic etching of silicon and some underdeveloped chemical micromachining concepts. *J. Vac. Sci. Technol.*, A8(4):3596–3605, jul/aug 1990.

[42] J. S. Kilby. Invention of the integrated circuit. *IEEE Trans. on Electron Devices*, ED-23:648–654, 1976.

[43] E. S. Kim, R. Muller, and R. Hijab. Front to backside alignment using resist patterned etch control and one etching step. *J. of Microelectromechanical Systems*, 1(2):95–100, June 1992.

[44] A. Koide, K. Sato, and S. Tanaka. Simulation of two dimensional etch profile of silicon during orientation-dependent anisotropic etching. In *Transducers '91*, pages 216–220, Institute of Electrical Engineers, 1991.

[45] G. Koppleman. Oyster, a simulation tool for micro electromechanical design. *Sensors and Actuators*, 20:179–185, 1989.

[46] Y. Linden, L. Tenerenz, Tiren, and B. Hok. Fabrication of three-dimensional silicon structures by means of doping selecting etching (dse). *Sensors and Actuators*, 16:67–82, 1989.

[47] George H. Martin. *Kinematics and Dynamics of Machines.* McGraw-Hill, New York, 1982.

[48] F. Maseeh, R. Harris, and S. Senturia. A CAD architecture for MEMS. In *Transducers 90*, pages 44–49, Institute of Electrical Engineers, 1990.

[49] G. K. Mayer, H. L. Offereins, H. Sandmaier, and K. Kuhl. Fabrication of non-underetched convex corners in anisotropic etching of (100)-silicon in aqueous KOH with respect to novel micromechanic elements. *J. Electrochem. Soc.*, 137(12):3947–3951, December 1990.

[50] Carver Meade and Lynn Conway. *Introduction to VLSI systems.* Addison Wesley, Reading Mass., 1980.

[51] W. Menz, W. Bacher, M. Harmening, and A. Michel. The LIGA technique - a novel concept for microstructures and the combination with Si-technologies by injection molding. In *MEMS '91*, pages 69–73, Institute of Electrical Engineers, 1991.

[52] S. Middelhoek and A. C. Hoogerwerf. Smart sensors: when and where? *Sensors and Actuators*, 8:39–48, 1985.

[53] S. Middlehoek, J. B. Angell, and D. J. W. Noorlag. Microprocessors get integrated sensors. *IEEE Spectrum*, pages 42–46, February 1980.

[54] R. Mlcak, H. L. Tuller, P. Greiff, J. Sohn, and L. Niles. Photoassisted electrochemical micromachining of silicon in HF electrolytes. *Sensors and Actuators*, 40:49–55, 1994.

[55] L. O'Connor. MEMS. *Mechanical engineering*, pages 40–47, February 1992.

[56] H. L. Offeriens, K. Kuhl, and H. Sandmaier. Methods for the fabrication of convex corners in anisotropic etching of (100) silicon in aqueous KOH. *Sensors and Actuators*, A25-27:9–13, 1991.

[57] K. E. Petersen. Fabrication of an integrated, planar silicon ink-jet structure. *IEEE Trans. on Elect. Devices*, 26:1918–1920, 1979.

[58] K. E. Petersen. Silicon as a mechanical material. *Proceedings of the IEEE*, 79(8):420–457, May 1982.

[59] K. S. Pister, M. W. Judy, S. R. Burgett, and R. S. Fearing. Microfabricated hinges. *Sensors and Actuators*, 33:249–256, 1992.

[60] F. Pourahmadi and J. Twerdok. Modeling micromachined sensors with finite elements. *Machine Design*, pages 44–60, july 1990.

[61] B. Puers and W. Sansen. Compensation structures for convex corner micromachining in silicon. *Sensors and Actuators*, A21-23:1036–1041, 1990.

[62] A. Reisman, M. Berkenblit, S. A. Chan, F. B. Kaufman, and D. C. Green. The controlled etching of silicon in catalyzed ethylenediamine-pyrocatecol-water solutions. *J. Electrochem. Soc.: Solid State Science and Technology*, pages 1406–1415, August 1979.

[63] W. R. Runyan and K. E. Bean. *Semiconductor Integrated Circuit Processing Technology*. Addison-Wesley, New York, 1990.

[64] U. Schnakenberg, W. Benecke, and B. Lochel. NH4 OH - based etchants for silicon micromachining. *Sensors and Actuators*, A21-A23:1031–1035, 1990.

[65] H. Seidel, L. Csepregi, A. Heuberger, and H. Baumgartel. Anisotropic etching of crystaline silicon in alkaline solutions. *J. Electrochem. Soc.*, 137:3613–3631, 1990.

[66] S. D. Senturia, R. M. Harris, B. P. Johnson, S. Kim, M. A. Shulman, and J. K. White. A computer-aided design system for microelectromechanical systems (MEMCAD). *J. of Microelectromechanical Systems*, 1:3–13, March 1992.

[67] C. H. Sequin. Computer simulation of anisotropic crystal etching. In *Transducers '91*, pages 801–806, San Francisco, CA, USA, 1991.

[68] D. W. Shaw. Morphology analysis in localized crystal growth and dissolution. *J. Cryst. Gr.*, 47:509–517, 1979.

[69] D. W. Shaw. Localized etching with acidic hyrogen peroxide solutions. *J. Electrochem. Soc.: Solid State Science and Technology*, pages 874–880, April 1981.

[70] A. H. Slocum. Precision machine design: macromachine design philosphy and its applicability to the design of micromachines. In *MEMS '92*, pages 37–42, Institute of Electrical Engineers, 1992.

[71] C. Steinbruchel, H. W. Lehmann, and K. Frick. Mechanism of dry etching of silicon dioxide. *J. Electrochem. Soc.: Solid State Science and Technology*, pages 180–186, January 1985.

[72] G. Stix. Micron machinations. *Scientific American*, pages 107–117, nov 1992.

[73] K. Suzuki and H. Tangigawa. Single crystal silicon rotational micromotors. In *MEMS '91*, pages 15–20, Institute of Electrical Engineers, 1991.

[74] O. Tabata, R. Asahi, H. Funabashi, K. Shimoaka, and S. Sugiyama. Anisotropic etching of silicon in TMAH solutions. *Sensors and Actuators*, A34:51–57, 1992.

[75] Y. C. Tai and R. S. Muller. IC-processed electrostatic synchronous micromotors. *Sensors and Actuators*, 20:49–50, 1989.

[76] W. C. Tang, T. H. Nguyen, and R. T. Howe. Laterally driven polysilicon resonant microstructures. *Sensors and Actuators*, 20:25–32, 1989.

[77] T. Thurgate. Segment based etch algorithm and modeling. *IEEE Transactions on computer-aided design*, pages 1101–1109, sep 1991.

[78] W. Tiller and E.G. Hanson. Offsets of two-dimensional profiles. *IEEE Comput. Graphics Appl.*, 4:36–46, 1984.

[79] W. Trimmer. Microrobots and micromechanical systems. *Sensors and actuators*, 19:267–287, 1989.

[80] C. C. Tseng, D. Botez, and S. Wang. Optical bends and rings fabricated by preferential etching. *Appl. Phys. Letters*, 26:699–701, 1975.

[81] W. T. Tseng, C. C. Tseng, and S. Wang. Optical waveguides fabricated by preferential etching. *Appl. Optics*, 14:1200–1206, 1975.

[82] D. B. Tuckerman and R. F. W. Pease. High performance heat sinking for VLSI. *IEEE Elect. Devices Letters*, 2:126–129, 1981.

[83] M. Turunen, J. Lenkkeri, J. Levoska, and S. Leppavuori. Laser-induced deposition and etching of materials: a new technology for sensor fabrication. *Sensors and Actuators*, 17:75–79, 1989.

[84] U. Wallrabe, P. Bley, B. Krevet, W. Menz, and J. Mohr. Theoretical and experimental results of an electrostatic micro motor with large gear ratio fabricated by the LIGA process. In *MEMS '92*, pages 139–140, Institute of Electrical Engineers, 1992.

[85] D. F. Weirauch. Correlation of the anisotropic etching of single crystal silicon spheres and wafers. *J. Appl. Phys.*, 46:1478–1483, 1975.

[86] K. Wise and K. Nafaji. Microfabrication techniques for integrated sensors and microsystems. *Science*, 25:1335–1342, November 1991.

[87] K. D. Wise. Integrated microelectromechanical systems: a perspective on MEMS in the 90s. In *MEMS '91*, pages 33–27, Institute of Electrical Engineers, 1991.

[88] X. Wu and W. H. Ko. Compensating corner undercutting in anisotropic etching of (100) silicon. *Sensors and Actuators*, 18:207–215, 1989.